

## Microstructural stability of the Kirkendall plane

**Citation for published version (APA):**

Dal, van, M. J. H. (2001). *Microstructural stability of the Kirkendall plane*. [Phd Thesis 1 (Research TU/e / Graduation TU/e), Chemical Engineering and Chemistry]. Technische Universiteit Eindhoven.  
<https://doi.org/10.6100/IR548020>

**DOI:**

[10.6100/IR548020](https://doi.org/10.6100/IR548020)

**Document status and date:**

Published: 01/01/2001

**Document Version:**

Publisher's PDF, also known as Version of Record (includes final page, issue and volume numbers)

**Please check the document version of this publication:**

- A submitted manuscript is the version of the article upon submission and before peer-review. There can be important differences between the submitted version and the official published version of record. People interested in the research are advised to contact the author for the final version of the publication, or visit the DOI to the publisher's website.
- The final author version and the galley proof are versions of the publication after peer review.
- The final published version features the final layout of the paper including the volume, issue and page numbers.

[Link to publication](#)

**General rights**

Copyright and moral rights for the publications made accessible in the public portal are retained by the authors and/or other copyright owners and it is a condition of accessing publications that users recognise and abide by the legal requirements associated with these rights.

- Users may download and print one copy of any publication from the public portal for the purpose of private study or research.
- You may not further distribute the material or use it for any profit-making activity or commercial gain
- You may freely distribute the URL identifying the publication in the public portal.

If the publication is distributed under the terms of Article 25fa of the Dutch Copyright Act, indicated by the "Taverne" license above, please follow below link for the End User Agreement:

[www.tue.nl/taverne](http://www.tue.nl/taverne)

**Take down policy**

If you believe that this document breaches copyright please contact us at:

[openaccess@tue.nl](mailto:openaccess@tue.nl)

providing details and we will investigate your claim.

# Microstructural stability of the Kirkendall plane

## PROEFSCHRIFT

ter verkrijging van de graad van doctor aan de  
Technische Universiteit Eindhoven, op gezag van de  
Rector Magnificus, prof.dr. R.A. van Santen, voor een  
commissie aangewezen door het College voor  
Promoties in het openbaar te verdedigen  
op dinsdag 9 oktober 2001 om 16.00 uur

door

Marcus Johannes Henricus van Dal

geboren te Diessen

Dit proefschrift is goedgekeurd door de promotoren:

prof.dr. F.J.J. van Loo

en

prof.dr. G. de With

Druk: Universiteitsdrukkerij, Technische Universiteit Eindhoven

Kaft: Titaan/nikkel diffusiekoppel

Kaftontwerp: Katrien Bos, Mark van Dal

CIP-DATA LIBRARY TECHNISCHE UNIVERSITEIT EINDHOVEN

Dal, Marcus J.H. van

Microstructural stability of the Kirkendall plane / by Marcus J.H. van Dal. -  
Eindhoven : Technische Universiteit Eindhoven, 2001.

Proefschrift. - ISBN 90-386-2982-6

NUGI 813

Trefwoorden: metalen ; vastestofchemie / metalen ; diffusie / metalen ;  
microstructuur / metaallegeringen ; vastestofchemie / metaallegeringen ;  
diffusie / metaallegeringen ; microstructuur / Kirkendall effect

Subject headings: metals ; solid state chemistry / metals ; diffusion /  
metals ; microstructure / metal alloys ; solid state chemistry / metal  
alloys ; diffusion / metal alloys ; microstructure / Kirkendall effect

## Contents

<b>Preface</b>	vii
<b>1. Introduction</b>	<b>1</b>
1.1 The discovery of the Kirkendall effect	1
1.2 Consequences of the Kirkendall effect	2
1.3 Motivation of the present work	4
1.4 Outline of the present work	6
<b>2. Experimental methods</b>	<b>9</b>
2.1 Starting materials and melting of alloys	9
2.2 Preparation of diffusion couples	11
2.3 Diffusion couple cross-sectioning and analysis	12
<b>3. Diffusion in solids</b>	<b>15</b>
3.1 Interdiffusion: Matano-Boltzmann analysis	15
3.2 Interdiffusion: Sauer-Freise analysis	18
3.3 Intrinsic diffusion: the Kirkendall effect and the phenomenological approach of Darken	21
3.4 Experimental determination of the Kirkendall velocity: the multi-foil technique	25
3.5 Thermodynamic factor and tracer diffusion coefficient	31
3.6 Relationship between the phase diagram and the interdiffusion behaviour in solid single-phase binary systems	36

---

<b>4. Reconsideration of the Kirkendall effect:</b>	
<b>Bifurcation and instability of the Kirkendall plane</b>	<b>41</b>
4.1 Introduction	41
4.2 The Kirkendall velocity and displacement of inert markers during binary interdiffusion	42
4.3 Microstructural stability of the Kirkendall plane	47
4.4 Multiple, stable and unstable Kirkendall planes in a single phase: manifestation of the Kirkendall effect in the $\beta'$ -AuZn intermetallic	49
4.5 General criterion of Kirkendall plane instability	56
4.6 Manifestation of the Kirkendall effect in disordered binary systems	59
Appendix 4.1: Numerical solution of Eq. (4.4) (Mathematica v3.0)	65
<b>5. Diffusion in multi-phase systems</b>	<b>71</b>
5.1 Introduction	71
5.2 Relations between the thermodynamics and the growth kinetics of binary line-compounds	74
5.3 Thermodynamic properties of the Co-silicides	80
5.4 Diffusion in the CoSi <sub>2</sub> intermetallic compound	82
5.5 Growth of the B20-type intermetallic CoSi in the CoSi <sub>2</sub> /Co <sub>2</sub> Si diffusion couples	87
5.6 Relative mobilities of species in the C23-type intermetallic Co <sub>2</sub> Si at 1100°C	93
5.7 Deficiencies of the proposed analysis	95
<b>6. Manifestations of the Kirkendall effect accompanying reactive diffusion</b>	<b>101</b>
6.1 Introduction	101
6.2 On migration of inert markers upon interdiffusion in a binary multi-phase system	102
6.3 Kirkendall effect in the multi-phase diffusion couples of the Co-Si system	104
6.4 Kirkendall effect in the multi-phase Ti/Ni diffusion couple	113

---

<b>7. Final considerations and recommendations for future work</b>	<b>117</b>
7.1 Unstable and stable Kirkendall planes: their mechanical consequences	118
7.2 More than two Kirkendall planes: is it possible?	119
7.3 Periodic layer formation as a manifestation of the Kirkendall effect	120
7.4 The influence of the Kirkendall effect on the microstructural evolution in the ternary system Ti-Ni-Cr	122
<b>Summary</b>	<b>127</b>
<b>Samenvatting</b>	<b>135</b>
<b>Dankwoord</b>	<b>145</b>
<b>List of Publications</b>	<b>147</b>
<b>Curriculum Vitae</b>	<b>150</b>



## Preface

The Kirkendall effect, named after its discoverer Dr. Ernest O. Kirkendall, is important in connection with any solid/solid bonding between dissimilar materials, which, in turn, is of significance in a wide range of technological fields. The theoretical background of the effect is incorporated in all textbooks on solid-state diffusion. Although Ernest Kirkendall published only three papers in his short scientific career, it is astonishing to see the enormous impact his work had in the theoretical development and understanding of diffusion in solids.



Dr. Ernest O. Kirkendall

Ernest Kirkendall was born in Michigan in 1914<sup>1</sup>. He graduated from Wayne College (later Wayne University) in 1934, was awarded a master's degree in 1935 and a doctor of science in 1938 from the Metallurgy Department at the University of Michigan. He was an instructor at Wayne University from 1937 to 1941 and an assistant professor from 1941 to 1946 during which period he wrote his famous paper "Zinc Diffusion in Alpha Brass" together with his graduate student Alice Smigelskas. Many researchers had criticised the ideas that he posed in this last paper, however, Kirkendall kept trying until his interpretation had been accepted. Shortly after he stopped his scientific career.

---

<sup>1</sup> All information on Ernest Kirkendall's life was taken from:  
H. Nakajima, *JOM* **49** (1997) 15.



The present work attempts to be complementary to Kirkendall's work. During our studies on the manifestations of the Kirkendall effect we have encountered many new aspects. With a phenomenological and comprehensive approach the observed phenomena will be rationalised. Mainly binary (both single- and multi-phase) systems will be discussed. It is intended here to demonstrate theoretically as well as experimentally the Kirkendall effect in all its appearances and, thereby, to gain more understanding of diffusion in solids in general.

# Chapter 1

## Introduction

### 1.1 The discovery of the Kirkendall effect

In 1947, Ernest Kirkendall published his third and last paper in a series on the diffusion of zinc in  $\alpha$ -brass [1-3]. In this paper [3], he presented the results of a so-called diffusion couple experiment that consisted of a brass bar (with a composition of 30 wt.% zinc and 70 wt.% copper) electroplated with pure copper (of about 2.5 mm thick on all sides). Prior to the electroplating procedure, inert molybdenum wires (130  $\mu\text{m}$  thick) were stretched length-wise along each of the two plane surfaces to mark the original interface of the brass-copper diffusion couple. Fig. 1.1 shows a schematic drawing of the cross-section of the bar.

The diffusion couple assembly was annealed at 785°C and as a result of the concentration difference the copper and zinc atoms started to interdiffuse. After heat treatments for different times (typically several hundreds of hours), a cross-section of the bar was cut and the distance between the two sets of molybdenum wire was measured. Kirkendall found that the wires shifted inwards, moving parabolically with time.

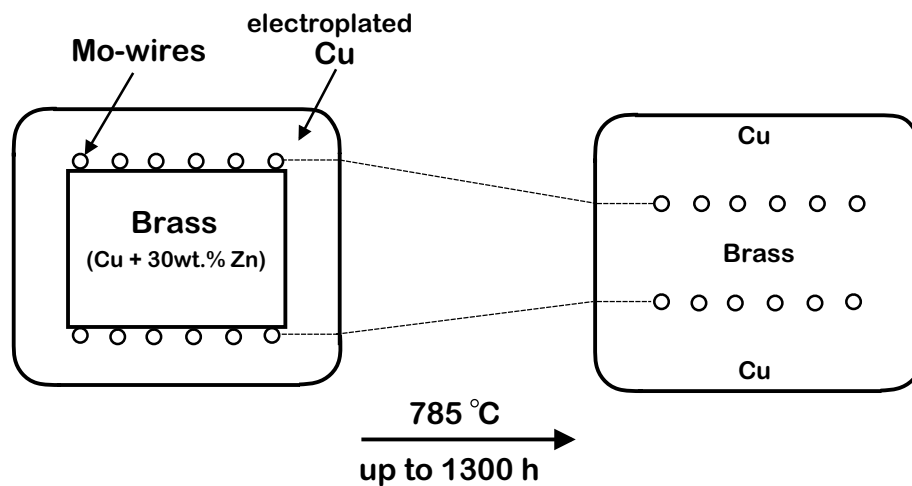


Figure 1.1: Schematic representation of a cross-section of the diffusion couple as prepared by Smigelskas and Kirkendall [3] before and after heat treatment at 785 °C. The molybdenum wires placed at the original contact surface moved towards each other. It was concluded that the Zn atoms diffused much faster outwards than the Cu atoms inwards.

On the basis of volume changes accompanying the interdiffusion process this could not be explained. He concluded:

*“The movement of the insoluble molybdenum wires was conclusive evidence that the  $\alpha$ -brass was being forced back as a whole (...) as a result of the diffusing out of the zinc atoms individually”.*

In other words, the experimental observation made by Kirkendall meant that Zn atoms diffused much faster outwards than Cu atoms inwards causing the inner brass core to shrink, which in turn resulted in the movement of the inert molybdenum wires.

## 1.2 Consequences of the Kirkendall effect

Kirkendall’s conclusion was received with much surprise. Before the 1940’s it was commonly believed that diffusion in solids took place via a direct exchange or ring mechanism (Fig. 1.2a and b) which implied the equality of diffusion of the moving elements in metals and alloys.

The fact that in a solid-state diffusion process it was possible for species to diffuse with different rates changed the existing theories on solid state diffusion completely.

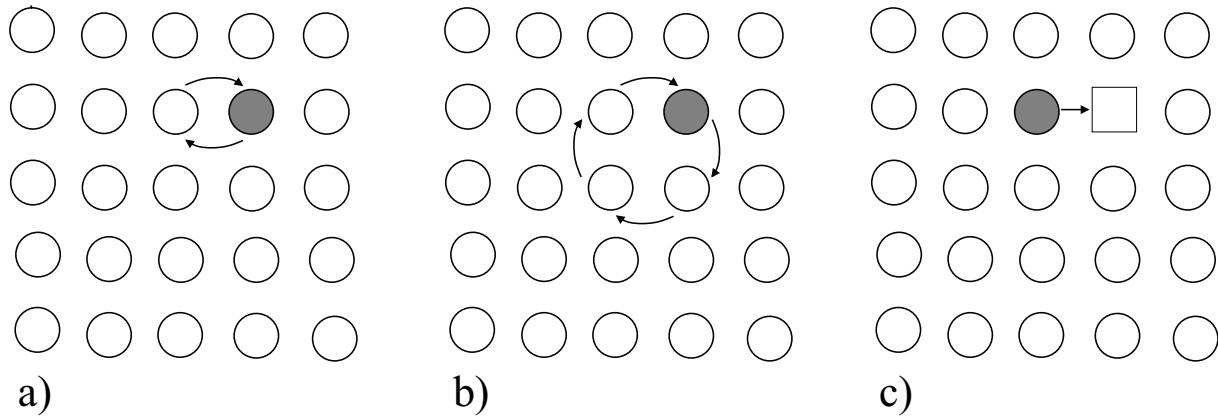


Figure 1.2: Atomic diffusion mechanisms showing: a) a direct exchange mechanism; b) ring mechanism and c) vacancy mechanism.

The impact of Kirkendall's finding can be appreciated from a reply on his paper [3] by one of the leading figures on solid state science at that time, Dr. R.F. Mehl [4]:

*"If verified, this "Kirkendall effect" would greatly modify not only the treatment of diffusion data but also the theory of the mechanism of diffusion. It would, for example, be no longer possible to represent diffusion data in a substitutional solid solution by one coefficient, applying to both metal atoms since the separate coefficients are equal, but one would have to show two coefficients, one each for the two metal atoms; the solution to the diffusion equation under these circumstances would be extraordinarily complex; and obviously this result would imply a diffusion mechanism differing from that of simple atom interchange."*

Nevertheless, more and more studies devoted to the behaviour of inert markers during a solid-state interdiffusion process pointed out the validity and, moreover, the generality of the Kirkendall effect. In the ten years after its discovery, the Kirkendall effect was observed in binary systems like Ag-Au [5-8], Ag-Pd [6], Ag-Zn [7,9], Al-Mg [7], Au-Ni [6], Cu-Ni [5,6,8,10-12], Cu-Sb [13], Cu-Zn [7], Fe-Ni [6], Fe-Si [14], Mo-Ti [15], U-Zr [16].

The first theoretical description of the Kirkendall effect was made by Darken [17]. For the case of binary systems, Darken used two individual (independent) diffusivities - one for each component - to describe the interdiffusion process. He showed that with two fundamental equations the Kirkendall experiment permits the calculation of these individual diffusion coefficients and, coupled with activity data, offers a means of measuring the mobilities of the separate atoms in the binary diffusion process.

Another consequence of Kirkendall's finding is that interdiffusion processes exhibiting a Kirkendall effect could not be mediated by the direct exchange or ring mechanism since these assumed the individual diffusion coefficients to be equal. Seitz [18] (and later also Bardeen [19]) showed from an atomistic point of view that interdiffusion accompanied by a *vacancy mechanism* (Fig. 1.2c) led to Darken's equations if it is assumed that the concentration of vacant sites is in thermal equilibrium. For the Kirkendall effect to occur, vacancies must be created at the one side and annihilated at the other side of the interdiffusion zone so that a vacancy flux is created to maintain local equilibrium.

Nowadays, we know that the Kirkendall effect manifests itself in many phenomena such as the development of diffusional porosity (Kirkendall voiding, see e.g. Refs. [3,5,6,10,14,20]), generation of internal stress [21,22] and even by deformation of the material on a macroscopic scale [23]. These diffusion-induced processes are of concern in a wide variety of structures including composite materials, coatings, welded components and thin-film electronic devices.

### 1.3 Motivation of the present work

The initiative to start a fundamental study on the Kirkendall effect was triggered by an experimental observation in a study on diffusion in the Ti-Ni system performed by Bastin and Rieck [24]. In their work, the authors showed a diffusion couple consisting of a piece of Ti and Ni pressed together and annealed at 800°C for 72 h. The initial contact surface was marked by 10 µm thick tungsten wires (Fig. 1.3a). Fig. 1.3b shows the cross-section of the diffusion couple after interaction. One can see that three intermetallic phases are formed: Ti<sub>2</sub>Ni, TiNi and TiNi<sub>3</sub>, which is in accordance with the Ti-Ni phase diagram [25]. However, a

quite peculiar observation was the appearance of the W-wire after the interaction: it split up in several pieces and these parts were located differently across the interaction zone.

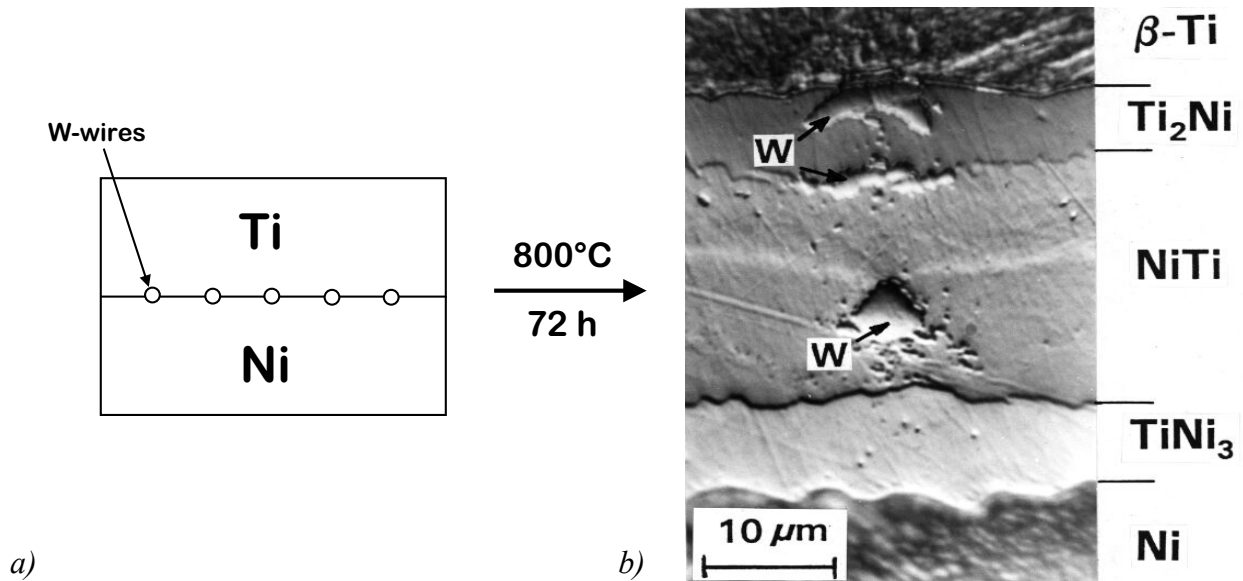


Figure 1.3: a) Schematic presentation of a Ti/Ni diffusion couple before annealing and b) a cross-section of the couple after annealing at 800 °C for 72 h taken from the work of Bastin and Rieck [24]. Prior to the heat treatment tungsten wires were introduced at the initial contact interface between Ti and Ni. After interaction the wire was split into several parts.

Now we can ask ourselves the following question. Is the Kirkendall plane, as marked by inert particles introduced prior to annealing between the initial end-members of a diffusion couple, unique? In other words, could the inert particles originating from one original contact surface migrate differently inside the zone of interdiffusion, so that two (or more) actual “Kirkendall planes” can be expected?

For binary two-phase systems, the problem has already been analysed theoretically [26]. The conclusion of this work was that in an  $\alpha/\beta$  diffusion couple it is necessary to consider two different Kirkendall-frames of references, one for the  $\alpha$  and one for the  $\beta$  phase. It was also shown that, depending upon the individual diffusion coefficients of the components in both phases, the interfacial composition of the diffusion couple and the composition of the end-members of the couple, the phase interface must be able to create and annihilate vacancies.

The latter means that the vacancy flux can, in principle, be in one direction in one phase and in the opposite direction in the other phase so that these fluxes are moving away from each other. As a result, the appearance of more than one plane marked by inert particles is expected inside the interaction zone. For the case of a binary system with a continuous solid solution, Cornet and Calais [27] described a hypothetical diffusion couple in which several “Kirkendall planes” can emerge. However, no experimental verification of these models was ever shown.

In the present work, we will try to seek such experimental evidences. In our quest on exploring new manifestations of the Kirkendall effect, several types of diffusion couple techniques will be used in order to gain more insight in the Kirkendall effect itself. We will design diffusion couple experiments taking different components as starting materials with which we will demonstrate new phenomena concerning the behaviour of inert markers present along the anticipated interdiffusion zone. It will be shown both theoretically and experimentally that a Kirkendall plane can be single, multiple, stable and unstable. Single-phase as well as multi-phase systems will be investigated. A phenomenological approach will be introduced, which can be used to predict the number of the Kirkendall planes and their positions and appearances.

#### **1.4 Outline of the present work**

The main objective of the present work is to provide better insight into the phenomenology of the Kirkendall effect in order to improve the general understanding of the Kirkendall effect and solid-state diffusion.

In Chapter 2 the experimental procedures used in this investigation will be given. Chapter 3 will deal with a general background on solid state diffusion in *single-phase* solid solutions. The theory will be illustrated by experimental results obtained in our study on diffusion phenomena and the Kirkendall effect in the Ni-Pd and Fe-Pd systems. In Chapter 4, a reconsideration of the Kirkendall effect is presented, in which the main findings of the present work are summarised. Again the theory will be illustrated with experimental results (mainly the observations made during our study on diffusion and the Kirkendall effect in the  $\beta'$ -AuZn phase of the binary Au-Zn system). Chapter 5 elaborates on diffusion phenomena in *multi-*

---

*phase* systems where the Co-Si system is taken for a case study. The results of the latter chapter will be used in Chapter 6 to explain the manifestations of the Kirkendall effect in multi-phase systems. The last chapter (Chapter 7) will conclude the present thesis with final considerations and recommendations for future work.



## References

1. E. Kirkendall, L. Thomassen and C. Upthegrove, *Trans. AIME* **133** (1939) 186.
2. E.O. Kirkendall, *Trans. AIME* **147** (1942) 104.
3. A.D. Smigelskas and E.O. Kirkendall, *Trans. AIME* **171** (1947) 130.
4. Discussion following ref. [3], *Trans. AIME* **171** (1947) 135.
5. L.C.C. daSilva and R.F. Mehl, *Trans. AIME* **191** (1951) 155.
6. W. Seith and A. Kottmann, *Angew. Chem.* **14** (1952) 379.
7. Th. Heumann and A. Kottmann, *Z. Metallkde.* **44** (1953) 139.
8. R.W. Balluffi and L.L. Seigle, *J. Appl. Phys.* **25** (1954) 607.
9. H. Bückle, *Z. Metallkde.* **37** (1946) 175.
10. R.S. Barnes, *Nature* **166** (1950) 1032.
11. W. Seith and R. Ludwig, *Z. Metallkde.* **45** (1954) 401.
12. W. Seith and R. Ludwig, *Z. Metallkde.* **45** (1954) 550.
13. Th. Heumann and F. Heinemann, *Z. Elektrochem.* **60** (1956) 1160.
14. E. Fitzner, *Z. Metallkde.* **44** (1953) 462.
15. P.G. Shewmon and J.H. Bechtold, *Acta Met.* **1** (1953) 355.
16. Y. Adda, J. Philibert and H. Faraggi, *Rev. Métall.* **54** (1957) 597.
17. L.S. Darken, *Trans. AIME* **175** (1948) 184.
18. F. Seitz, *Phys. Rev.* **74** (1948) 1513.
19. J. Bardeen, *Phys. Rev.* **76** (1949) 1403.
20. Th. Heumann and K.J. Grundhoff, *Z. Metallkde.* **63** (1972) 173.
21. G. B. Stephenson, *Scripta metall.* **20** (1986) 465.
22. G. B. Stephenson, *Acta metall.* **36** (1988) 2663.
23. I. Daruka, I.A. Szabó, D.L. Beke, C. Cserhádi, A.A. Kodentsov and F.J.J. van Loo, *Acta mater.* **44** (1996) 4981.
24. G.F. Bastin and G.D. Rieck, *Met. Trans.* **5** (1974) 1817.
25. J.L. Murray, Ed., Phase diagrams of binary titanium alloys, ASM International, Metals Park, Ohio (1987) pp. 197-211.
26. F.J.J. van Loo, B. Pieraggi and R.A. Rapp, *Acta metall. mater.* **38** (1990) 530.
27. J.-F. Cornet and D. Calais, *J. Phys. Chem. Solids* **33** (1972) 1675.

## Chapter 2

### Experimental methods

During this investigation, a large number of different binary (and ternary) *diffusion couples* were prepared. A diffusion couple consists of two pieces of dissimilar material, joined together in such a way that there is intimate contact between the two contact surfaces. This couple is heated for an extended period at an elevated temperature (below the melting points of the materials) so that both species are allowed to diffuse into each other. After cross-sectioning the sample, the interaction zone was analysed with optical microscopy, Scanning Electron Microscopy (SEM) and Electron Probe Microanalyser (EPMA).

#### 2.1 Starting materials and melting of alloys

Table 2.1 shows the specifications of the starting materials used for the diffusion couples prepared in the present investigations.

In some cases, alloys had to be melted which was performed in an arc-melt furnace. The materials were cut in small pieces, weighted into the desired amounts and placed together on a water-cooled Cu-bottom plate of the furnace. Then the furnace was closed and evacuated until

Table 2.1

*Specifications of the as-bought material used as a starting material for the present study.*

Material	Type	Purity (at.%)	Supplier
Au	Sheet (25 x 25 x 0.25 mm <sup>3</sup> )	99.995	Goodfellow, UK
Au	Wire (1.4 mm)	99.9999	Goodfellow, UK
Co	Rod (12 mm)	99.98	Goodfellow, UK
Cr	Pieces	99.99	Goodfellow, UK
Cu	Rod (12 mm)	99.995	Goodfellow, UK
Fe	Sheet (25 x 25 x 2.0 mm <sup>3</sup> )	99.98	Goodfellow, UK
Fe	Foil (25 μm)	99.95	Goodfellow, UK
Ni	Rod (10 mm)	99.99	Goodfellow, UK
Ni	Foil (21 μm)	99.9	Goodfellow, UK
Pd	Sheet (25 x 25 x 1.0 mm <sup>3</sup> )	99.99	Goodfellow, UK
Pd	Foil (20 μm)	99.95	Goodfellow, UK
Si	Pieces	99.99	Hoboken, Belgium
SiC	Rod, HIPSiC (12 mm)	99.9999	Goodfellow, UK
Ti	Rod (12 mm)	99.99	Alfa Products, Germany
Zn	Shots	99.98	Alfa Products, Germany

the pressure was below  $1 \cdot 10^{-7}$  mbar. After the evacuation procedure, the vacuum chamber was purged three times with Ar gas to finally obtain a pure Ar atmosphere of approximately 0.3 bar. Now a current of 250 A is employed on the tungsten electrode and the electrode is directed to the Cu-bottom plate so that a highly energetic arc is produced. The arc is then immediately pointed at the material causing it to melt (with approximate temperature of up to 3000 °C). In order to improve homogeneity the alloys were re-melted three times. The suitable diffusion couple dimensions were obtained by cutting the ingots into slices (8 x 8 x 3 mm<sup>3</sup>) using a slow-speed saw.

A different procedure was employed in the case of binary Au-Zn alloys, because of the possible evaporation of Zn during melting in the arc furnace. The Au-Zn alloys were melted in alumina crucibles in a flowing Ar gas atmosphere under flux consisting of ZnCl<sub>2</sub> and NaCl

(mass ratio 3:1) at 800-1000 °C. For this purpose a vertical furnace was used. After melting, the alloys were quenched in ice water and the flux was removed by dissolving it in water.

In all cases, the weight loss was less than 1 wt.% and the composition of the end-members was checked by means of Scanning Electron Microscope (SEM).

## 2.2 Preparation of diffusion couples

Before being assembled into a diffusion couple, the starting end-members were equilibrated and recrystallised by preheating them at the temperature of interest in a vacuum furnace for typically 24 h. The average grain size in the materials was in the range 100-300  $\mu\text{m}$ . The end-members were then ground into plan-parallel slices using a 180-grid SiC grinding paper and afterwards polished one-sided by successively 30  $\mu\text{m}$  and 10  $\mu\text{m}$  diamond impregnated discs to finish with 0.05  $\mu\text{m}$  alumina slurry.

Three types of diffusion couples were prepared:

1. Pure end-member diffusion couples (e.g. Ni/Pd, Ti/Ni, Co/Si etc.);
2. Incremental (partial) diffusion couples (e.g. Ni/Ni<sub>70</sub>Pd<sub>30</sub> (i.e. an alloy consisting of 70 at.% of Ni and 30 at.% of Pd), Au/AuZn<sub>2</sub>, Co<sub>2</sub>Si/CoSi<sub>2</sub>, etc.);
3. “Multi-foil” diffusion couples in which each end-member consists of a pile of foils next to a bulk piece of component material. More details will follow in section 3.4.

Prior to annealing, thorium dioxide (ThO<sub>2</sub>) particles were introduced at the polished surfaces of the end-members to mark the initial interface (the Kirkendall plane: see section 3.3). A suspension of ThO<sub>2</sub>-particles in acetone was prepared of which a drop was placed on the polished bonding faces of the diffusion couple. After a while, the acetone has evaporated leaving behind the homogeneously distributed ThO<sub>2</sub>-particles.

We used ThO<sub>2</sub>-particles with a grain size of 0.5 – 5  $\mu\text{m}$  to mark the initial contact surface of the diffusion couple for several reasons. Firstly, ThO<sub>2</sub> is a very stable oxide. This means that it is fair to assume that ThO<sub>2</sub> is not likely to react during the annealing procedure. Secondly, one has to be sure that the ThO<sub>2</sub> particles are “immobile”. It is clear that in this respect the

size of the markers is an important parameter. Too large particles (several hundreds of micrometers) could interfere with the interdiffusion process. However, in the case of too small particles, dragging of the particles by a moving phase boundary could occur so that then the displacement of the marker is not governed by the Kirkendall effect. The problem of dragging of small particles by moving phase boundaries has been analysed by van Gurp *et al.* [1]. An extensive study on the migration of inclusions in a field of an inhomogeneous concentration gradient can be found in Ref. [2]. As a rule of thumb for Kirkendall markers one can say that the particle's dimensions should be small with respect to the diffusion width and large with respect to the atomic distances in the diffusion matrix. Thirdly, the ThO<sub>2</sub> particles are easily traceable in the back-scattered electron microscope images, which is paramount to obtain the position of the Kirkendall plane after interaction.

The diffusion couple annealings were performed in a vacuum furnace under a gas pressure of about  $5 \cdot 10^{-7}$  mbar. It is extremely important that the diffusion couple is annealed under a sufficiently high and constant load to avoid pore formation. The latter was obtained by applying a load of approximately 5 MPa. In the samples presented in this work no pore formation was detected unless it is stated explicitly. Temperature (from 800 to 1400 °C) was controlled within  $\pm 2$  °C. More technical details of the vacuum furnace can be found elsewhere [3].

For the diffusion couples in which a highly volatile species such as Zn was used as starting material one can not apply high vacuum. In such a case the couples were annealed in a tube furnace under a flowing Ar + 5 vol.% H<sub>2</sub> gas mixture. The couple halves are held together in a specially designed steel clamp. This clamp, which keeps the end-members of the couple in intimate contact during annealing, was placed in the hot zone of the horizontal tube furnace. After the diffusion anneal, such a clamp can be rapidly removed from the furnace and immediately quenched in cold water.

### 2.3 Diffusion couple cross-sectioning and analysis

Cross-sections of the diffusion couples were prepared by cutting the couple with a slow-speed saw using a diamond-impregnated blade. The cut parts were imbedded in a conductive resin

and were ground and polished with a final finish of 0.25  $\mu\text{m}$  diamond paste. Sometimes a suspension of  $\text{SiO}_2$  particles in water was used as a final polishing step to obtain a more pronounced appearance of the microstructure. Finally, the samples were cleansed with ethanol and blown dry in hot air.

All samples were inspected by optical microscopy to gain a first impression of reaction layer thicknesses and morphology. Polarised light was used to identify non-cubic phases. In some cases, a solution of 2%  $\text{HNO}_3$  in ethanol was used to etch the polished samples to reveal the formed phases.

Elemental analysis was performed with a Scanning Electron Microscope (SEM, JEOL 840A) equipped with an electron dispersive X-ray (EDX) detector. All micrographs (back-scattered and secondary electron images) were taken with this electron microscope. Linescans for determining concentration profiles across the interaction zone (in atomic fractions) were carried out with Electron Probe Microanalyser (EPMA, JEOL JXA 8600 Superprobe) using an EDX detector.

**References**

1. G.J. van Gorp, W.F. van der Weg and D. Sigurd, *J. Appl. Phys.* **49** (1978) 4011.
2. Ya. E. Geguzin and M.A. Krivoglaz, Migration of macroscopic inclusions in solids, Consultants Bureau, New York-London (1973) pp. 200-206.
3. W.J.J. Wakelkamp, Diffusion and phase relations in the systems Ti-Si-C and Ti-Si-N. Ph.D. thesis, Eindhoven, The Netherlands, (1991).

## Chapter 3

### Diffusion in solids<sup>1</sup>

#### 3.1 Interdiffusion: Matano-Boltzmann analysis

Many reactions and processes that are important in material technology rely on the transfer of mass from one solid to the other. The process, whereby atoms of one solid material diffuse into the other allowing a new concentration profile to be set up, is called *interdiffusion*. The best way to demonstrate a diffusion process in solids is perhaps with the use of a *diffusion couple* (see Chapter 2). As an example, Fig. 3.1 shows the molar fraction of Ni  $N_{\text{Ni}}$  as a function of the diffusion parameter  $x$  corresponding to a Ni/Pd diffusion couple after heat treatment at 1100°C for 196 h.

A one-dimensional interdiffusion process can be described by Fick's first and second law [1]:

$$\tilde{J}_i = -\tilde{D} \frac{dC_i}{dx}, \quad (3.1)$$

$$\frac{dC_i}{dt} = \frac{d}{dx} \left[ \tilde{D} \frac{dC_i}{dx} \right], \quad (3.2)$$

---

<sup>1</sup> Part of the experimental results presented in this chapter are published in a paper: M.J.H. van Dal, M.C.L.P. Pleumeekers, A.A. Kodentsov and F.J.J. van Loo, *Acta Mater.* **48** (2000) 385.



where flux  $\tilde{J}_i$  is the amount (moles) of  $i$  atoms going through a certain area per unit of time ( $\text{mol}/\text{m}^2\text{s}$ ),  $\tilde{D}$  is the interdiffusion coefficient ( $\text{m}^2/\text{s}$ ),  $C_i$  is the concentration of component  $i$  ( $\text{mol}/\text{m}^3$ ),  $t$  is the diffusion (or annealing) time (s) and  $x$  is the diffusion parameter (m). The interdiffusion flux  $\tilde{J}_i$  is defined with respect to the volume- or laboratory-fixed frame of reference. Eq. (3.2) is only valid when the total volume of the couple does not change, i.e. the partial molar volumes  $V_A$  and  $V_B$  are constant (see section 3.2).

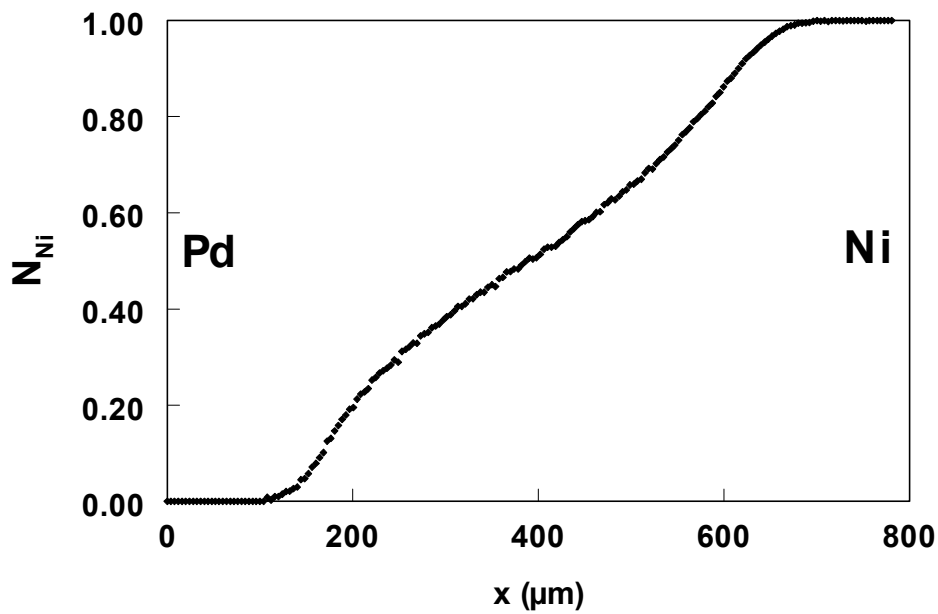


Figure 3.1: Concentration profile of a Ni/Pd diffusion couple annealed at  $1100^\circ\text{C}$  for 196 h.

Matano was the first to apply Fick's equations to determine the concentration-dependent interdiffusion coefficient from a concentration profile [2]. For this purpose he used the solution of Eq. (3.2) given by Boltzmann [3]. Taking the boundary conditions:

$$\begin{aligned} C_i &= C_i^- & x < 0 & \quad t = 0 \\ C_i &= C_i^+ & x > 0 & \quad t = 0 \end{aligned} \tag{3.3}$$

and substituting the so-called Boltzmann variable  $\lambda = x/\sqrt{t}$  in Eq. (3.2), the interdiffusion coefficient  $\tilde{D}$  can be written as:

$$\tilde{D}(C_i^*) = -\frac{1}{2t} \left( \frac{dx}{dC_i} \right)^* \int_{C_i^-}^{C_i^*} x dC_i. \quad (3.4)$$

In accordance with the boundary conditions (3.3), the integral term  $\int x dC_i$  integrated over the entire concentration range (from  $C_i^-$  to  $C_i^+$ ) should be equal to zero, hence:

$$\int_{C_i^-}^{C_i^+} x dC_i = 0. \quad (3.5)$$

In fact, Eq. (3.5) defines the plane  $x_0 = 0$ , called the *Matano plane*. This interface corresponds to the position of the original contact plane of the diffusion couple in the laboratory-fixed frame of reference if  $V_i$  is constant. The interdiffusion fluxes  $\tilde{J}_i$  can, therefore, be measured with respect to the Matano plane.

Eq. (3.4) and (3.5) can be solved graphically using the concentration curve (Fig. 3.2).

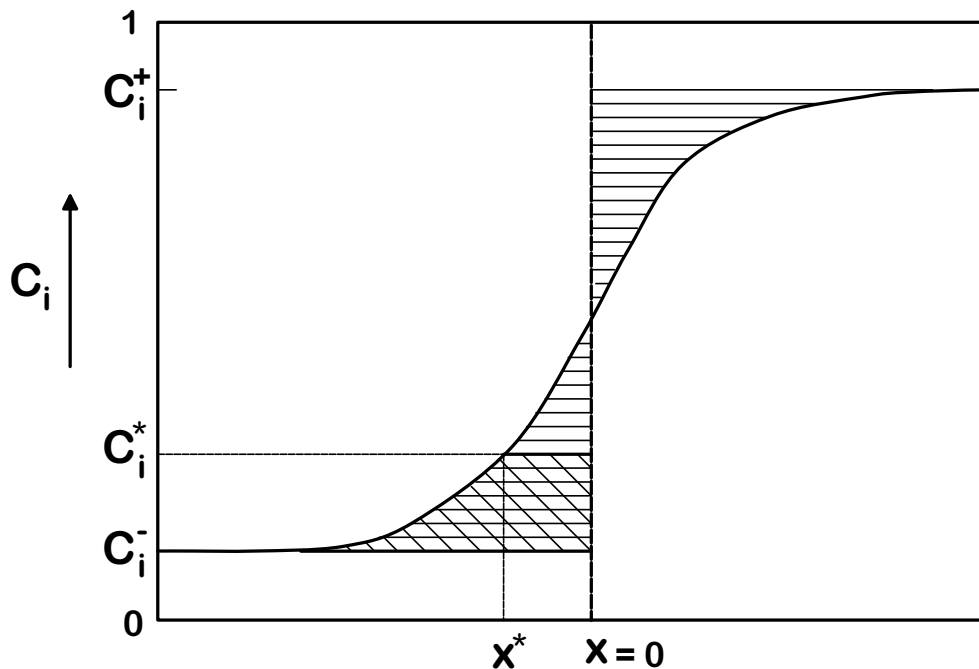


Figure 3.2: Concentration-penetration curve for component  $i$  in a binary diffusion couple between two alloys with starting compositions  $C_i^-$  and  $C_i^+$ , respectively.

The position of the Matano plane is defined in such a way that the hatched areas in Fig. 3.2 are equal. The interdiffusion coefficients are measured with respect to this Matano plane at each position (or concentration) of the concentration profile. The value of the integral in Eq. (3.4) at the position  $x^*$  is given by the double-hatched area in Fig. 3.2; the reciprocal of the concentration gradient has to be taken where  $C_i = C_i^*$ . This analysis is known as the *Matano-Boltzmann analysis*.

### 3.2 Interdiffusion: Sauer-Freise analysis

If the total volume changes during the reaction, the Matano-Boltzmann method can not be applied because Fick's second law (Eq. 3.2) needs a correction term [4]. For instance, for the Ni-Pd system this is the case as can be seen from a plot of the molar volume as a function of composition [5] (Fig. 3.3).

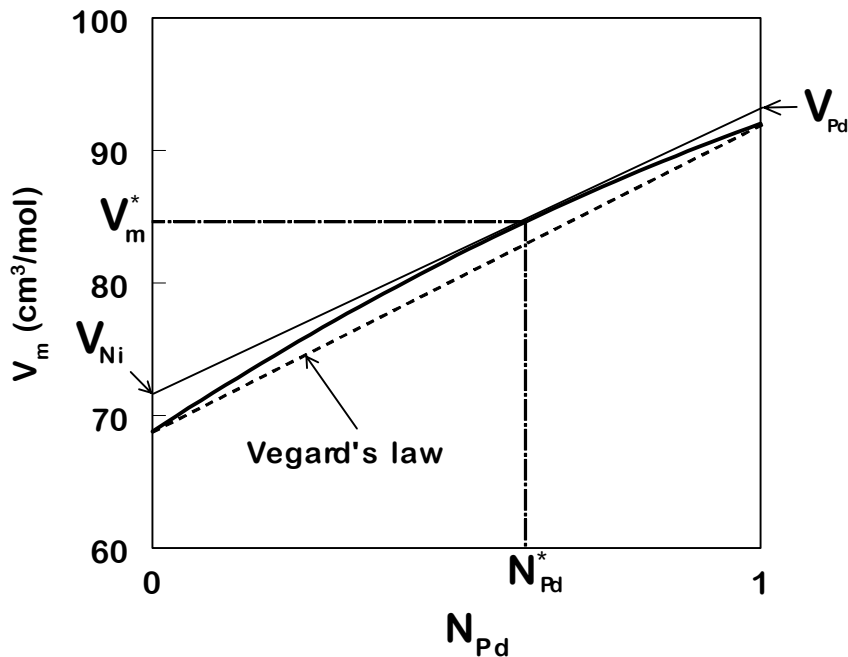


Figure 3.3: Molar volumes of Ni-Pd alloys at 900 °C [5].

The partial molar volumes of Ni and Pd,  $V_{Ni}$  and  $V_{Pd}$ , are related to the molar volume  $V_m$  by:

$$V_m = V_{Ni} N_{Ni} + V_{Pd} N_{Pd} \quad (3.6)$$

and can be obtained graphically at every concentration as the intersections of the tangent with the y-axis at  $N_{Pd} = 0$  and  $N_{Pd} = 1$  (see Fig. 3.3). As one can see the molar volume of the Ni-Pd solid solution exhibits a positive deviation from Vegard's law (corresponding to the dashed line in Fig. 3.3). This means that the Ni/Pd diffusion couple will change its total volume: it will swell as a whole.

In order to incorporate the total volume change, Sauer and Freise [6] derived a new solution for Fick's second law (Eq. (3.2)):

$$\tilde{D}(Y^*) = \frac{V_m}{2t} \left( \frac{dx}{dY} \right)^* \left[ (1 - Y^*) \int_{-\infty}^{x^*} \frac{Y}{V_m} dx + Y^* \int_{x^*}^{+\infty} \frac{1 - Y}{V_m} dx \right] \quad (3.7)$$

where  $Y$  is defined as  $\frac{(N_i - N_i^-)}{(N_i^+ - N_i^-)}$ ;  $N_i$  is the molar fraction of component  $i$ , with  $N_i^-$  and  $N_i^+$  being the mole fraction of component  $i$  at the unreacted left-hand ( $x = -\infty$ ) and right-hand ( $x = +\infty$ ) ends of the couple, respectively. To solve Eq. (3.7), we need to construct two graphs, namely  $Y/V_m$  versus  $x$  and  $(1-Y)/V_m$  versus  $x$ . Fig. 3.4 shows these graphs for the Ni/Pd couple of Figure 3.1.

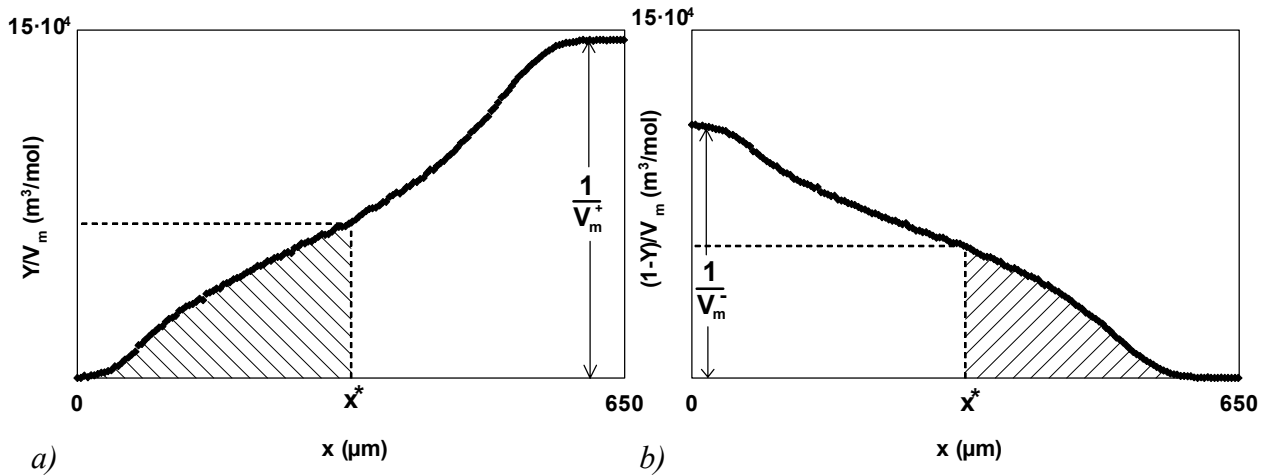


Figure 3.4: Penetration curves of a Ni/Pd diffusion couple (1100 °C; 196 h) constructed according to the Sauer and Freise method.  $Y = (N_{Ni} - N_{Ni}^-)/(N_{Ni}^+ - N_{Ni}^-)$ ;  $V_m^+$  and  $V_m^-$  are the molar volumes of the right-hand and left-hand end-member, respectively, which are in this case equal to the molar volumes of pure Ni and Pd.

The two integrals in Eq. (3.7)  $\int_{-\infty}^{x^*} \frac{Y}{V_m} dx$  and  $\int_{x^*}^{+\infty} \frac{1-Y}{V_m} dx$  correspond to the hatched areas.

In our study on diffusion phenomena in the Ni-Pd system we have made several pure end-member diffusion couples in the temperature range 900-1200°C. The concentration profile of each couple was measured and using the *Sauer-Freise analysis* the interdiffusion coefficients as a function of the mole fraction of Ni at different temperatures were determined (Fig. 3.5). (Note: the maximum of the concentration dependence is situated at 45-50 at.% of Ni).

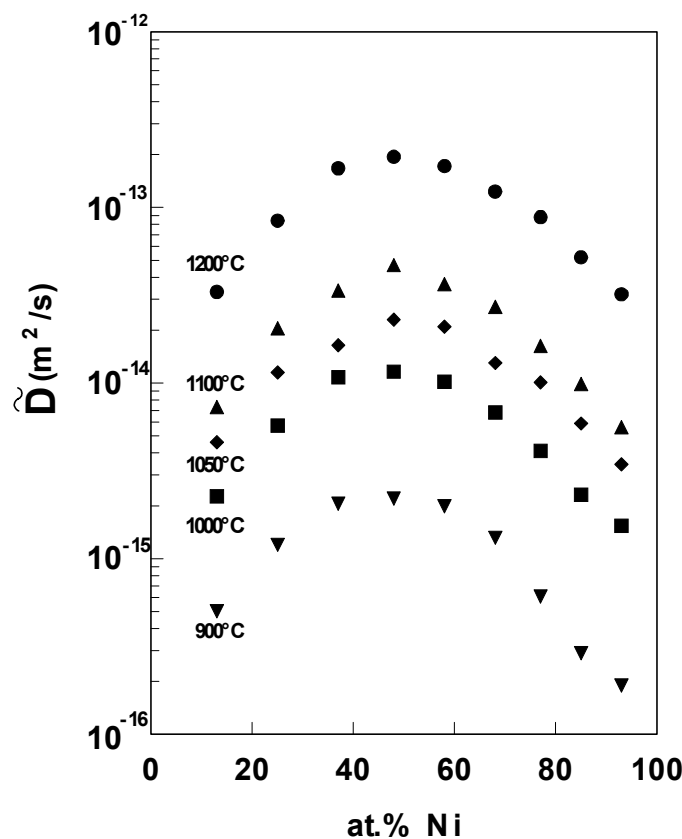


Figure 3.5: Concentration dependence of the interdiffusion coefficient  $\tilde{D}$  in the Ni-Pd system at different temperatures.

Proof that the interdiffusion coefficient found in this way is a material constant, which is only depending on the temperature and concentration, can be found from experiments on incremental diffusion couples. Two alloys were melted, Ni<sub>30</sub>Pd<sub>70</sub> and Ni<sub>70</sub>Pd<sub>30</sub>, and with these alloys four different incremental diffusion couples were annealed at 1100°C taking one pure end-member placed against an alloy end-member.

Again using the Sauer-Freise method the interdiffusion coefficients were determined as function of the mole fraction of Ni (Fig. 3.6). One can see that within the limits of experimental error these values are consistent with those obtained by investigating the diffusion couples with pure Ni and Pd as end-members. In other words, the interdiffusion coefficient is a single-valued function of temperature and composition.

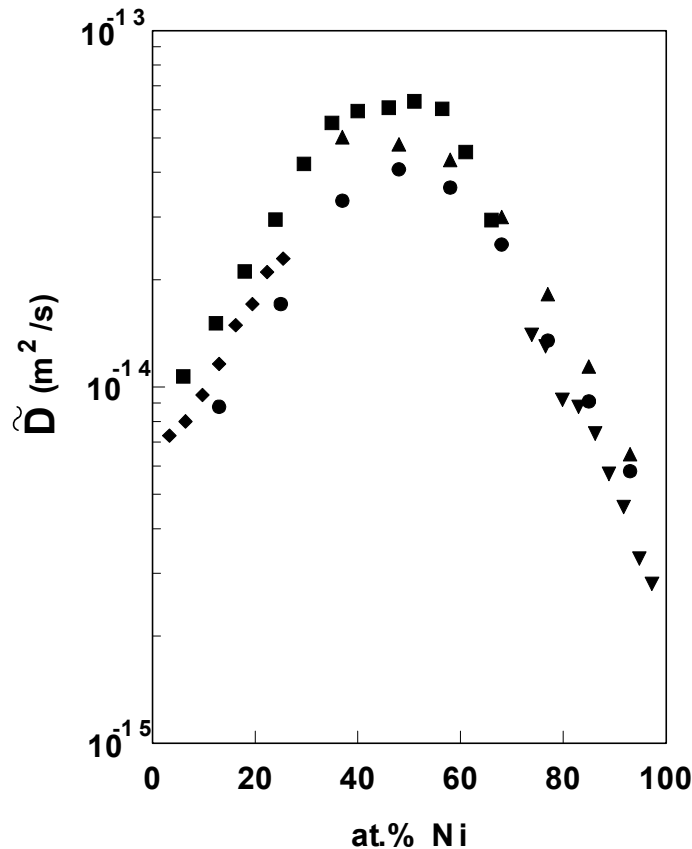


Figure 3.6: Interdiffusion coefficients in the Ni-Pd system at 1100 °C obtained with different diffusion couples: • - Ni/Pd; ▲ - Ni/Ni<sub>30</sub>Pd<sub>70</sub>; ▼ - Ni/Ni<sub>70</sub>Pd<sub>30</sub>; ◆ - Pd/Ni<sub>30</sub>Pd<sub>70</sub>; ■ - Pd/Ni<sub>70</sub>Pd<sub>30</sub>.

### 3.3 Intrinsic diffusion: the Kirkendall effect and the phenomenological approach of Darken

The interdiffusion coefficient as obtained from the concentration profile is only a measure for the intermixing of the species involved: it gives no information on the mobilities of the

individual species. As was proved by Kirkendall's experiment [7] (see Fig. 1.1) and later described by Darken [8], a solid-solid interdiffusion process is the result of two independent component fluxes in opposite directions that need not necessarily be equal.

The inequality of these fluxes leads to a net mass flow accompanying the interdiffusion process, which causes the couple to shrink on one side and to swell on the other side. This process can be made visible by the movement of inert inclusions (markers) present in the interdiffusion zone, which will move towards the fastest diffusing species: *the Kirkendall effect* (Fig. 3.7).

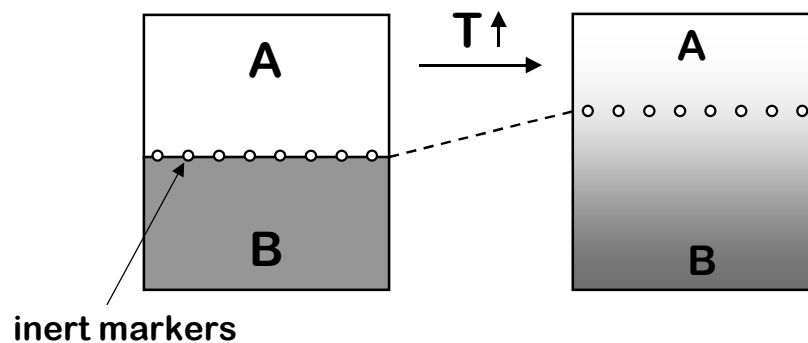


Figure 3.7: Schematic representation of an A/B diffusion couple demonstrating a typical “Kirkendall” experiment. Inert markers are placed at the original contact surface of A and B and after interaction they shifted towards the A-side showing that A is the fastest diffusing species.

The velocity of such inclusions in an A-B binary system, i.e. *the Kirkendall velocity*  $v$ , can thus be expressed as:

$$v = -(V_A J_A + V_B J_B). \quad (3.8)$$

The intrinsic fluxes of A and B,  $J_A$  and  $J_B$ , can be described with Fick's first law:

$$J_A = -D_A \frac{\partial C_A}{\partial x}, \quad (3.9a)$$

$$J_B = -D_B \frac{\partial C_B}{\partial x}, \quad (3.9b)$$

where  $D_i$  is the *intrinsic diffusion coefficient* of component  $i$  ( $\text{m}^2/\text{s}$ ).

Contrary to the interdiffusion flux, these intrinsic diffusion fluxes are defined with respect to inert particles, present (or deliberately introduced) throughout the couple prior to annealing (i.e. a Kirkendall frame of reference). In most cases, however, inert markers are only put at the original contact plane between the initial end-members. The position of these markers after annealing corresponds to the so-called *Kirkendall plane* (see also Fig. 3.7).

Given the fact that  $dC_A = -(V_B / V_A) dC_B$  [9], we can now write for the Kirkendall velocity:

$$v = V_B (D_B - D_A) \frac{\partial C_B}{\partial x}. \quad (3.10)$$

Following Darken's approach [8], the interdiffusion flux  $\tilde{J}$  can be written as the sum of the intrinsic flux  $J_i$  and the Kirkendall drift  $C_i \cdot v$ :

$$\tilde{J} = J_i + C_i \cdot v. \quad (3.11)$$

Substituting Eq. (3.10) in Eq. (3.11), one arrives at a general expression for the interdiffusion coefficient:

$$\tilde{D} = C_B V_B D_A + C_A V_A D_B. \quad (3.12)$$

Eqs. (3.10) and (3.12) are often denoted as the Darken equations and can be regarded as completely descriptive of isothermal linear diffusion in a binary system.

Darken [8] also showed that the inert particles originating from the initial contact surface, corresponding to the Kirkendall plane, move parabolically in time with respect to the laboratory-fixed frame:  $x_K = k\sqrt{t}$  where  $x_K$  is the displacement of the Kirkendall plane (m) and



$k$  is a constant ( $\text{m}\cdot\text{s}^{-1/2}$ ). This is true since the Kirkendall plane is the only marker plane that starts moving from the beginning, i.e. from  $t = 0$  and we are dealing with diffusion-controlled processes. This means that its velocity  $v_K$  is equal to:

$$v_K = dx/dt = x_K/2t. \tag{3.13}$$

From the position of the Kirkendall plane one can deduce information on the intrinsic diffusivities of species. It can be shown that the ratio of intrinsic diffusivities in an A-B diffusion system equals [10]:

$$\frac{D_A}{D_B} = \frac{V_A}{V_B} \left[ \frac{N_A^+ \int_{-\infty}^{x_K} \frac{(N_A - N_A^-)}{V_m} dx - N_A^- \int_{x_K}^{\infty} \frac{(N_A^+ - N_A)}{V_m} dx}{-N_B^+ \int_{-\infty}^{x_K} \frac{(N_A - N_A^-)}{V_m} dx + N_B^- \int_{x_K}^{\infty} \frac{(N_A^+ - N_A)}{V_m} dx} \right] \tag{3.14}$$

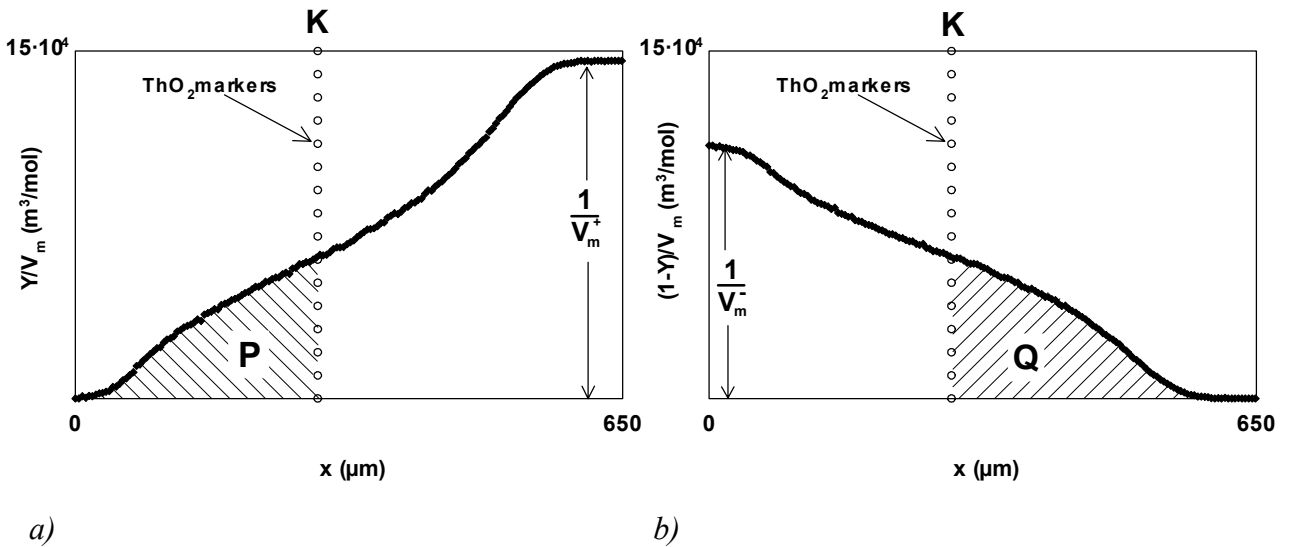


Figure 3.8: Penetration curves of a Ni/Pd diffusion couple ( $1100\text{ }^\circ\text{C}$ ;  $196\text{ h}$ ) constructed according to the Sauer and Freise method.  $Y = (N_{Ni} - N_{Ni}^-)/(N_{Ni}^+ - N_{Ni}^-)$ ;  $V_m^+$  and  $V_m^-$  are the molar volumes of Ni and Pd, respectively.  $\text{ThO}_2$  particles mark the Kirkendall plane K.

In the case of the Ni/Pd couple, we have used  $\text{ThO}_2$  particles to mark the original contact surface between the two end-members (see Chapter 2). These markers were easily traced in the cross-section of the diffusion couple after interaction. The position of the Kirkendall plane

can now be transferred on the concentration profile. Eq. (3.14) simplifies for the pure end-member Ni/Pd diffusion couple ( $N_{\text{Ni}}^+ = 1$  and  $N_{\text{Ni}}^- = 0$ ) into:

$$\frac{D_{\text{Ni}}}{D_{\text{Pd}}} = \frac{V_{\text{Ni}}}{V_{\text{Pd}}} \cdot \frac{P}{Q}, \quad (3.15)$$

where  $P$  and  $Q$  correspond to the hatched areas in Fig. 3.8. Together with Eq. (3.12), the intrinsic diffusion coefficient of Ni and Pd can be obtained at the concentration corresponding to the Kirkendall plane:  $D_{\text{Ni}}(N_{\text{Ni}} = 40.3 \text{ at.}\%) = 4.9 \cdot 10^{-14} \text{ m}^2/\text{s}$  and  $D_{\text{Pd}}(N_{\text{Ni}} = 40.3 \text{ at.}\%) = 6.5 \cdot 10^{-14} \text{ m}^2/\text{s}$ .

### 3.4 Experimental determination of the Kirkendall velocity: the multi-foil technique

The intrinsic diffusion coefficients of species over the entire concentration range can be found when the interdiffusion coefficients and the Kirkendall velocity are known as a function of concentration. We have already shown that the interdiffusion coefficient can be determined from the concentration profile by applying the Sauer-Freise method. Knowledge of the net mass flow accompanying the interdiffusion process, i.e. the velocity of inert markers described by Eq. (3.12), can be obtained experimentally with the “multi-foil diffusion couple technique”.

The “multi-foil” technique for studying interdiffusion phenomena has been introduced by Heumann and Walther [11]. The characteristic feature of a “multi-foil” sample is that each end-member of the diffusion couple is composed of several foils with fiducial markers in between. The total number of foils within the end-members and their thickness may vary depending on the interaction rate in the material system at the temperature of interest. Interdiffusion in such a multi-layered system will cause the markers to move relative to a laboratory-fixed frame of reference with the Kirkendall velocity  $v$  (m/s) (Eq. 3.10).

By measuring the shift of the markers, the “Kirkendall displacement” can be determined over the entire diffusion zone and, subsequently, a displacement curve can be constructed (Fig. 3.9). It should be mentioned here that the maximum of this  $y-x_0$  plot need not be at the

Kirkendall plane defined by  $x_0 = 0$ ; also the appearance of the plot can be different (see Chapter 4).

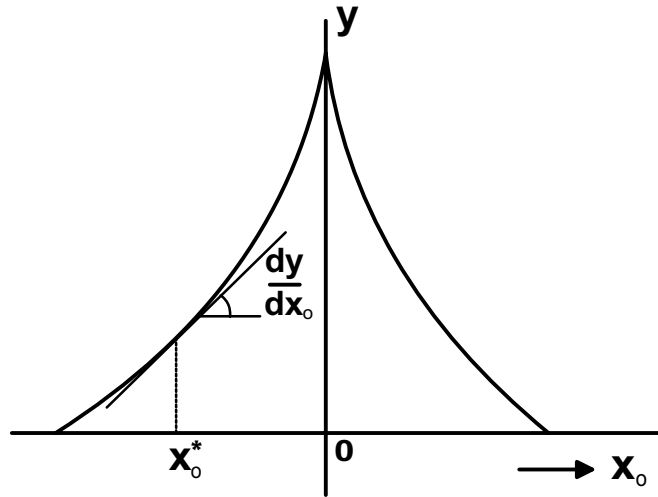


Figure 3.9: Schematic representation of marker displacement,  $y$ , vs. their original position  $x_0$  in a multi-foil diffusion couple.

Levasseur and Philibert [12] proposed a method to obtain the Kirkendall velocity from the displacement curve. Later, this analysis was developed further due mainly to the work of Cornet *et al.* [13,14] and of van Loo *et al.* [15]. The Kirkendall velocity can be found as:

$$v = \frac{1}{2t} \left( y - x_0 \cdot \frac{dy}{dx_0} \right) \quad (3.16)$$

with  $x_0$  being the original location of the markers and  $y$  the displacement of the markers relative to  $x_0$ , hence,  $x_0 = x - y(x)$ . Indeed, for the special case that  $x_0 = 0$  (i.e. the Kirkendall plane) Eq. (3.16) transforms into  $v = y/2t$  (Eq. 3.13).

We employed the multi-foil technique for the Ni-Pd system. Twenty foils (20  $\mu\text{m}$  thick) of Pd and nineteen foils (21  $\mu\text{m}$  thick) of Ni were pressed together between the plan-parallel slices ( $\approx 1.0$  mm thick) of pure metals.  $\text{ThO}_2$ -particles ( $\approx 0.5\text{-}5$   $\mu\text{m}$ ) were used as fiducial markers between the foils. The couple was annealed at  $1100^\circ\text{C}$  for 121 h. Fig. 3.10 shows a cross-section of the couple after the heat treatment. The  $\text{ThO}_2$ -markers are clearly visible as straight rows of inclusions exhibiting a “white” contrast in the back-scattered electron micrograph.

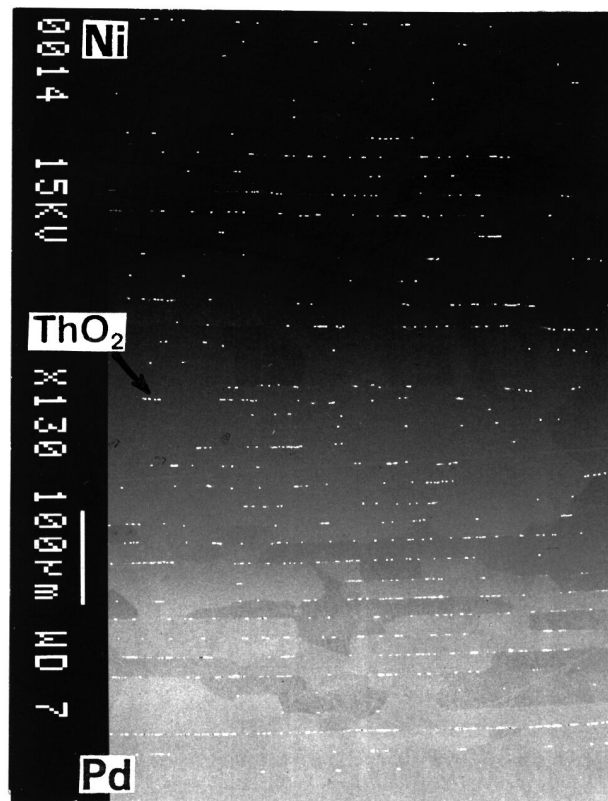
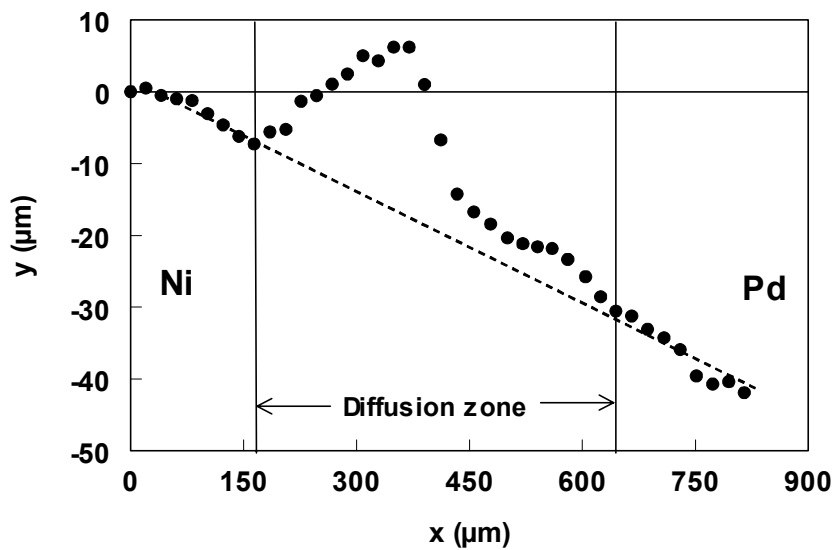


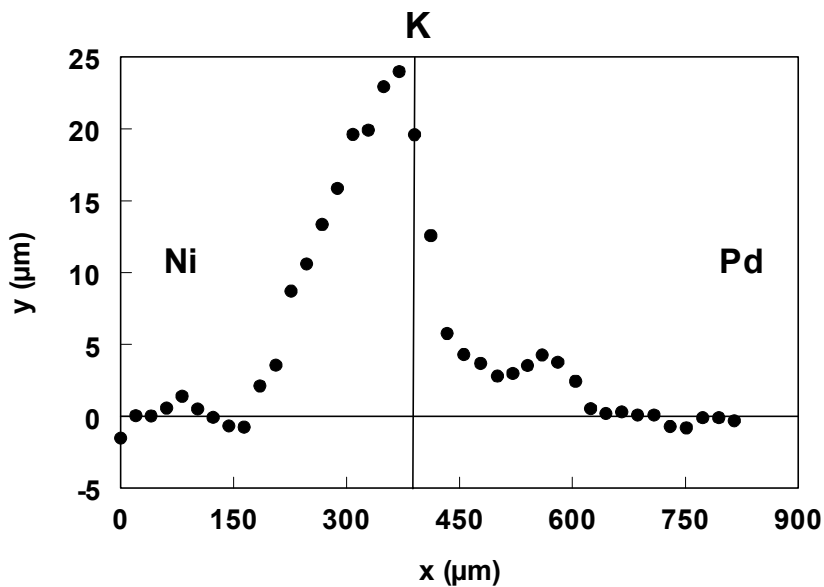
Figure 3.10: Back-scattered electron image of a Ni/Pd multi-foil diffusion couple annealed at 1100°C for 121 h in vacuum. The rows of ThO<sub>2</sub>-particles used as fiducial markers correspond to the interfaces between the initial foils. Note that no pore formation occurred after the heat treatment.

From the concentration profile measured across the interaction zone, the interdiffusion coefficients for various compositions of the Ni-Pd solid solution at 1100°C were computed using the Sauer-Freize method. As was expected, the results are compatible with the values found by analysing the incremental couples and the couples with the pure metals as end-members. This means that the initial foil interfaces and the ThO<sub>2</sub>-particles present across the diffusion zone do not interfere with the overall diffusion process.

The displacement of markers within the diffusion zone was calculated taking the first “marked” plane at the pure Ni-side of the couple as a reference (Fig. 3.10). The original marker positions were determined using the average values of the foil thicknesses (nickel or palladium) in the parts of the couple where no interdiffusion has taken place yet after annealing at this temperature for 9 h.



a)



b)

Figure 3.11: Displacement curves ( $y(x)$ ) a) determined experimentally and b) corrected for plastic deformation for a Ni/Pd multi-foil diffusion couple annealed at  $1100^\circ\text{C}$  for 121 h (K indicates the Kirkendall plane).

It turned out that the markers located outside the interdiffusion zone are also shifted. Obviously, this is a direct outcome of the sample deformation (creep) caused by the pressure applied during the joining and annealing. To take into account the possible effect of plastic deformation and determine the genuine Kirkendall displacement, a correction procedure similar to that proposed by Heumann and Grundhoff [16] was used. The approach is quite

simple. As a first approximation, the deformation rate of the end-members of the couple is assumed to be equal and constant. In such a case the line in Fig. 3.11a connecting marker position inside the “unreacted” parts of the couple, i.e. outside the interdiffusion zone, represents the displacement of the markers resulting from the plastic deformation.

The difference between the apparent marker displacement and the value corresponding to this “baseline” (dashed line in Fig. 3.11a) gives the actual Kirkendall shift. In this manner the displacement curve shown in Fig. 3.11b was constructed. The maximum of the displacement, which is situated in the vicinity of the Kirkendall plane, was found to be  $24 \pm 2 \mu\text{m}$ .

The displacement curve was subsequently plotted versus  $x_0$  (which is equal to  $x - y(x)$ ) and using the analysis shown in Fig. 3.9 the Kirkendall velocity  $v$  as a function of  $x$  was determined (Fig. 3.12). In fact, Fig. 3.12 displays the mass flow accompanying the interdiffusion process in the Ni/Pd couple arising from the inequality of the fluxes of Ni and Pd atoms. It can be seen that the velocity of the markers has a positive value, indicating that Pd is the fastest diffusing component over the composition range studied. Later, we will discuss such Kirkendall velocity curves more thoroughly.

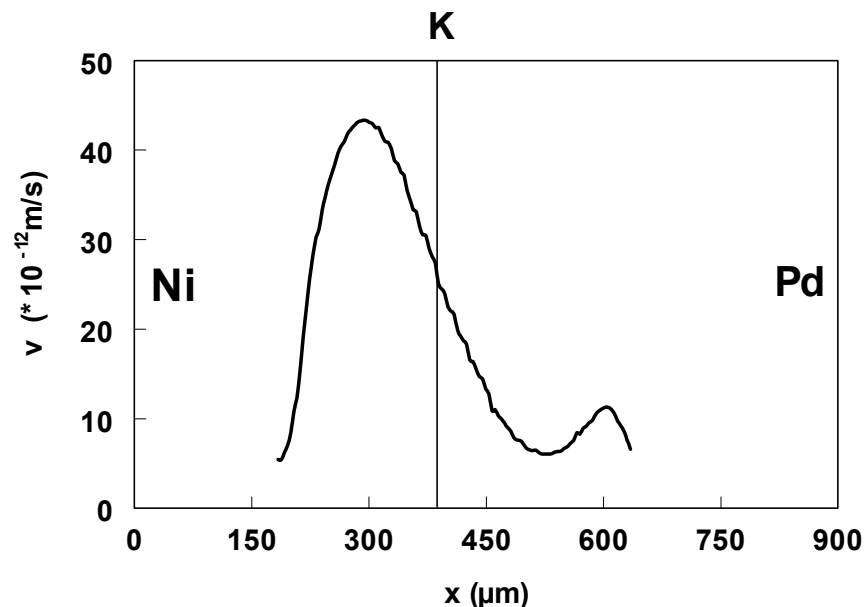


Figure 3.12: Marker (or Kirkendall) velocity curve in the Ni/Pd multi-foil diffusion couple annealed at  $1100^\circ\text{C}$  for 121 h calculated using experimental data of the present study (K indicates the Kirkendall plane).

Combining Eq. (3.10) and (3.12), one can obtain an expression for the ratio of the intrinsic diffusion coefficients [15]:

$$\frac{D_A}{D_B} = \frac{1 + Q C_A}{1 - Q C_B (V_B / V_A)} \quad (3.17a)$$

with

$$Q = \frac{v}{\tilde{D} \cdot (dC_A / dx)} \quad (3.17b)$$

Knowing the interdiffusion coefficient  $\tilde{D}$  and the Kirkendall velocity  $v$ , the intrinsic diffusivities can be calculated with Eq. (3.12) and (3.17). The intrinsic diffusion coefficients of Ni and Pd as a function of the molar fraction of Ni are presented graphically in Fig. 3.13.

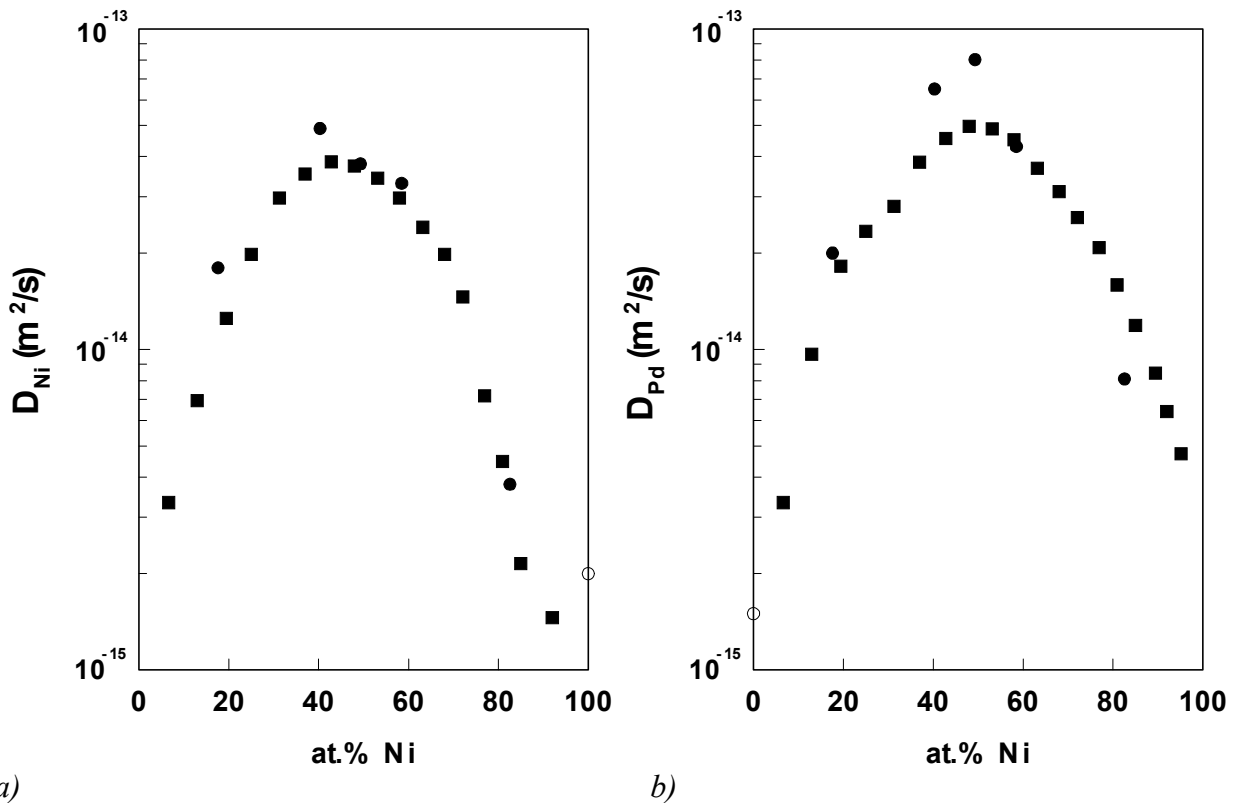


Figure 3.13: Intrinsic diffusion coefficients a) of nickel,  $D_{Ni}$ , and b) of palladium,  $D_{Pd}$ , in the Ni-Pd alloys at 1100 °C obtained with pure end-member and incremental couples (●) and derived from the multi-foil experiment (■). The values for self-diffusion coefficient of nickel [17] and palladium [18] are given for comparison (○).

As comparison, the intrinsic diffusivities, which were determined from the pure end-member and the incremental diffusion couples, are included. These values were obtained at the position of the Kirkendall plane using Eqs. (3.12) and (3.14). One can see that the data are compatible. As a conclusion one can say that the present analysis provides means to determine intrinsic diffusion coefficients in a binary metallic system over the whole concentration range from, in principle, one single experiment.

### 3.5 Thermodynamic factor and tracer diffusion coefficient

From a fundamental point of view, the concentration gradient as the driving force for diffusion as given by Fick's laws (Eqs. (3.1) and (3.2)) is not correct. Instead, the difference in chemical potential is the real driving force for diffusion. Thus, the flux of a component A in, for instance, an A-B binary alloy should be written in terms of gradient in chemical potential  $\mu$  [19]:

$$J_A = -B_A C_A \frac{\partial \mu_A}{\partial x}, \quad (3.18)$$

where  $B_A$  is called the atomic mobility of A. The chemical potential of A  $\mu_A$  can be written in terms of activity,  $a_A$ :

$$\mu_A = \mu_A^\theta + RT \ln a_A, \quad (3.19)$$

where  $\mu_A^\theta$  is the standard chemical potential ( $T = 298$  K;  $p^\theta = 1$  bar) in J/mol and R is the gas constant (8.3143 J/molK). Substituting Eq. (3.19) in Eq. (3.18) and knowing that  $dN_A = (V_m^2 / V_B) dC_A$  [9] and  $C_A = N_A / V_m$  one can obtain:

$$J_A = -B_A RT \frac{V_m}{V_B} \left( \frac{\partial \ln a_A}{\partial \ln N_A} \right) \frac{dC_A}{dx}, \quad (3.20)$$



with  $\frac{d \ln a_A}{d \ln N_A} = \frac{d \ln a_B}{d \ln N_B}$  being the *thermodynamic factor* ( $a_A$  and  $a_B$  are the chemical activities of components with pure elements A and B under the experimental conditions as the reference state).

The mobility of A,  $B_A$ , can be experimentally determined from a tracer experiment. If one deposits an “infinitely” thin layer of a radioactive isotope of A on the surface of an homogeneous A-B alloy, the activity as a function of the distance in the diffusion direction after annealing can be measured using the sectioning technique. By applying the method of Gruzin [20], in which it is assumed that the atoms A and isotopes  $A^*$  move identically, a so-called *tracer diffusion coefficient*  $D_A^*$  can be derived. The tracer diffusion coefficient is directly connected to the atomic mobility by the Nernst-Einstein relation:

$$D_i^* = B_i RT . \quad (3.21)$$

More details of this technique can be found elsewhere (see for instance [21]).

When we now take Eq. (3.9a), (3.20) and (3.21), we arrive at a general relation between the intrinsic and tracer diffusion coefficients:

$$D_A = D_A^* \frac{V_m}{V_B} \left( \frac{\partial \ln a_A}{\partial \ln N_A} \right). \quad (3.22)$$

If the pertinent thermodynamic data are available, Eq. (3.22) allows the calculation of intrinsic diffusivities from tracer diffusion coefficients.

Often a so-called vacancy wind factor  $W$  is added to Eq. (3.22) introduced by Manning [22]. According to Manning’s atomistic approach, the vacancy wind effect stems from the fact that the interdiffusion in solids is mediated by a vacancy mechanism. The faster moving atoms during an interdiffusion process will be enhanced by the “vacancy wind” directed in the opposite way and the Kirkendall shift will be higher. However, the effect is relatively small in

the binary systems investigated (within the limits of error) and thus not discussed here. For more information the reader is referred to Refs. [21,22].

Unfortunately, there are no tracer diffusion data available for the Ni-Pd system. However, we also have performed an extensive study on diffusion phenomena in the completely miscible Fe-Pd system at 1100°C. For this system, thermodynamic data on the binary solid solution and tracer diffusivities for the entire concentration range of Fe-Pd alloys are available at the temperature of interest. This gives an ideal opportunity to test the validity of the diffusion equations as discussed up to now.

Thermodynamic activities of iron in Fe-Pd alloys were determined from oxidation experiments at 1200-1400°C by Aukrust and Muan [23]. Later, Alcock and Kubic [24] performed a comprehensive study of the thermodynamic properties of Fe-Pd solid solutions over the temperature range 700-1000°C using the EMF-method. It is interesting to mention some peculiarities in the thermodynamic behaviour of the Fe-Pd system in this temperature range. Iron-rich solid solutions exhibit positive deviations from Raoultian behaviour for the activity of iron and negative deviation for the activity of the palladium. Palladium-rich solid solutions, on the other hand, exhibit negative deviations from Raoult's law for the activity of both elements.

By extrapolating the reported EMF-values to 1100°C [24] and correcting for the non-stoichiometry of wüstite [25] used as an electrode material, the activities of iron in the Fe-Pd alloys were derived. The thermodynamic factor at this temperature was calculated for various compositions (Fig. 3.14).

Tracer diffusion coefficients in the Fe-Pd system at 1100-1250°C were measured by Fillion and Calais [18]. Using the data at 1100°C and values of the thermodynamic factor, the corresponding intrinsic coefficients for Fe and Pd were computed with Eq. (3.22).

The intrinsic diffusivities of the components in the Fe-Pd solid solution at 1100°C were also obtained from the "multi-foil" couple experiment. To this end, twenty-four foils of Pd (20 µm) and eight foils of Fe (25 µm) were pressed together between the slices of pure end-members and annealed in vacuum. Again, ThO<sub>2</sub>-particles were used as inert markers.

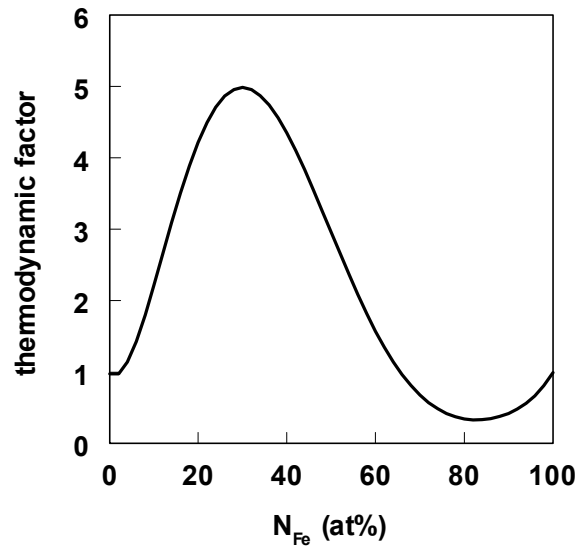


Figure 3.14: Concentration dependence of the thermodynamic factor for diffusion in the Fe-Pd alloys at 1100 °C calculated according data of Alcock and Kubic [24] extrapolated to 1100 °C and correcting for the non-stoichiometry of wüstite [25].

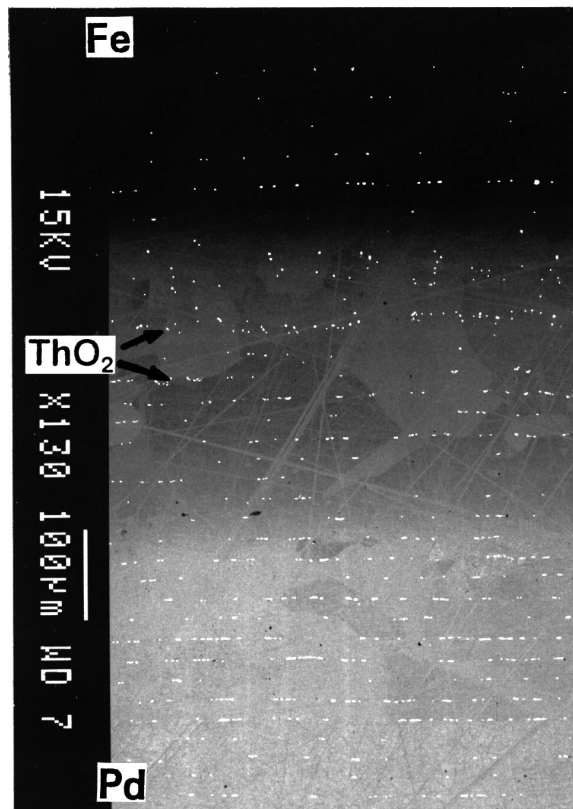


Figure 3.15: Back-scattered electron image of an Fe/Pd multi-foil diffusion couple annealed at 1100 °C for 144 h in vacuum. The rows of  $\text{ThO}_2$ -particles used as fiducial markers correspond to the interfaces between the initial foils. Note: the marker planes near the Kirkendall plane are scattered.

At this point it has to be mentioned that we found peculiar behaviour of the Fe/Pd diffusion couple with respect to the Kirkendall effect. Fig. 3.15 shows the cross-section of the Fe/Pd multi-foil couple after interaction at 1100°C for 144 h. If one looks carefully at the appearance of the markers near the Kirkendall plane and compares this with the Ni/Pd multi-foil couple (Fig. 3.10) one sees that the markers are much more scattered across the interaction zone. We will come back to this observation later on, as it is one of the most important findings of the present work.

The displacement of the individual marker planes was determined as accurate as possible and using the procedure described above, the intrinsic diffusion coefficients of Fe and Pd were determined. The results are presented in Fig. 3.16 along with the values calculated from the tracer diffusivities of the species and thermodynamic data. Within the limits of experimental error, one can see excellent agreement between the two sets of data.

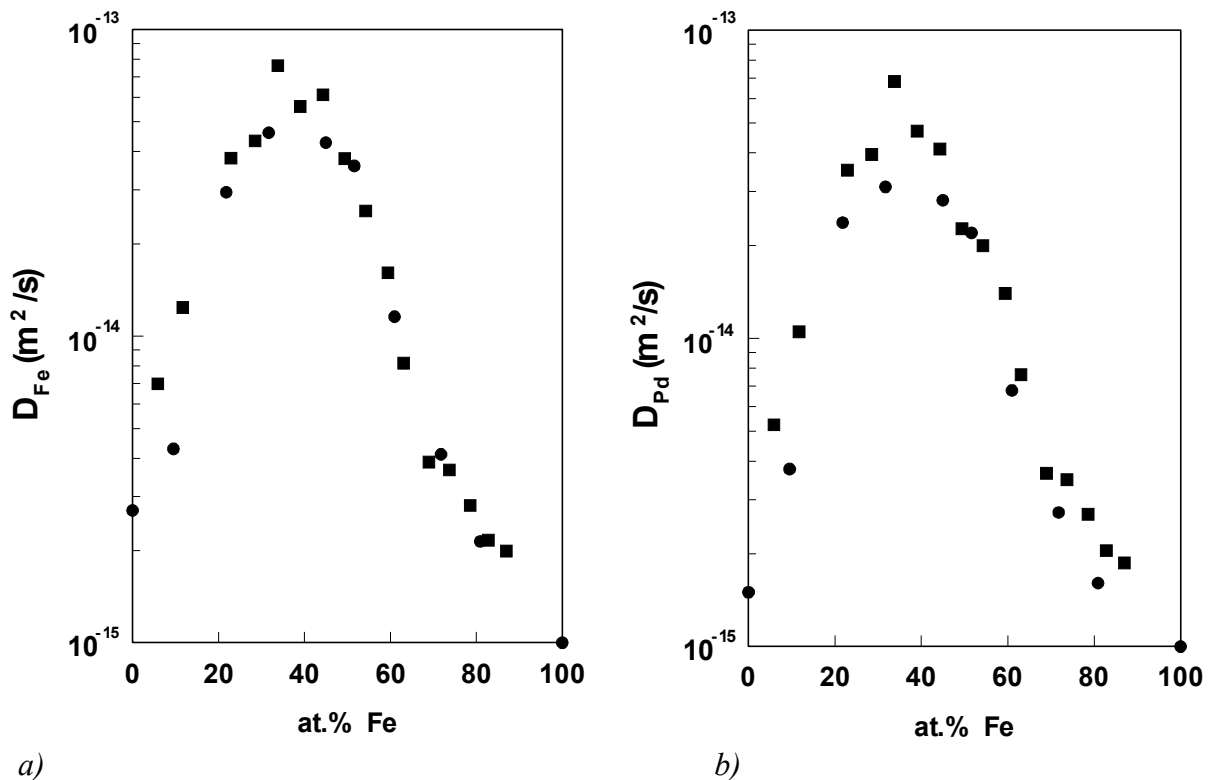


Figure 3.16: Intrinsic diffusion coefficient a) of iron,  $D_{Fe}$ , and b) of palladium,  $D_{Pd}$ , in the Fe-Pd solid solution at 1100 °C: ■ - determined experimentally using the multi-foil technique; ● - calculated using data of Refs. [18, 23-25].

### 3.6 Relationship between the phase diagram and the interdiffusion behaviour in solid single-phase binary systems

In this section we will look at the relationship between the phase diagrams, governed by the thermodynamics of the system, and the interdiffusion behaviour. Four systems exhibiting a certain region of mutual solubility have been investigated: the Ni-Pd, Fe-Pd, Cu-Pd and Au-Ni system.

The first one is the Ni-Pd binary system [5] (Fig. 3.17). One can see a complete solid solubility over the entire concentration range even down to room temperature. The interesting feature of this system is the minimum in melting temperature ( $1237^{\circ}\text{C}$ ) at 45.4 at.% of Pd. It has been postulated by Vignes and Birchenall [26] that the interdiffusion behaviour of alloys is related to the melting point. In the proximity of the temperature of the solidus the amount of thermal vacancies increases, resulting in the enhancement of the atomic mobilities. Indeed, the maximum of the concentration dependence coincides (within experimental accuracy) with the minimum on the liquidus of the binary Ni-Pd system (at 45-50 at.% of Ni) (Fig. 3.5).

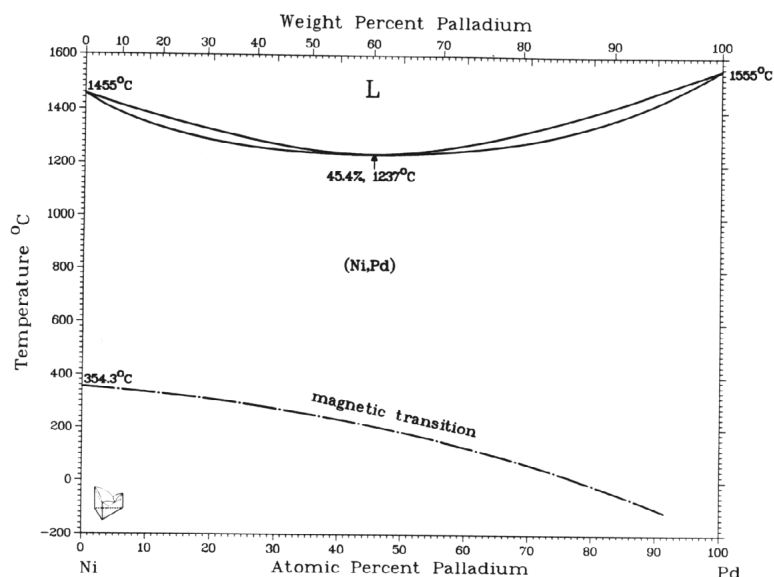


Figure 3.17: Binary Ni-Pd phase diagram [5].

Fig. 3.18a shows the binary phase diagram of the Fe-Pd system [27]. As is in the Ni-Pd system, a minimum in the solidus and liquidus exists at the equiatomic composition.

However, at lower temperature Fe-Pd alloys exhibit a tendency towards ordering which is manifested by the formation of the intermetallic phases with compositions around FePd and FePd<sub>3</sub>. This effect is probably responsible for the experimental observation that the maximum in the interdiffusion rates in the Fe-Pd system was found at approximately 30-35 at.% of iron (Fig. 3.18b).

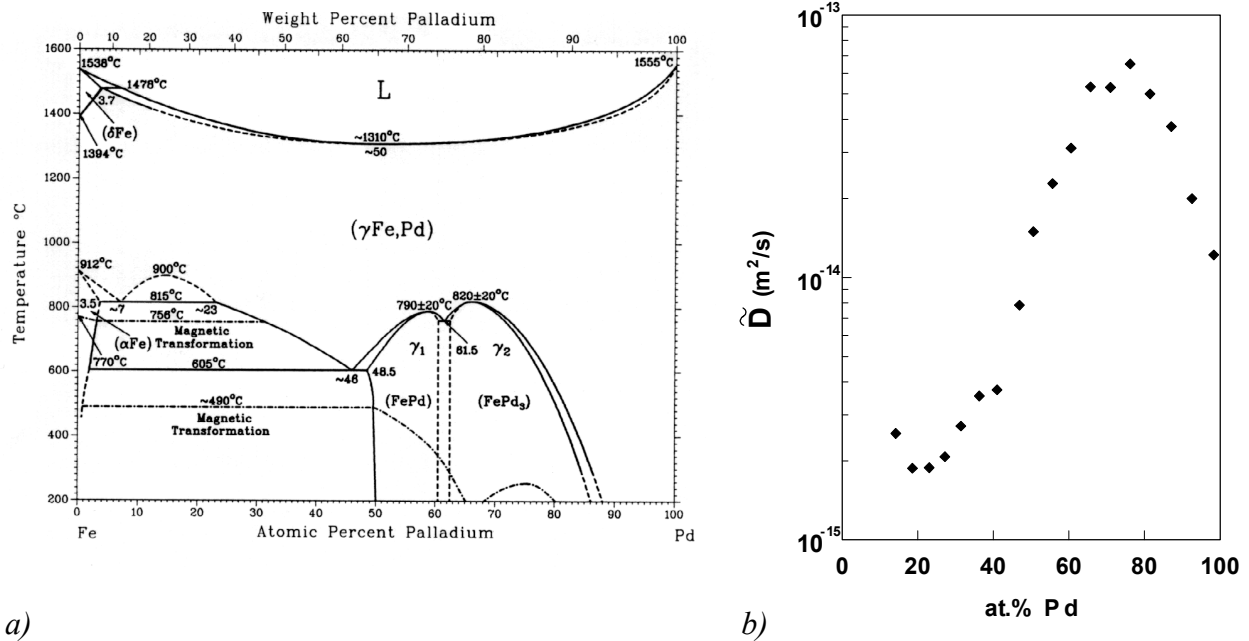


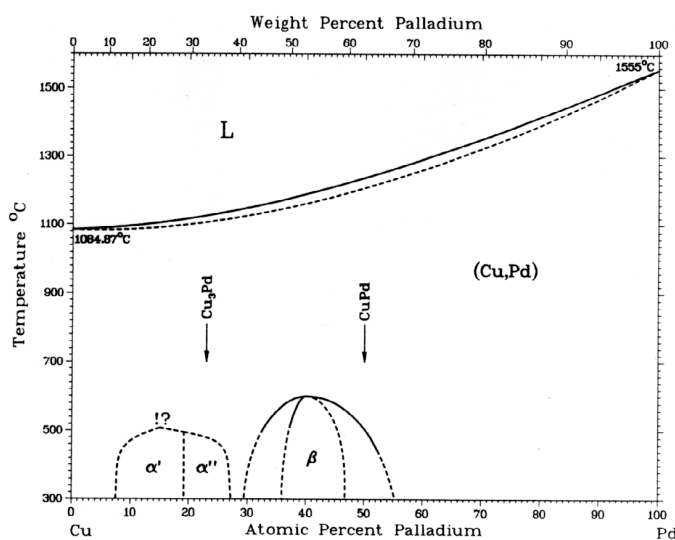
Figure 3.18: a) The binary Fe-Pd phase diagram [27] and b) concentration dependence of the interdiffusion coefficient in Fe-Pd alloys at 1100 °C obtained with the Matano-Boltzmann analysis.

This is quite far from the position of the minimum on the liquidus curve on the Fe-Pd phase diagram [27] (which is at about 50 at.% of Fe). The maximum of the concentration dependence of *intrinsic* diffusivities in the Fe-Pd alloys is also located near the Fe-content of about 30-35% (Fig. 3.16). However, the tracer diffusion coefficient as a function of concentration of the solid solution was reported to have a maximum [18] close to the equiatomic composition, which is in accordance with the minimum in the phase diagram. The appearance of the maximum on the interdiffusion coefficient vs. composition curve at 1100 °C can not be explained solely in terms of the proximity of the melting point. It is clear that the tendency towards ordering contributes (in terms of the thermodynamic factor) to the

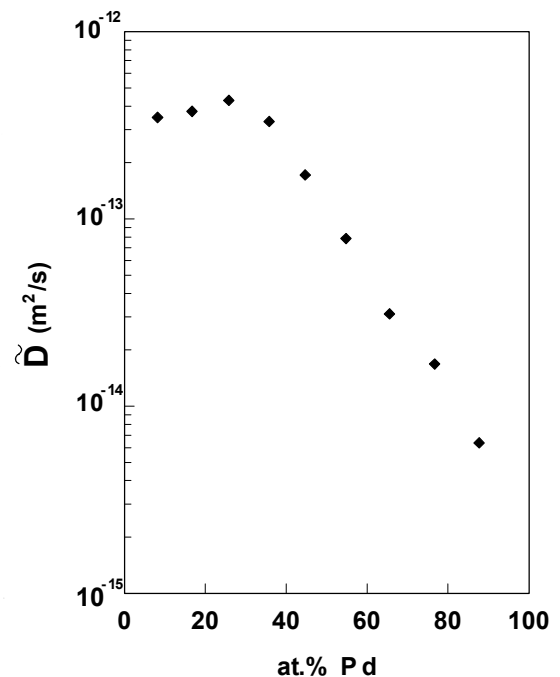
overall interdiffusion process; this does not affect the tracer diffusion coefficient but it enhances intrinsic diffusion (see Fig. 3.14 and Eq. 3.22).

A similar observation was encountered in the Cu-Pd system (Fig. 3.19a). As in the Fe-Pd phase diagram, the formation of intermetallics at lower temperature ( $\text{Cu}_3\text{Pd}$  and  $\text{CuPd}$ ) points out a tendency towards ordering in solid solutions above the decomposition temperatures (around  $600^\circ\text{C}$ ) [27].

There is no minimum melting temperature of the Cu-Pd alloys. Fig. 3.19b shows the interdiffusion coefficients as a function of mole fraction determined from the penetration plots of a diffusion couple annealed at  $1050^\circ\text{C}$  for 48 h. The maximum of the interdiffusion coefficient was found at approximately 20 at.% of Cu. Again, the proximity of the alloy composition to the melting temperature and the tendency of the alloy towards ordering both influence the interdiffusion behaviour.



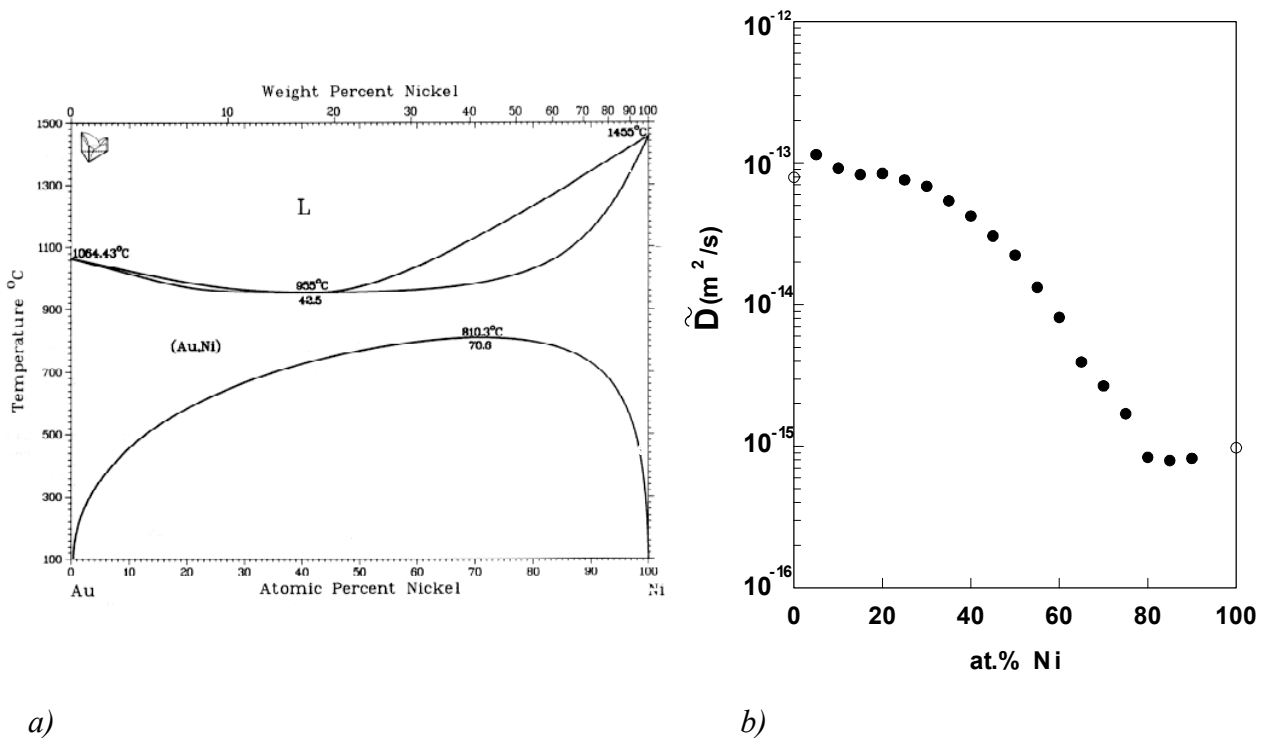
a)



b)

Figure 3.19: a) The binary Cu-Pd phase diagram [27] and b) concentration dependence of the interdiffusion coefficient in Cu-Pd alloys at  $1050^\circ\text{C}$  obtained from a Cu/Pd diffusion couple annealed for 48 h at  $1050^\circ\text{C}$  using the Matano-Boltzmann analysis.

The last system studied in this respect is the Au-Ni system<sup>2</sup> [27] (Fig. 3.20a). The composition dependencies of inter- and intrinsic diffusivities for temperatures above the critical point of the binodal curve on the Au-Ni phase diagram ( $T > 810.3^\circ\text{C}$ ) (Fig. 3.20b), show a reversal near the high Ni-end with a minimum at about 80-85 at.% of nickel. This is thought to result from the fact that thermodynamic driving force for diffusion goes to zero. This leads to low interdiffusion in the Au-Ni solid solution in the vicinity of the corresponding composition range. However, it is to be emphasised that the minimum in the interdiffusion rate found in this alloy system does not exactly coincide with the maximum on the miscibility curve ( $\sim 70.6$  at.% of Ni). In the proximity of the melting point minimum, the amount of thermal vacancies increases which results in an enhancement of the atomic mobilities. The interplay between these two effects explains why the minimum of the interdiffusion rate is found at a composition richer in Ni than the maximum of the miscibility gap.



a)

b)

Figure 3.20: a) The binary Au-Ni phase diagram, and b) concentration dependence of the interdiffusion coefficient  $\tilde{D}$  in the Au-Ni system at  $900^\circ\text{C}$ . The open symbols correspond to the self-diffusion of Ni in Au and vice versa taken from [28,29].

<sup>2</sup> The results of the study on intrinsic diffusion and the Kirkendall effect in the Au-Ni system are published in a paper:

M.J.H. van Dal, M.C.L.P. Pleumeekers, A.A. Kodentsov and F.J.J. van Loo, *J. Alloys Comp.* **309** (2000) 132.



**References**

1. A. Fick, *Pogg. Ann.* **94** (1855) 59.
2. C. Matano, *J. Phys. Japan* **8** (1933) 109.
3. L. Boltzmann, *Ann. Physik* **53** (1894) 959.
4. F.J.J. van Loo, *Acta Met.* **18** (1970) 1107.
5. A. Nash and P. Nash, *Bulletin Alloy Phase Diagrams* **5** (1984) 446.
6. F. Sauer and V. Freise, *Z. Elektrochem.* **66** (1962) 353.
7. A.D. Smigelskas and E.O. Kirkendall, *Trans. AIME* **171** (1947) 130.
8. L.S. Darken, *Trans. AIME* **175** (1948) 184.
9. L.E. Trimble, D. Finn and A. Cosgarea Jr., *Acta Met.* **13** (1965) 501.
10. F.J.J. van Loo, *Prog. Solid St. Chem.* **20** (1990) 47.
11. Th. Heumann and G. Walther, *Z. Metallkde.* **48** (1957) 151.
12. J. Levasseur and J. Philibert, *Phys. Status Solidi* **21** (1967) K1.
13. J.-F. Cornet and D. Calais, *J. Phys. Chem. Solids* **33** (1972) 1675.
14. J.-F. Cornet, *J. Phys. Chem. Solids* **35** (1974) 1247.
15. F.J.J. van Loo, G.F. Bastin and G.D. Rieck, *Sci. Sintering* **11** (1979) 9.
16. Th. Heumann and K.J. Grundhoff, *Z. Metallkde.* **63** (1972) 173.
17. H. Mehrer, Ed., Landolt-Börnstein: Diffusion in Solid Metals and Alloys. **Vol. 26** Springer Verlag (1990).
18. J. Fillion and D. Calais, *J. Phys. Chem. Solids* **38** (1977) 81.
19. S. Prager, *J. Chem. Phys.* **21** (1953) 1344.
20. P.L. Gruzin, *Dokl. Akad. Nauk S.S.S.R.* **86** (1952) 289.
21. J. Philibert, Atom Movements. Les Éditions de Physique, (1991).
22. J.R. Manning, *Acta metall.* **15** (1967) 817.
23. E. Aukrust and A. Muan, *Acta metall.* **10** (1962) 555.
24. C.B. Allcock and A. Kubik, *Acta metall.* **17** (1969) 437.
25. L.S. Darken and R.W. Gurry, *J. Amer. Chem. Soc.* **67** (1945) 1398.
26. A. Vignes and C.E. Birchenall, *Acta metall.* **16** (1968) 1117.
27. T.B. Massalski, J.I. Murray, L.H. Bennet and H. Baker, Eds., *Binary Alloy Phase Diagram*, ASM International, Metals Park, Ohio, (1986).
28. J.E. Reynolds, B.L. Averbach and M. Cohen, *Acta Met.* **5** (1957) 29.
29. A.D. Kurtz, B.L. Averbach and M. Cohen, *Acta Met.* **3** (1955) 442.

## Chapter 4

### Reconsideration of the Kirkendall effect: Bifurcation and instability of the Kirkendall plane<sup>1</sup>

#### 4.1 Introduction

The initial concentration step in the standard diffusion couple contains all the future of this couple like the initial fireball of the Big Bang contained the future of our Universe. Moreover, likewise to small fluctuations in the Fireball leading to the modern non-homogeneous structure of the Universe, small fluctuations of inert Kirkendall markers distribution in the vicinity of the initial interface can lead to bifurcations and instabilities of Kirkendall planes.

From a naïve, purely intuitive point of view it seems strange that markers “overlapping” at first the whole concentration range of the diffusion couple, afterwards gather in a single plane corresponding to only one fixed (constant in time) composition, this plane usually being

---

<sup>1</sup> Parts of this chapter have been published as papers:

Section 4.2: M.J.H. van Dal, M.C.L.P. Pleumeekers, A.A. Kodentsov and F.J.J. van Loo, *Acta Mater.* **48** (2000) 385.

Sections 4.3 and 4.6: M.J.H. van Dal, A.M. Gusak, C. Cserhádi, A.A. Kodentsov and F.J.J. van Loo, *Defect and Diffusion Forum* **194-199** (2001) 195.

Sections 4.4 and 4.5: M.J.H. van Dal, A.M. Gusak, C. Cserhádi, A.A. Kodentsov and F.J.J. van Loo, accepted for publication in *Phil. Mag. A*.

called a Kirkendall plane. Existence of a Kirkendall plane means that this plane is some kind of “attractor” for markers. It is natural to ask why a system should have only one attractor. Is it possible for binary diffusion couple to have two or more attractors? Is there a possibility for a system to interdiffuse without any attractor at all (without a stable Kirkendall plane), with widening (broadening) in time of the distribution of markers?

In this chapter, we will have a closer look at the Kirkendall effect and Darken’s theory [1]. It will be demonstrated that the displacement of markers over the entire interaction zone can be found numerically if the intrinsic diffusivities are known. We will introduce the concept of the Kirkendall velocity curve with which it is possible to predict the location of the Kirkendall plane in any diffusion couple. With this concept it will be made clear that a Kirkendall plane can be multiple, single, stable or unstable and this will be verified by experimental examples.

## 4.2 The Kirkendall velocity and displacement of inert markers during binary interdiffusion

In section 3.4, it was shown that measuring the Kirkendall displacement over the whole interaction zone (in terms of a multi-foil couple) provides a means to determine the intrinsic diffusivities as a function of the concentration. Here we will investigate whether the displacement of the markers is uniquely defined if the intrinsic diffusivities of the species are known as function of composition at the annealing temperature.

Consider a binary A-B solid solution system with, for simplicity reasons, a constant interdiffusion coefficient and equal partial molar volumes. The concentration distribution of, for example, component A across the A/B interaction zone after a certain time  $t$  can be then described by Fick’s second law (see Eq. (3.2)):

$$\frac{\partial N_A}{\partial t} = \frac{\partial}{\partial x} \left( \tilde{D} \frac{\partial N_A}{\partial x} \right), \quad (4.1)$$

where  $N_A$  is the molar fraction of A. Since we assumed  $\tilde{D} = \text{constant}$ , the solution is given by an error function:

$$N_A = \frac{1}{2} \operatorname{erfc}\left(\frac{x}{2\sqrt{\tilde{D}t}}\right). \quad (4.2)$$

The corresponding intrinsic diffusion coefficients  $D_A$  and  $D_B$  are either equal or concentration dependent in a specific way, which follows from Darken's equation (3.12):

$$\tilde{D} = N_B D_A + N_A D_B = D_A + N_A (D_B - D_A) = \text{constant}. \quad (4.3)$$

The relation between the Kirkendall velocity and marker displacement is given by Eq. (3.16). This equation can be re-written as:

$$g(x) = 2tv(x), \quad (4.4a)$$

$$g(x) = y(x) + [g(x) - x] \frac{dy}{dx}. \quad (4.4b)$$

The last equation has a singularity for  $x = g(x) = 2vt$ , which corresponds to the position of the Kirkendall plane. The solution for this first order differential equation is given by:

$$y(x) = \frac{1}{\mu(x)} \left( \mu(x_0) y(x_0) + \int_{x_0}^x \mu(\xi) \frac{g(\xi)}{g(\xi) - \xi} d\xi \right), \quad (4.5a)$$

with

$$\mu(x) = \exp\left[ \int \frac{1}{g(x) - x} dx \right], \quad (4.5b)$$

and can be found numerically using an appropriate computer program (e.g. Mathematica v3.0). A solution to Eq. (4.4b) written in Mathematica is given in Appendix 4.1.

Since it is assumed that  $V_A = V_B = V_m$ , the Kirkendall velocity as given by Darken (Eq. (3.10)) can be expressed as:

$$v = (D_A - D_B) \frac{dN_A}{dx}. \quad (4.6)$$

If now, for instance, the ratio of the intrinsic diffusivities of the components  $D_A/D_B$  is assumed to be constant, then the Kirkendall velocity at position  $x$  inside the diffusion zone can be found by combining Eq. (4.2), (4.3) and (4.6):

$$v = \tilde{D} \left( \frac{\frac{D_A}{D_B} - 1}{N_A + N_B \frac{D_A}{D_B}} \right) \left( \frac{-1}{\sqrt{\pi}} \frac{1}{2\sqrt{\tilde{D}t}} \exp \left[ - \left( \frac{x}{2\sqrt{\tilde{D}t}} \right)^2 \right] \right). \quad (4.7)$$

The position of the Kirkendall plane,  $x_K$ , is defined by  $v_K = x_K/2t$  (see section 3.3) and can be determined graphically as the intersection point of the velocity curve and the line  $v = x/2t$ . Evidently, the straight line  $v = x/2t$  should cross  $x = 0$ , which corresponds to the original position of the initial contact surface, i.e. the location of the Kirkendall markers at  $t = 0$ .

Fig. 4.1 shows the Kirkendall velocity and displacement curves obtained with the assumptions listed above, taking  $\tilde{D} = 10^{-14} \text{ m}^2/\text{s}$ ,  $D_A/D_B = 3$  and  $t = 10^6 \text{ sec}$ .

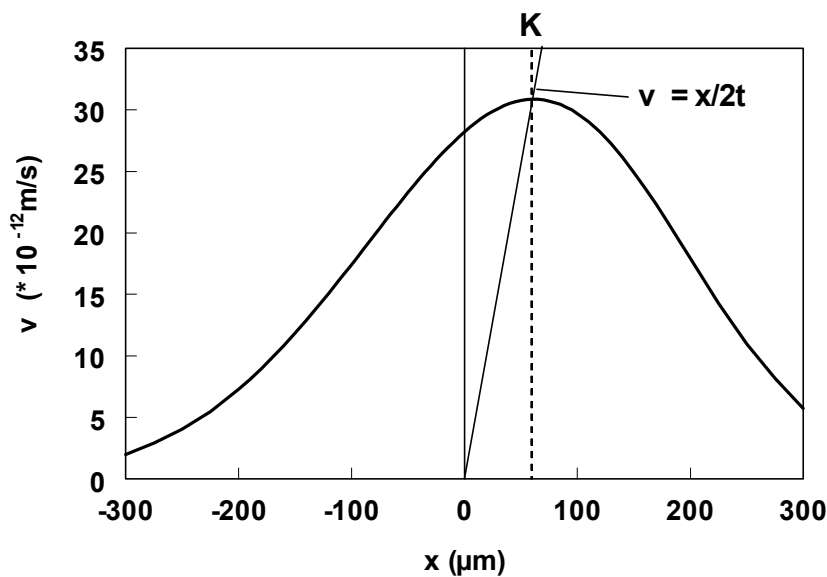
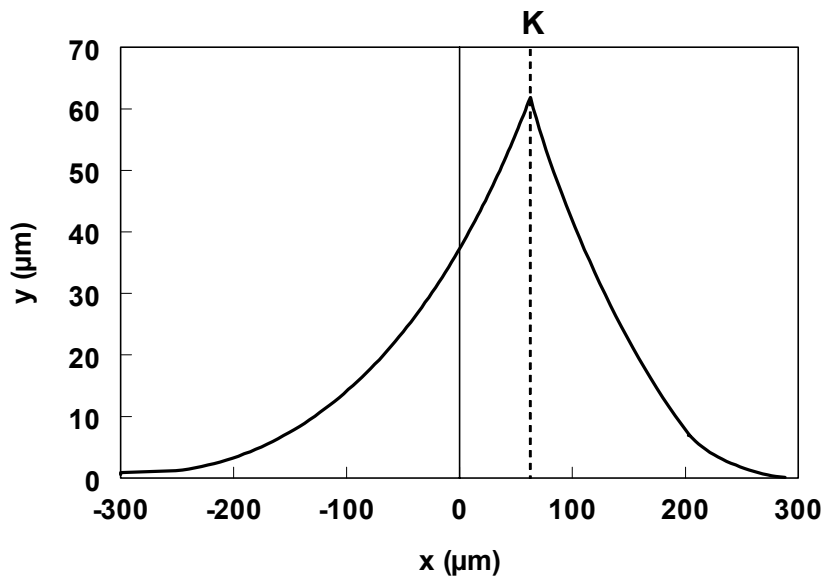


Figure 4.1 a) (continued)



b)

Figure 4.1: a) The Kirkendall velocity and b) the Kirkendall displacement in a hypothetical A-B diffusion system ( $V_A = V_B$ ) with a constant interdiffusion coefficient  $\tilde{D} = 10^{-14} \text{ m}^2/\text{s}$  and constant ratio of intrinsic diffusivities  $D_A/D_B = 3$  ( $t = 10^6 \text{ s}$ ); K indicates the Kirkendall plane.

As it was expected based on the consideration of Philibert [2], the maximum of the velocity curve and displacement curve both coincide with the position of the Kirkendall plane for the case of constant ratio of intrinsic diffusivities. This type of marker behaviour was for long time a generally accepted feature of the manifestation of the Kirkendall effect in binary solid solution systems. However, Cornet *et al.* [3,4] have demonstrated that this is not necessarily true. It can be illustrated by the following example.

Let us again suppose that the interdiffusion coefficient in a hypothetical binary solution system is constant and equal to  $10^{-14} \text{ m}^2/\text{s}$ . But now we assume that the difference between the intrinsic diffusivities of the components is constant, e.g.  $D_A - D_B = 10^{-14} \text{ m}^2/\text{s}$ .

In this particular case, the Kirkendall velocity can be found in a similar way as in the previous example:

$$v = (D_A - D_B) \left( \frac{-1}{\sqrt{\pi}} \frac{1}{2\sqrt{\tilde{D}t}} \exp \left[ - \left( \frac{x}{2\sqrt{\tilde{D}t}} \right)^2 \right] \right) \quad (4.8)$$

and the displacement curve can be calculated using the procedure explained above. These constructions are given in Figs. 4.2a and b.

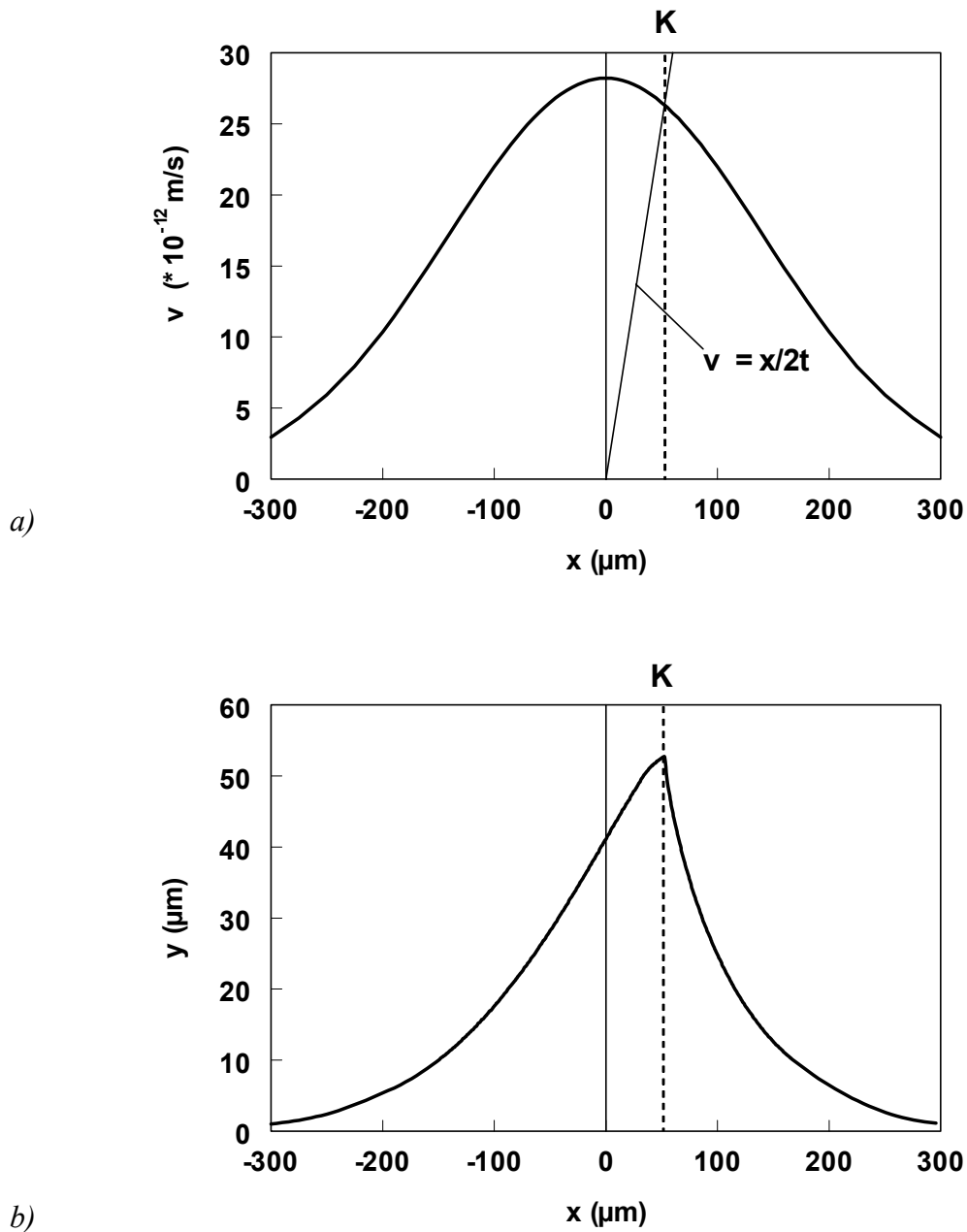


Figure 4.2: a) The Kirkendall velocity and b) the Kirkendall displacement in a hypothetical A-B diffusion system ( $V_A = V_B$ ) with a constant interdiffusion coefficient  $\tilde{D} = 10^{-14} \text{ m}^2/\text{s}$  and constant difference of intrinsic diffusivities  $D_A - D_B = 10^{-14} \text{ m}^2/\text{s}$  for the interaction time  $10^6 \text{ s}$ ; K indicates the Kirkendall plane.

One sees that the maximum of the Kirkendall velocity is situated at the Matano plane and not at the Kirkendall plane. On the other hand, the maximum of the displacement and the position of the Kirkendall plane coincide. In fact, taking real values for  $D_A$  and  $D_B$ , there is no reason why the maximum in the velocity curve, the maximum in the displacement curve and the Kirkendall plane should coincide (Fig. 3.11) (see also Refs. [3,4]).

The analysis discussed in this section clearly demonstrated that the displacement of inert markers is uniquely defined for a diffusion system and can be numerically determined.

### 4.3 Microstructural stability of the Kirkendall plane

From the previous considerations it becomes clear that one can deduce the position and velocity of the Kirkendall plane via the intersection point of the straight line  $v = x/2t$  and the Kirkendall velocity curve. In this respect it is interesting that in the classical paper by Cornet and Calais [3], a hypothetical diffusion couple was shown in which the velocity curve exhibited multiple maxima. The authors stated that inside such a diffusion couple more than one Kirkendall plane could appear. This idea can be best explained by an example of a hypothetical A/B diffusion couple in which on the A-rich side of the interaction zone A is the fastest diffusing species and on the B-rich side B diffuses faster.

In Fig. 4.3, the corresponding velocity curve is given schematically. It is possible for the line  $v = x/2t$  to intersect the Kirkendall velocity curve up to three times as is shown in the figure. This implies that in such a diffusion couple three “Kirkendall” planes might exist, which move parabolically in time. As a result, the markers originally introduced between the end-members would rearrange during interdiffusion into three distinct parallel rows of inclusions, situated at the positions  $K_1$ ,  $K_2$  and  $K_3$ .

However, one should realise that only two of the three predicted “Kirkendall planes” can be found experimentally within the reaction zone. This can be appreciated by analysing the stability of the Kirkendall plane at the possible intersections. If markers, which ended up at the position  $K_1$  in Fig. 4.3, would (for whatever perturbation) be slightly ahead of this plane, they would slow down (lower velocity) and if these markers were behind this plane, they



would move faster (higher velocity). In other words, the plane located at  $K_1$  tends to “attract” inert markers in its vicinity. The same can be said for the plane at  $K_3$ . Hence, a *stable* Kirkendall plane will emerge in the interdiffusion zone when the straight-line  $v = x/2t$  intersects the velocity curve at a position where the Kirkendall velocity has a *negative* gradient.

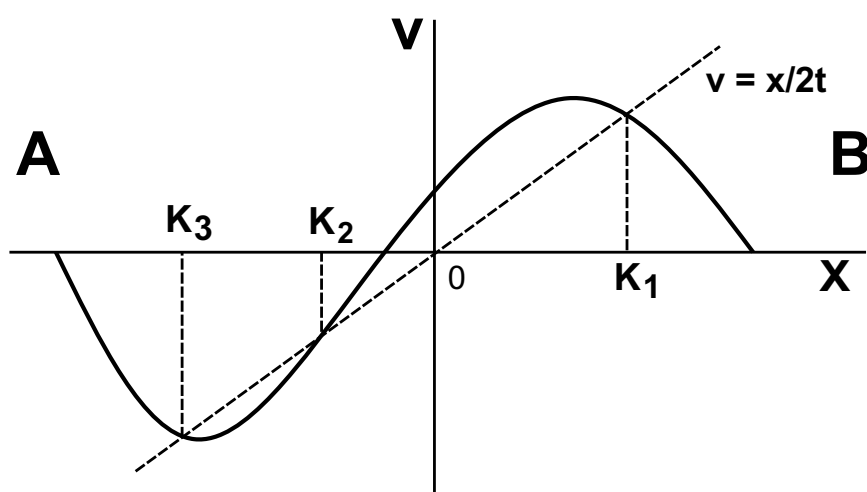


Figure 4.3: The Kirkendall velocity in a hypothetical A-B diffusion system (schematically), in which the intrinsic diffusion coefficients of A and B are chosen arbitrarily in such a way that on the A-side of the diffusion zone A is the faster diffusing component and on the B-side the component B has the highest diffusivity. In principle, three “Kirkendall” planes ( $K_1$ ,  $K_2$ ,  $K_3$ ) can emerge.

Following a similar line of argument, it can be concluded that an *unstable* Kirkendall plane will appear inside a diffusion zone when the gradient of the velocity is *positive* at the intersection point. Indeed, the markers which are slightly ahead of the plane situated at  $K_2$  in Fig. 4.3 will move faster, and markers slightly behind this plane will migrate slower. If such an unstable Kirkendall plane is situated between two stable ones (like in the example in Fig. 4.3), the stable planes will accumulate all markers during the initial stage of interdiffusion. Therefore, only two Kirkendall planes (at the positions  $K_1$  and  $K_3$ ) are expected to appear in the A/B couple.

Experimental verification of these ideas were found in our studies on diffusion phenomena and the Kirkendall effect in the  $\beta'$ -ordered AuZn phase (B2 structure) of the binary Au-Zn system. Previous reports about interdiffusion in this intermetallic compound [5,6] indicate a rather

unusual behaviour of inert markers in the  $\beta'$ -AuZn phase layer developed during interaction between pure Au and a  $\gamma$ -'AuZn<sub>2</sub>' phase containing 64 at.% of Zn. The Kirkendall markers (tungsten wires of about 5  $\mu\text{m}$  thick) and the 'original interface revealed by traces of the joining plane' (presumably by grinding debris remaining at the contact surface between the couple halves) were observed at two different locations inside the  $\beta'$ -AuZn reaction layer. This conspicuous finding was, however, not identified by the authors as the formation of the multiple Kirkendall planes, and this phenomenon was not critically examined.

#### **4.4 Multiple, stable and unstable Kirkendall planes in a single phase: manifestation of the Kirkendall effect in the $\beta'$ -AuZn intermetallic**

The  $\beta'$ -ordered phase (B2; CsCl-structure) in the binary Au-Zn system exists in a wide homogeneity range (e.g. at 500°C this is approximately 38.0 – 57.0 at.% of Zn [7]), and the diffusivities of the components are strongly composition dependent. Of particular importance is that, according to self-diffusion measurements using <sup>65</sup>Zn and <sup>195</sup>Au radiotracers reported by Gupta and Lieberman [8], Au is the faster diffusing species in the Au-rich part of the  $\beta'$ -phase, whereas in the Zn-rich part Zn-atoms have higher mobility. In this situation, the Kirkendall velocity within the  $\beta'$ -intermetallic layer diffusion-grown from its adjacent phases will change direction (see Eq. (3.10), A = Au and B = Zn) and will have a shape similar as shown in Fig. 4.3.

Figure 4.4 shows a representative microstructure of the reaction zone developed during interaction at 500°C in a diffusion couple based on pure Au and  $\gamma$ -AuZn<sub>2</sub> intermetallic containing 64 at.% of Zn. ThO<sub>2</sub>-particles (0.5-5  $\mu\text{m}$ ) were used as fiducial markers between the initial end-members. One sees that the inert particles re-arranged upon interaction into two distinct marker planes (i.e. two Kirkendall planes) moving with different velocities within the newly formed layer of the  $\beta'$ -AuZn phase.

Another interesting feature that can be noticed from this back-scattered electron micrograph is the abrupt change in contrast near the equiatomic composition in the product layer. This is caused by the steep concentration gradient developed in the  $\beta'$ -AuZn phase upon

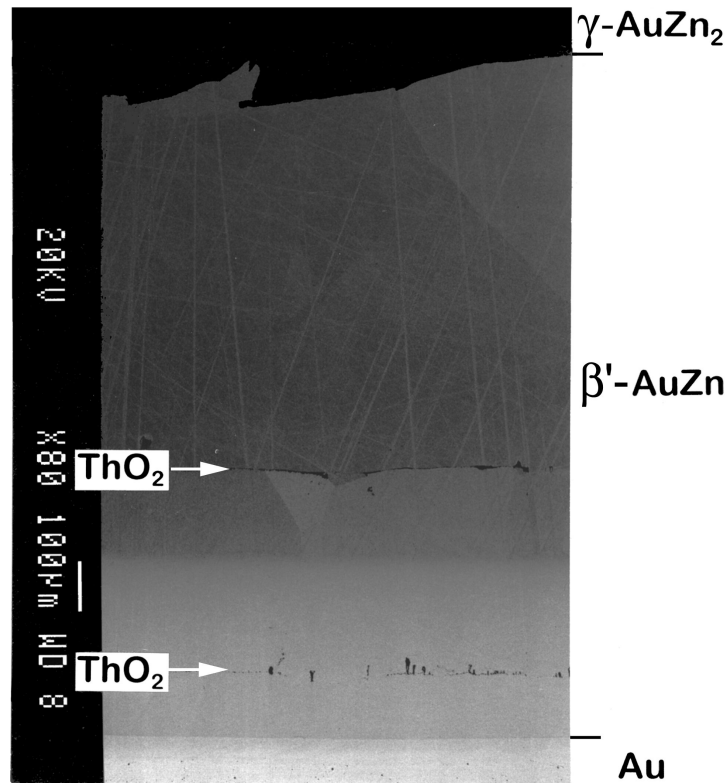


Figure 4.4: Back-scattered electron image (BEI) of a Au/Au<sub>36</sub>Zn<sub>64</sub> (“ $\gamma$ -AuZn<sub>2</sub>”) diffusion couple annealed at 500 °C for 17.25 h under flowing argon. After interdiffusion the ThO<sub>2</sub>-markers introduced between the couple halves are clearly visible as two distinct straight rows of inclusions.

interdiffusion. The physical meaning of the existence of this gradient is the slow diffusion in the near stoichiometric intermetallic AuZn, which reflects the highest degree of order in the B2-structure of the  $\beta'$ -phase near this composition [8,9]. Within this steep concentration gradient also the position where  $D_{\text{Au}} \approx D_{\text{Zn}}$  and, thus, where  $v \approx 0$  is located.

The corresponding velocity curve (that was constructed based on the positions of the Matano plane, the Kirkendall planes (K<sub>1</sub> and K<sub>3</sub>) and the approximate point where  $v \approx 0$  ( $D_{\text{Au}} \approx D_{\text{Zn}}$ ) relative to the phase boundaries) is shown in Fig. 4.5. Apparently, there is no theoretical restriction for the straight line  $v = x/2t$  to intersect a Kirkendall velocity curve of such a shape up to three times as shown in this figure. As already has been stated, since the Kirkendall planes at position K<sub>1</sub> and K<sub>3</sub> are stable they will accumulate the ThO<sub>2</sub> particles in the initial

stages of the interaction. As a consequence the unstable Kirkendall plane at position  $K_2$  is not visible and two Kirkendall planes will emerge inside the interaction zone.

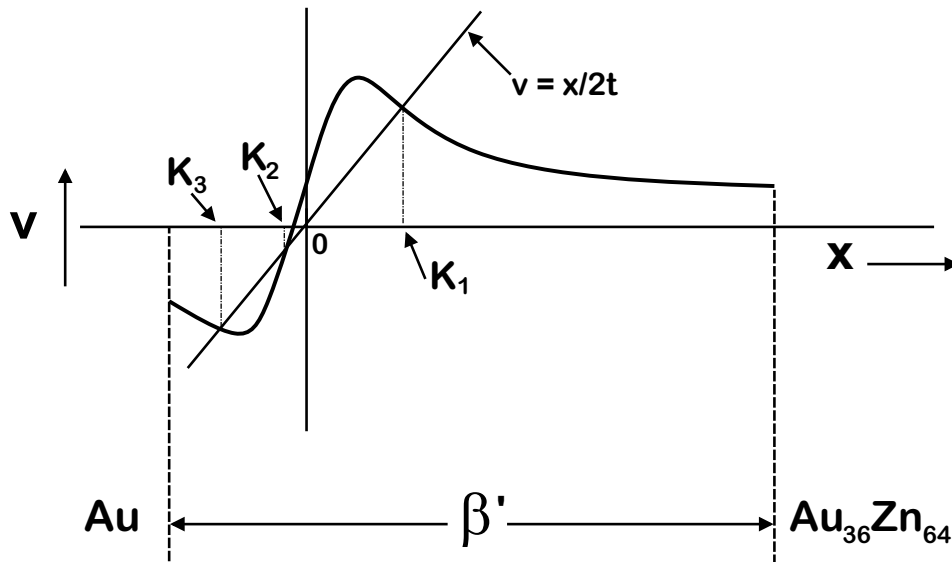
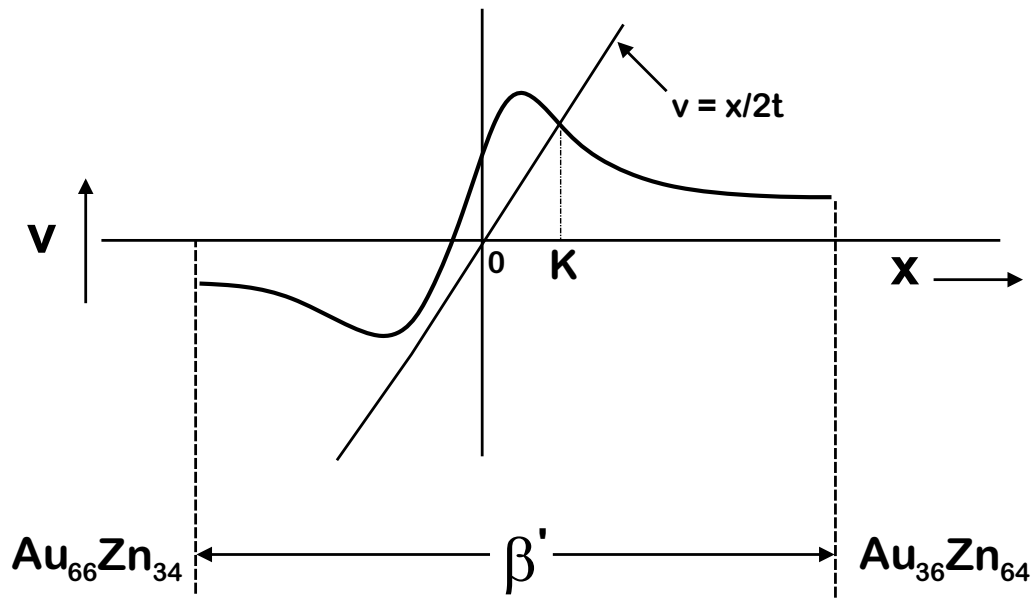


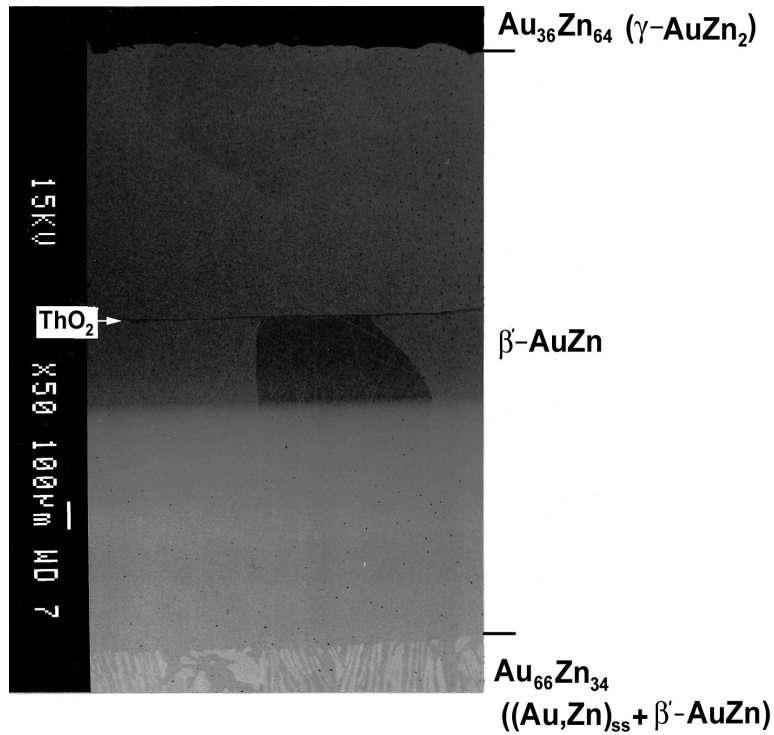
Figure 4.5: The Kirkendall velocity curve corresponding to the  $\beta'$ -AuZn product layer in the annealed ( $500^\circ\text{C}$ ; 17.25 h; Ar + 5 vol.%  $\text{H}_2$ ) Au/Au<sub>36</sub>Zn<sub>64</sub> ( $\gamma'$ -AuZn<sub>2</sub>) couple. This plot is based on the positions of the Matano plane, the Kirkendall planes ( $K_1$  and  $K_3$ ) and the point where  $v \approx 0$  (sudden change in contrast) relative to the phase boundaries.

It is important to realise that the number of intersections between the Kirkendall velocity curve and the line  $v = x/2t$  is determined not only by the shape of the curve, but also depends on the position of the Matano plane ( $x = 0$ ) in the diffusion couple. For instance, if one adds Zn to the pure Au end-member of the diffusion couple, the position of the Matano plane shifts towards the Zn-side of the reaction zone. Then, a situation may occur when the straight line  $v = x/2t$  intersects the velocity curve instead of three times only once as is shown in Fig. 4.6a. One can see that the intersection point and, hence, the corresponding stable Kirkendall plane should then be found at the Zn-rich part of the  $\beta'$ -AuZn product layer.

A typical example of such situation is given in Fig. 4.6b, showing a diffusion zone of an reaction couple annealed at  $500^\circ\text{C}$  composed of a  $\gamma'$ -AuZn<sub>2</sub> with a nominal composition Au<sub>36</sub>Zn<sub>64</sub> and a two-phase alloy Au<sub>66</sub>Zn<sub>34</sub>. The latter alloy after equilibration at  $500^\circ\text{C}$  consists of a saturated (Au,Zn)-solid solution and precipitates of the  $\beta'$ -phase. The sudden



a)



b)

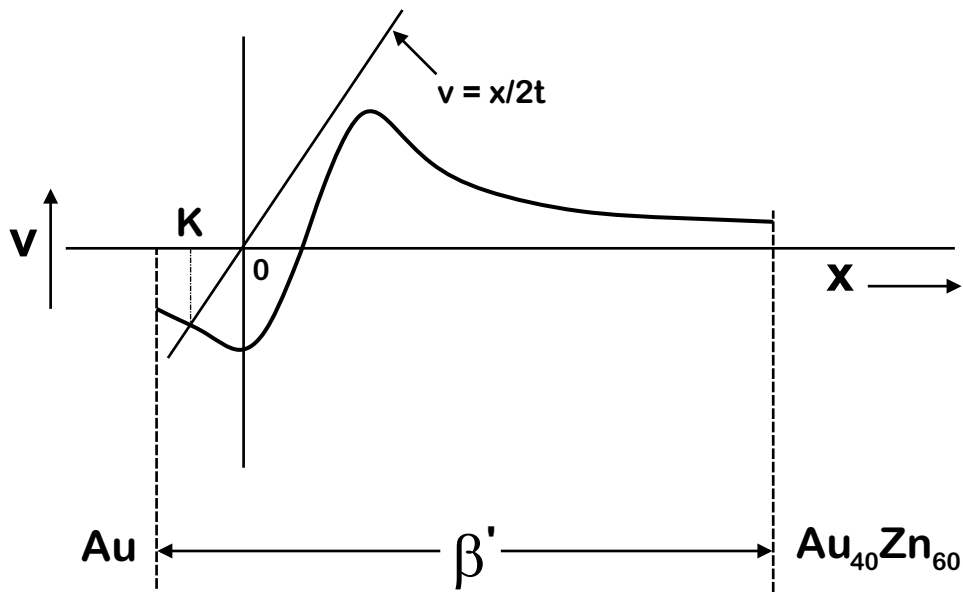
Figure 4.6: a) The Kirkendall velocity curve corresponding to the product layer of the  $\beta'$ -AuZn intermetallic formed during reaction between  $\gamma$ 'AuZn<sub>2</sub>' (Au<sub>36</sub>Zn<sub>64</sub>) and a two-phase Au<sub>66</sub>Zn<sub>34</sub> alloy ((Au,Zn)-solid solution +  $\beta'$ -AuZn) (500 °C; 17 h; Ar + 5 vol.% H<sub>2</sub>); b) BEI of the diffusion zone after annealing. The straight line  $v = x/2t$  intersects the velocity curve only once at the Zn-rich side of the  $\beta'$ -AuZn layer.

change in contrast at the near-stoichiometric composition in the newly formed  $\beta'$ -AuZn intermetallic is again clearly visible on the micrograph. As expected, the ThO<sub>2</sub> particles used as inert markers between the couple halves are found as a straight row of inclusions at one specific position (point K in Fig. 4.6a) in the Zn-rich of the  $\beta'$ - phase layer. The marker plane is also revealed by the differences in grain morphology inside the  $\beta'$ -layer. The differently nucleated grains of the product phase meet at the Kirkendall plane. Therefore, this plane can readily be seen within the reaction layer even without the presence of any inert particles. (This was also visible, although less pronounced, in the Au/Au<sub>36</sub>Zn<sub>64</sub> couple of Fig. 4.4).

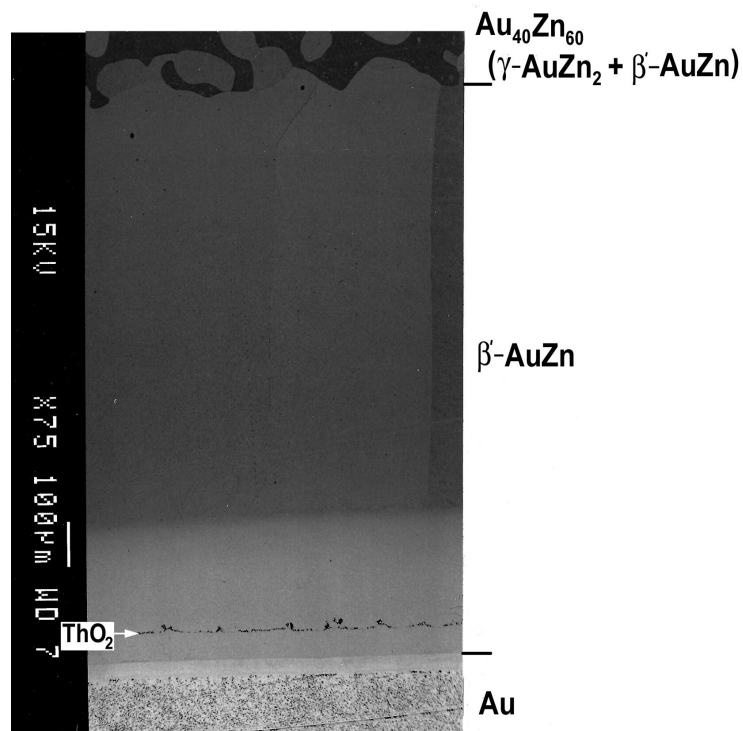
Extending this approach, it can be understood that if the position of the Matano plane shifts in the direction of Au-side of the incremental couple, the stable Kirkendall marker plane will appear in the Au-rich domain of the  $\beta'$ -AuZn intermetallic layer. This is demonstrated in Fig. 4.7a. Here, experimental proof came from the analysis of the diffusion zone morphology developed during interaction (500°C; 16 h; Ar + 5 vol.% H<sub>2</sub>) between pure Au and an equilibrated Au<sub>40</sub>Zn<sub>60</sub> alloy consisting of a  $\gamma$ -‘AuZn<sub>2</sub>’ matrix phase and  $\beta'$ -precipitates (Fig. 4.7b). As predicted, the Kirkendall marker plane appears in the Au-rich part of the  $\beta'$ -AuZn product layer.

Obviously, one more possible configuration of the marker velocity construction can be envisaged, in which the line  $v = x/2t$  intersects the velocity curve only once, but at a point where the gradient of the Kirkendall velocity is *positive*, like, for example, shown in Fig. 4.8a. In this case, the predicted Kirkendall marker plane is microstructurally unstable, and no stable Kirkendall plane is present next to the unstable one, i.e. no ‘attractor’ for markers exists in the diffusion zone. Therefore, no well-defined Kirkendall marker plane will develop upon interdiffusion in such a system.

A very telling example of the Kirkendall plane instability is provided by the experiments on a diffusion couple consisting of an equilibrated two-phase  $\gamma$ -AuZn<sub>2</sub> +  $\beta'$ -AuZn alloy with nominal composition Au<sub>40</sub>Zn<sub>60</sub> and a Au<sub>70</sub>Zn<sub>30</sub>-solid solution. A representative microstructure of the couple after annealing at 500°C for 6 h under flowing Ar + 5 vol.% H<sub>2</sub> gas mixture is given in Fig. 4.8b. Unlike the previous cases, no distinct row of the ThO<sub>2</sub>-inclusions used as fiducial markers between the end-members can be seen inside the product phase  $\beta'$ -AuZn.

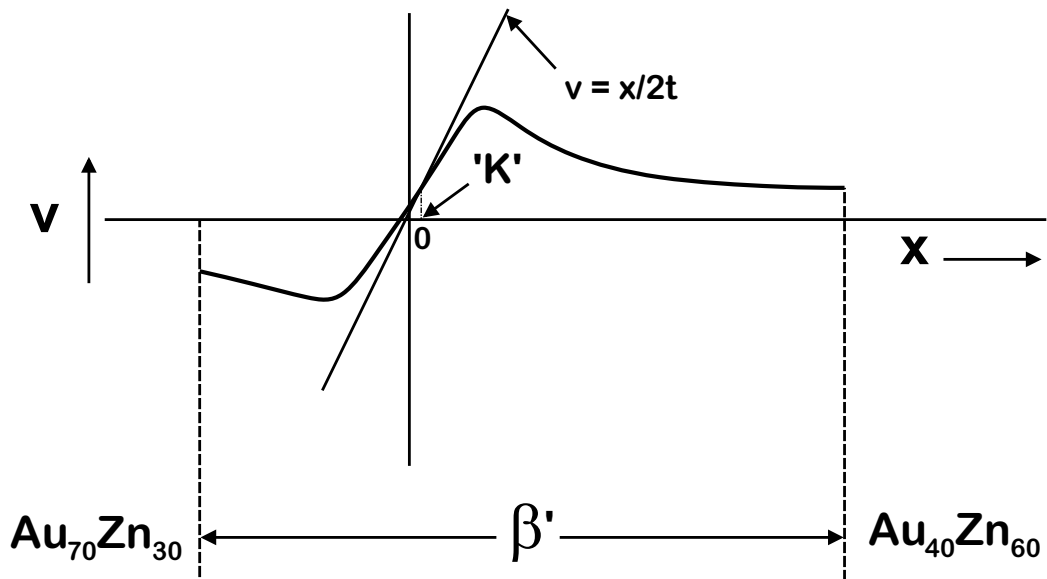


a)



b)

Figure 4.7: a) The Kirkendall velocity construction corresponding to the layer of  $\beta'$ -AuZn diffusion-grown at 500 °C for 17.5 h in Ar + 5 vol.%  $\text{H}_2$  between Au and a  $\text{Au}_{40}\text{Zn}_{60}$  two-phase alloy ( $\gamma$ -AuZn<sub>2</sub> +  $\beta'$ -AuZn) and b) corresponding microstructure of the reaction zone (BEI). Only one Kirkendall marker plane appears in the Au-rich part of the product layer.



a)

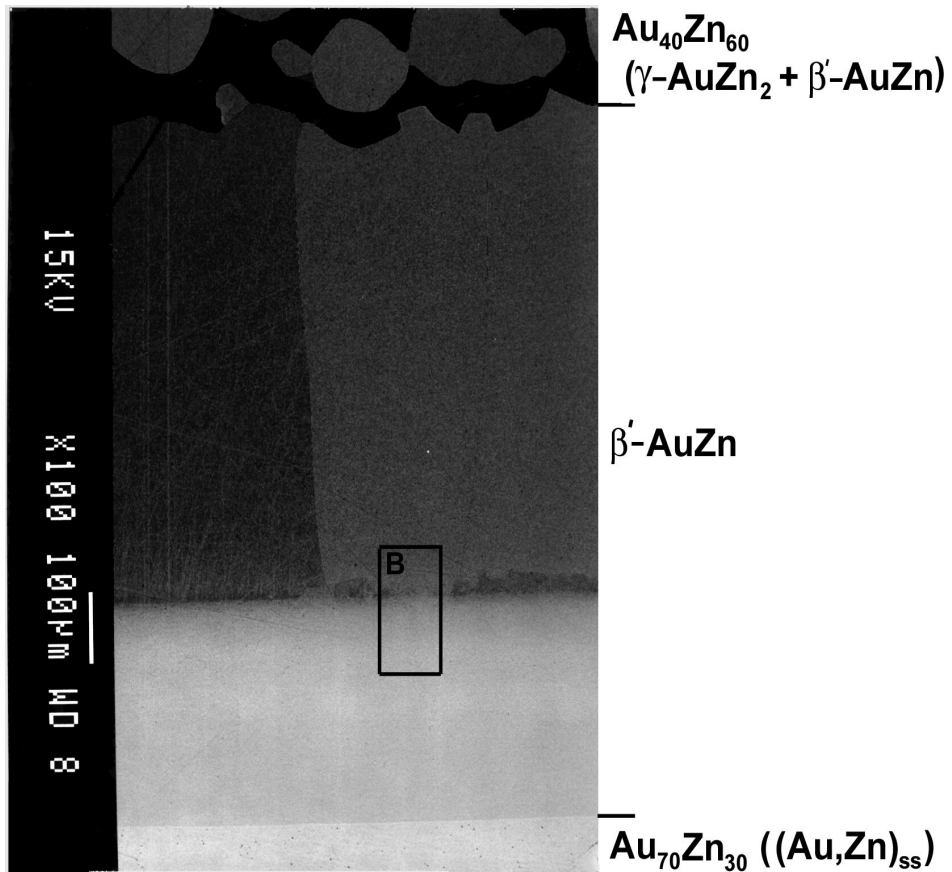


Figure 4.8 b) (continued)



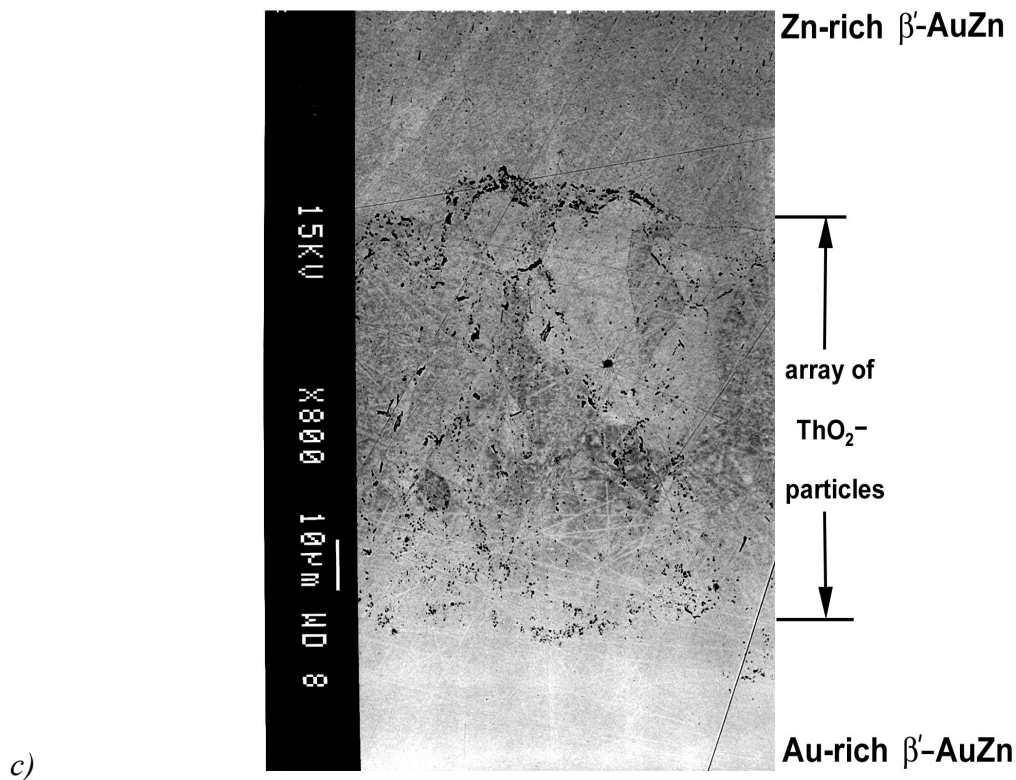


Figure 4.8: a) The Kirkendall velocity curve corresponding to the diffusion-grown layer of  $\beta'$ -AuZn in a  $Au_{70}Zn_{30}/Au_{40}Zn_{60}$  reaction couple ( $500^\circ\text{C}$ ; 6 h; Ar + 5 vol.%  $H_2$ ); b) corresponding microstructure of the reaction zone (BEI) and c) magnified area (B in Fig. 4.8b) of the product layer in the vicinity of the unstable Kirkendall plane location (BEI). The line  $v = x/2t$  intersects the velocity curve at a position 'K' where the gradient of the Kirkendall velocity is positive. The corresponding 'Kirkendall' plane is unstable.

However, close inspection of the intermetallic layer in the vicinity of the expected location of the unstable Kirkendall plane revealed the occurrence of the  $\text{ThO}_2$ -inclusions not in a distinct row, but spatially distributed in the diffusion direction (Fig. 4.8c).

#### 4.5 General criterion of Kirkendall plane instability

As explained in section 4.3, a Kirkendall plane is considered to be microstructurally unstable if at its location in a diffusion zone,  $x_K$ , the corresponding marker velocity has a positive gradient, i.e.:

$$\left. \frac{\partial v}{\partial x} \right|_{x_K} > 0. \quad (4.9)$$

Since we are dealing with a diffusion-controlled interaction, the instability criterion in a binary A-B system can be rewritten using Eq. (3.10) and the Boltzmann variable  $\lambda = x/\sqrt{t}$  as:

$$\frac{d}{d\lambda} \left( (D_B - D_A) \cdot V_B \frac{dC_B}{d\lambda} \right)_{\lambda_K} > 0, \quad (4.10)$$

where  $\lambda_K$  corresponds to the Kirkendall plane location. Combining this inequality and Fick's second law in a form  $-\frac{\lambda}{2} \frac{dC_B}{d\lambda} = \frac{d}{d\lambda} \left( \tilde{D} \frac{dC_B}{d\lambda} \right)$  with  $\tilde{D}$  being the interdiffusion coefficient defined as in Eq. (3.12), we arrive at the following expression:

$$\frac{d}{d\lambda} \left( \frac{D_B - D_A}{\tilde{D}} V_B \right) \tilde{D} \left. \frac{dC_B}{d\lambda} \right|_{\lambda_K} + \frac{D_B - D_A}{\tilde{D}} V_B \frac{d}{d\lambda} \left( \tilde{D} \frac{dC_B}{d\lambda} \right)_{\lambda_K} > 0 \quad (4.11)$$

or further

$$\frac{d}{dC_B} \left( \frac{D_B - D_A}{\tilde{D}} V_B \right)_{C_K} \left( \left. \frac{dC_B}{d\lambda} \right|_{\lambda_K} \right)^2 - \left. \frac{\lambda_K}{2} \frac{dC_B}{d\lambda} \right|_{\lambda_K} \frac{D_B - D_A}{\tilde{D}} V_B > 0, \quad (4.12)$$

with  $C_K$  corresponding to the concentration of B at the Kirkendall plane. The partial molar volumes  $V_i$  can be different but are constant in this treatment (Vegard's law holds, see section 3.2).

At the position of the Kirkendall plane ( $x = x_K$ ), the Kirkendall velocity equals  $x/2t$  (Eq. (3.13)). With the Boltzmann-parameter, this can be restated as:

$$\frac{\lambda_K}{2} = (D_B - D_A) V_B \left. \frac{\partial C_B}{\partial \lambda} \right|_{\lambda_K}. \quad (4.13)$$

Substituting Eq. (4.13) into Eq. (4.12), one obtains the following:

$$\tilde{D} \left( \frac{dC_B}{d\lambda} \right)^2 \left( \frac{d}{dC_B} \left( \frac{D_B - D_A}{\tilde{D}} V_B \right) - \left( \frac{D_B - D_A}{\tilde{D}} V_B \right)^2 \right) > 0. \quad (4.14)$$

After some algebra we have:

$$\frac{d}{dC_B} \left( \frac{\tilde{D}}{(D_B - D_A) V_B} \right) < -1. \quad (4.15)$$

Taking for simplicity  $V_A = V_B = V_m$ , the instability criterion for Kirkendall marker plane in a binary system is found as the simple expression:

$$\frac{d}{dN_B} \left( \frac{D_A}{D_B} \right)_{N_K} < 0, \quad (4.16)$$

where  $N_B$  is the mole fraction of component B. In words, this means that, when a Kirkendall plane is expected within a concentration range where the ratio of intrinsic diffusivities of A and B decreases with increasing composition of B, it will be unstable. Eq. (4.16) is an extra condition for the Kirkendall plane to Eqs. (3.10) and (3.13) and can be a useful tool in finding candidates for Kirkendall plane instability.

We will demonstrate the instability criterion for the diffusion couple in the Au-Zn system in which a single unstable Kirkendall plane was found discussed in the preceding section (Fig. 4.8). Fig. 4.9 shows the ratio of intrinsic diffusivities of Au and Zn in the concentration range 48-51 at.% of Zn calculated using tracer diffusion data of Gupta and Lieberman [8] (here it is assumed that  $D_{Au}/D_{Zn} = D_{Au}^*/D_{Zn}^*$ , i.e. the vacancy wind effect term is supposed to be equal to unity). Following the criterion (4.16), this should lead to an unstable Kirkendall plane in this concentration range. Indeed, the position of the unstable Kirkendall plane in the  $Au_{40}Zn_{60}/Au_{70}Zn_{30}$  diffusion couple (Fig. 4.8) coincided with the steep concentration gradient near the equiatomic composition, hence an unstable Kirkendall plane was expected.

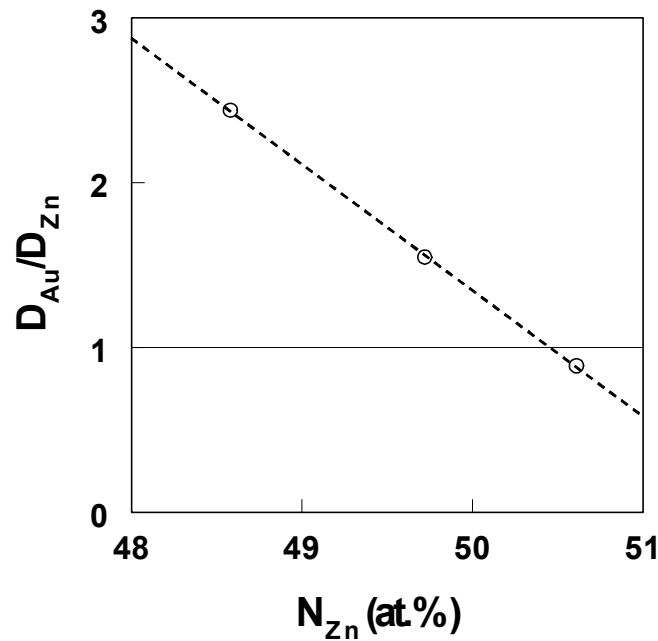


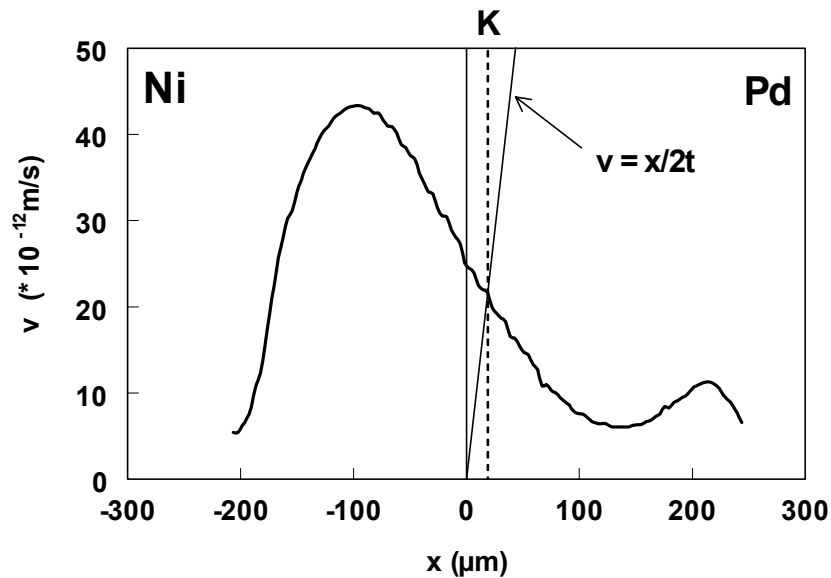
Figure 4.9: Ratio of intrinsic diffusion coefficients of Au and Zn in the AuZn compound at 500 °C taken from Ref. [8].

#### 4.6 Manifestation of the Kirkendall effect in disordered binary systems

Further experimental evidences for the existence of stable and unstable Kirkendall planes were found in the study on the manifestation of the Kirkendall effect in the Au-Ni, Ni-Pd and Fe-Pd systems. Figs. 4.10 a, b and c show the experimentally determined velocity curves of a Ni/Pd diffusion couple annealed at 1100 °C for 121 h, a Au/Ni diffusion couple annealed at 900 °C for 100 h and an Fe/Pd diffusion couple annealed at 1100 °C for 144 h, respectively. These curves were constructed with the multi-foil technique (see Chapter 3 and for the Au/Ni couple the reader is referred to Ref. [10]). In all curves the straight line  $v = x/2t$  intersects the velocity curve only once, which means that only one Kirkendall plane can be expected. However, in the case of the Au/Ni and Ni/Pd diffusion couples, the velocity curves in the intersection point have a negative slope while in the case of the Fe/Pd couple the straight line intersects the velocity curve with a positive gradient. According to the condition of instability Eq. (4.9), this should lead to single *stable* Kirkendall planes for the Au-Ni and Ni-Pd systems and a single *unstable* Kirkendall plane for the Fe-Pd system.

The (in)stability of a Kirkendall plane in the interdiffusion zone of a diffusion couple is revealed by the behaviour of the inert  $\text{ThO}_2$ -particles placed at the original contact surface of the initial end-member. Fig. 4.11a and b show back-scattered electron images of a Ni/Pd diffusion couple annealed at  $1100^\circ\text{C}$  for 196 h and a Au/Ni diffusion couple annealed at  $900^\circ\text{C}$  for 50 h, respectively. For the Ni/Pd couple the  $\text{ThO}_2$  particles exhibit a white contrast whereas for the Au/Ni couple, the  $\text{ThO}_2$ -particles show a dark-greyish contrast in the back-scattered electron image.

After interaction, the  $\text{ThO}_2$  markers are located in a straight row inside the interaction zone in both cases and they exhibit a plate-like shape. Apparently, the stable Kirkendall plane attracts the inert particles in its vicinity.



a)

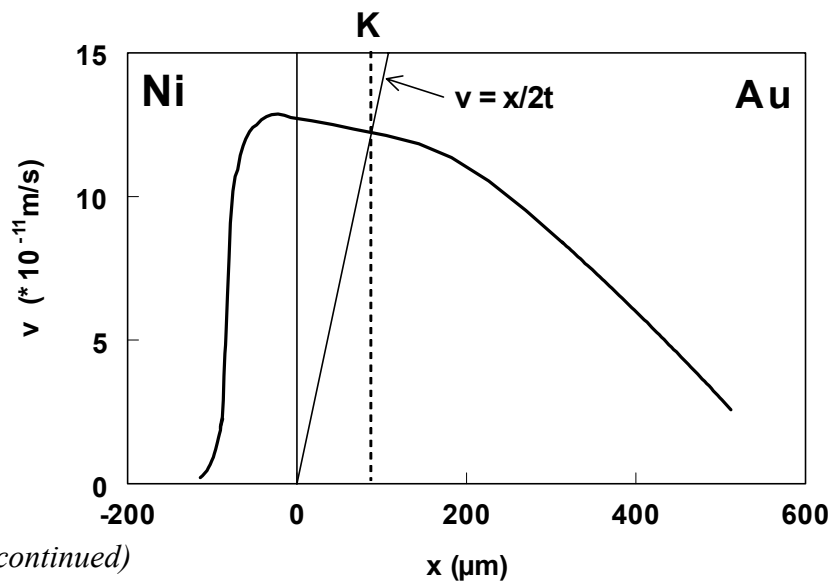


Figure 4.10 b) (continued)

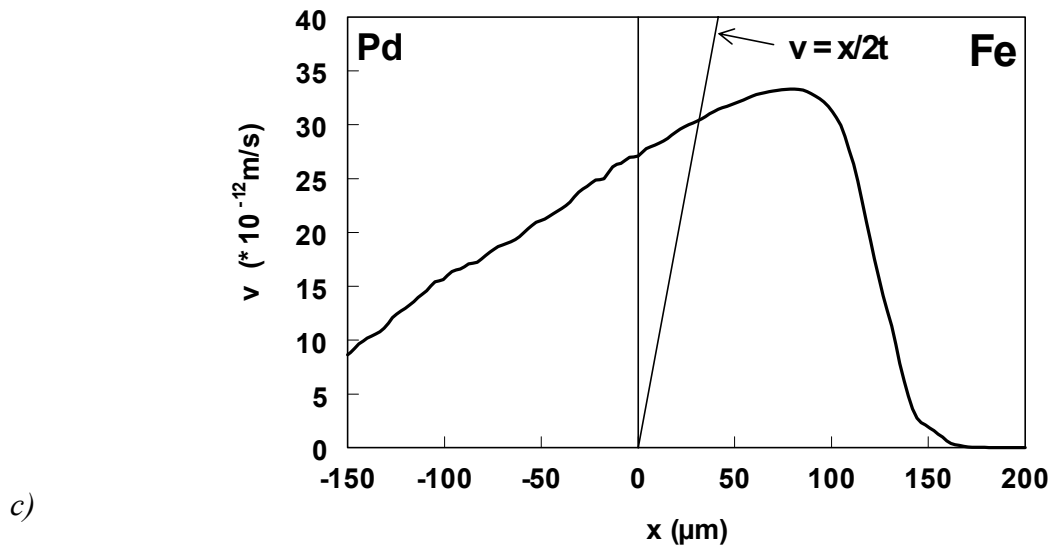
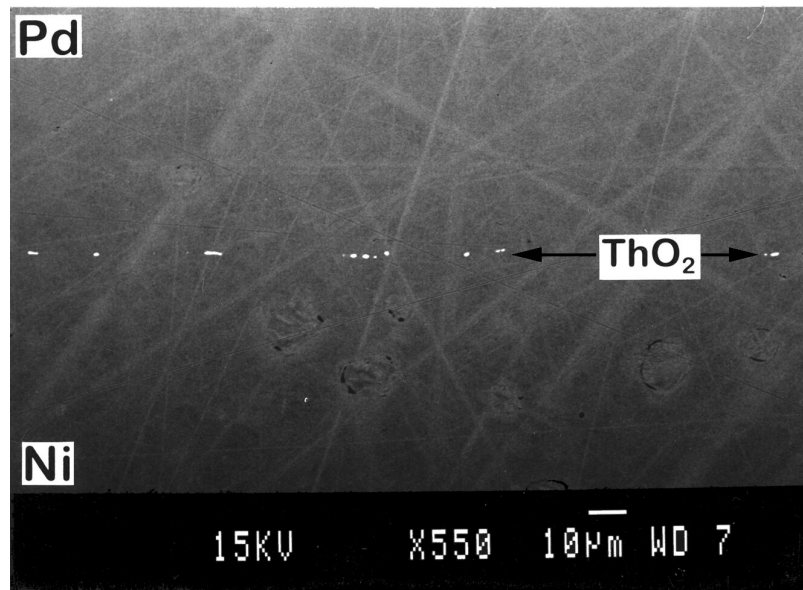


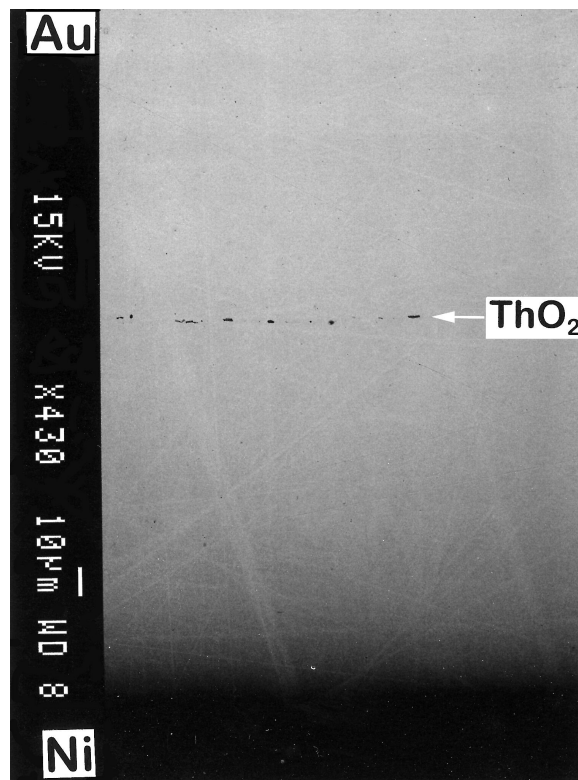
Figure 4.10: a) Experimentally determined Kirkendall velocity curves of (a) a multi-foil Ni/Pd diffusion couple annealed at  $1100^\circ\text{C}$  for 121 h, (b) a multi-foil Au/Ni couple annealed at  $900^\circ\text{C}$  for 100 h [10] and (c) a multi-foil Fe/Pd couple annealed at  $1100^\circ\text{C}$  for 144 h. Note:  $x = 0$  corresponds to the position of the original contact interface between the component materials.

A completely different picture can be observed if we look at the interdiffusion zone of the Fe/Pd diffusion couple. Fig. 4.11c shows a back-scattered electron image of an Fe/Pd diffusion couple annealed at  $1100^\circ\text{C}$  for 144 h. As one can see, a significant scattering of the particles occurred during interaction with respect to the initial spatial distribution. Additionally, the shape of the particles is more round-like. This is a similar observation as was done in the multi-foil couple (see Fig. 3.15 in section 3.5).

In the case of the Fe/Pd diffusion couples annealed  $1100^\circ\text{C}$  there is no “attractor” (i.e. no stable Kirkendall plane) present inside the interaction zone. The initial planar array of the markers at the contact interface tends to transform into an array of  $\text{ThO}_2$ -particles spatially distributed in the diffusion direction.



a)

*Figure 4.11 b) (continued)*

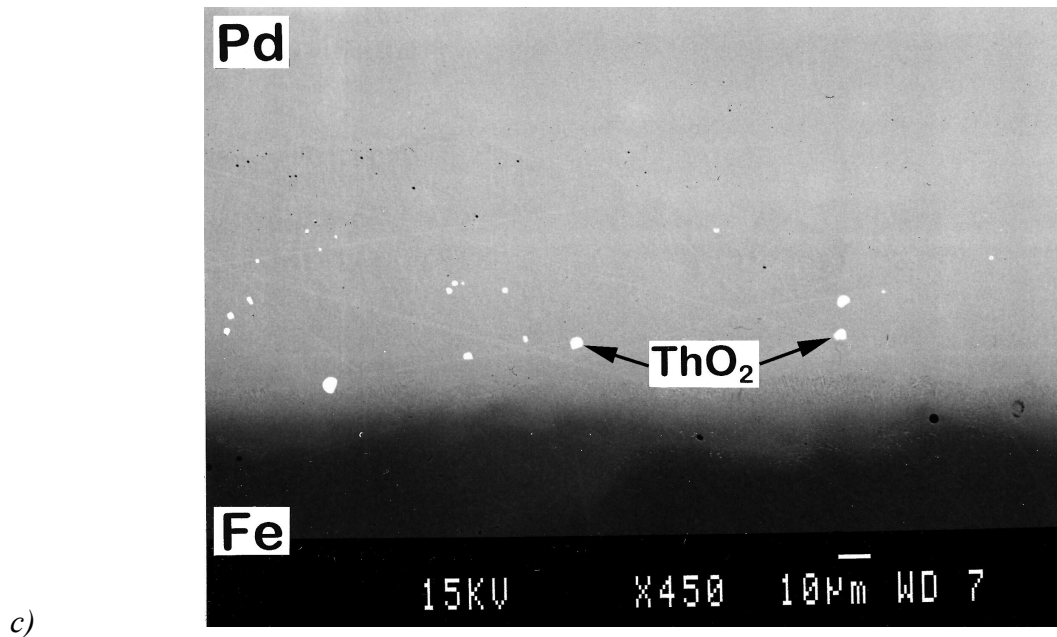


Figure 4.11: BEI of (a) a Ni/Pd couple after interdiffusion at 1100 °C in vacuum for 196 h; (b) a Au/Ni diffusion couple annealed at 900 °C in vacuum for 50 h and (c) an Fe/Pd couple after interdiffusion at 1100 °C in vacuum for 144 h. The ThO<sub>2</sub> markers exhibit a dark-grey contrast on the BEI image of the Au/Ni diffusion zone and a white contrast in the case of the Ni/Pd and Fe/Pd couples.



## References

1. L.S. Darken, *Trans. AIME* **175** (1948) 184.
2. J. Philibert, *Atom Movements and Mass Transport in Solids*, Les Éditions de Physique, (1991).
3. J.-F. Cornet and D. Calais, *J. Phys. Chem. Solids* **33** (1972) 1675.
4. J.-F. Cornet, *J. Phys. Chem. Solids* **35** (1974) 1247.
5. T. Shimozaki, private communication.
6. T. Shimozaki, Y. Goda, Y. Wakamatsu and M. Onishi, *Defect and Diffusion Forum* **95-98** (1993) 629.
7. H. Okamoto and T.B. Massalski, *Phase Diagrams of Binary Gold Alloys*. Metals Park, Ohio: American Society for Metals (1988) p. 331.
8. D. Gupta and D.S. Lieberman, *Phys. Rev. B* **4** (1971) 1070.
9. R. Hilgedieck and C. Herzig, *Z. Metallkde.* **74** (1983) 38.
10. M.J.H. van Dal, M.C.L.P. Pleumeekers, A.A. Kodentsov and F.J.J. van Loo, *J. Alloys. Comp.* **309** (2000) 132.

## Appendix 4.1: Numerical solution of Eq. (4.4) (Mathematica v3.0)

Mathematica v3.0 was used to numerically solve Eq. (4.4b):

$$g(x) = y(x) + [g(x) - x] \frac{dy}{dx} \quad (4.4b)$$

The idea was to start with a set of data (*gdata*) representing the Kirkendall velocity curve as determined from the known intrinsic diffusivities using Eq. (3.10). In such a case the program makes it possible to use any experimental set of data of the Kirkendall velocity curve for determination of the corresponding displacement curve. As an example, we demonstrate the program for the hypothetical diffusion couple in which constant ratio of intrinsic diffusivities of A and B ( $D_A/D_B = 3$ ) was assumed (Fig. (4.1)). An interpolation function (*f*) was used to fit the inserted Kirkendall velocity data (*gdata*). Subsequently this function was solved numerically (*NDSolve* in the program). Because the Kirkendall plane represents a singularity of Eq. (4.4b) the function *f* was solved in two ranges:  $-\infty < x < x_K$  and  $x_K < x < +\infty$ . The program parameter  $x_0$  corresponds to the position of the Kirkendall plane  $x_K$ . These two sections,  $g_1$  and  $g_2$ , were then put together to give the displacement curve *y*.

```

SetDirectory["D:\Mathematica"]
D:\Mathematica
Off[General::spell]; Off[General::spell1];

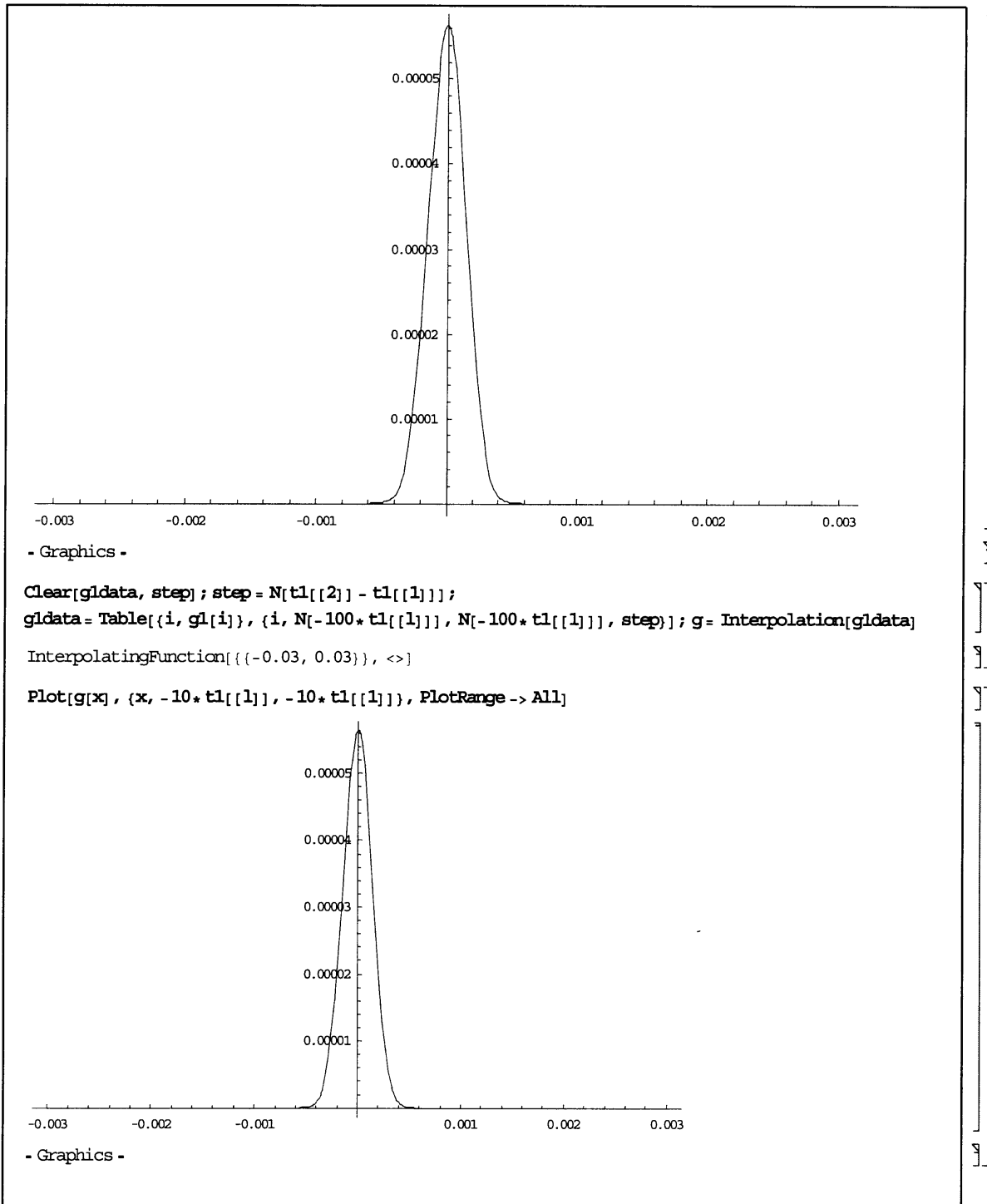
Clear[v, t1, t2, l, gdata]; v = ReadList["DDconstant.txt", Number, RecordLists -> True];
l = Length[v]; t1 = 10^(-6) * #[[1]] &/e v; t2 = 2 * 10^6 * #[[2]] &/e v; gdata = {};
Do[gdata = AppendTo[gdata, {-t1[[i]], t2[[i]]}], {i, l}];

Clear[A1, A2, D1, D2];
FindRoot[{A1 * Exp[-D1 * Abs[t1[[1]]]] == t2[[1]], A2 * Exp[-D2 * Abs[t1[[1]]]] == t2[[1]],
  A1 * D1 * Exp[-D1 * Abs[t1[[1]]]] == Abs[(t2[[2]] - t2[[1]]) / (t1[[2]] - t1[[1]])],
  A2 * D2 * Exp[-D2 * Abs[t1[[1]]]] == Abs[(t2[[1]] - t2[[1-1]]) / (t1[[1]] - t1[[1-1]])],
  {A1, t2[[1]]}, {A2, t2[[1]]}, {D1, Abs[1/t1[[1]]]}, {D2, Abs[1/t1[[1]]]}, MaxIterations -> 50]
{A1 -> 0.00224222, A2 -> 0.00224222, D1 -> 19774.7, D2 -> 19774.7}

Clear[a1, a2, d1, d2]; a1 = A1 /. %; a2 = A2 /. %; d1 = D1 /. %; d2 = D2 /. %;

Clear[f, g1];
f = Interpolation[gdata, InterpolationOrder -> 1]; g1[x_ /; x < -t1[[1]]] := a2 * Exp[-d2 * Abs[x]];
g1[x_ /; -t1[[1]] <= x && x <= -t1[[1]]] := f[x]; g1[x_ /; x > -t1[[1]]] := a1 * Exp[-d1 * Abs[x]];
Plot[g1[x], {x, -10 * t1[[1]], -10 * t1[[1]]}, PlotRange -> All]

```



```

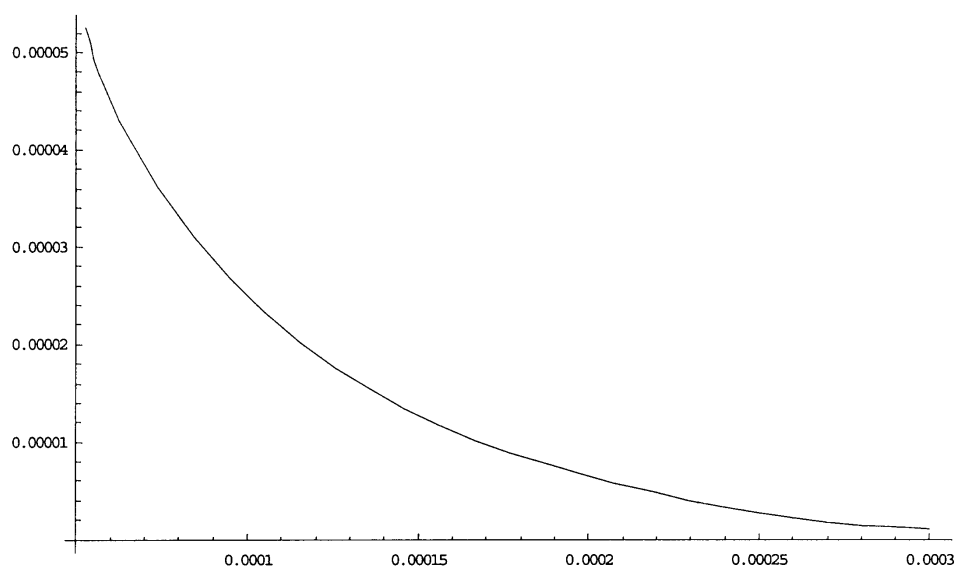
Clear[x0, x1, start]; start = (t1[[1]] + t1[[2]]) / 2; x1 = FindRoot[g[x] == x, {x, start}];
x0 = x /. x1[[1]]

0.000052653

Clear[y1, solut1];
solut1 = NDSolve[{y1[x] - y1'[x] * (x - g[x]) - g[x] == 0, y1[-100 * t1[[1]]] == 0}, y1, {x, x0, t1[[1]]}];
{{y1 -> InterpolatingFunction[{{0.000052653, 0.0003}}, <>]}}

Clear[g1]; g1 = Plot[Evaluate[y1[x] /. solut1[[1]]], {x, x0, -t1[[1]]}]

```



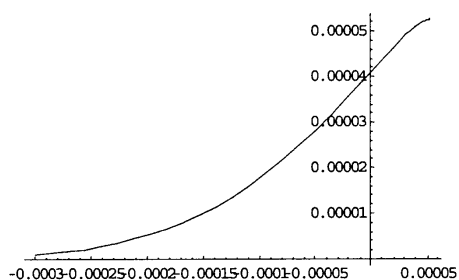
- Graphics -

```

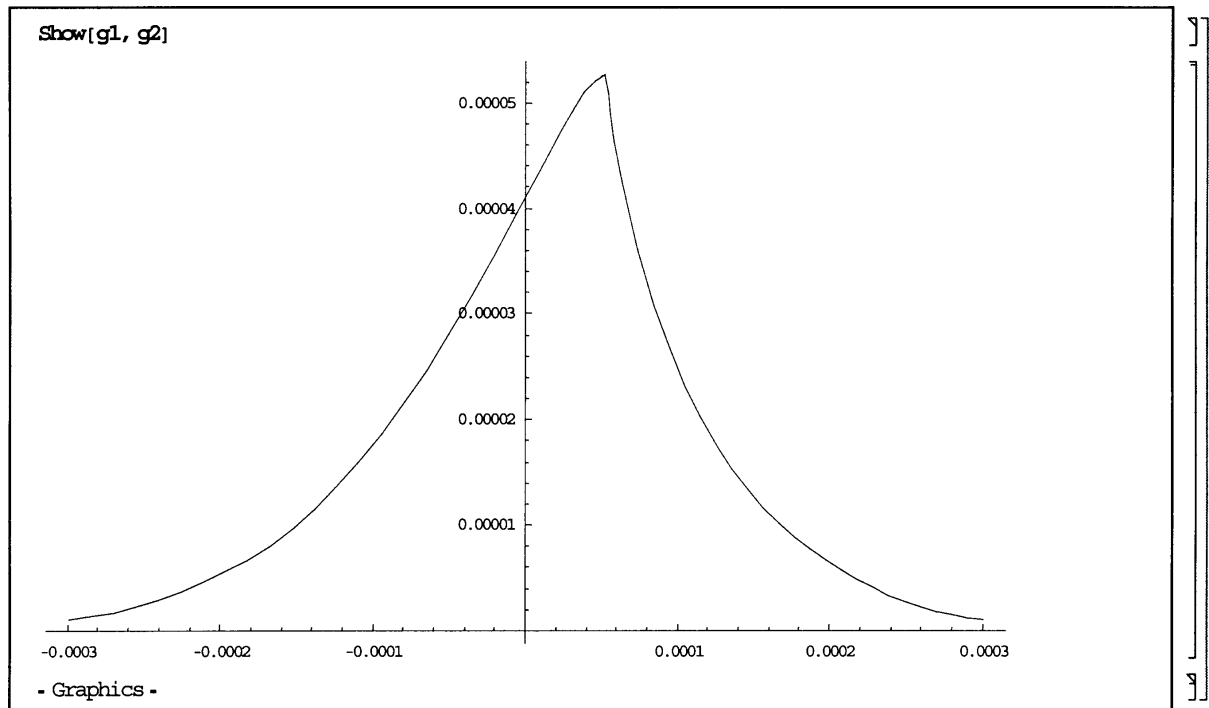
Clear[y2, solut2];
solut2 = NDSolve[{y2[x] - y2'[x] * (x - g[x]) - g[x] == 0, y2[-100 * t1[[1]]] == 0}, y2, {x, -t1[[1]], x0}];
{{y2 -> InterpolatingFunction[{{-0.0003, 0.000052653}}, <>]}}

Clear[g2]; g2 = Plot[Evaluate[y2[x] /. solut2[[1]]], {x, -t1[[1]], x0}]

```



- Graphics -



The proposed numerical program was verified by the experimental data obtained from the Ni/Pd multi-foil couple. Fig. A4.1 shows the displacement curves where the solid dots represent the experimental values of the multi-foil couple and the continuous line corresponds to the displacement curve as determined by applying the numerical program on the velocity curve from Fig. 3.12. As expected, they coincide satisfactorily. The position of the Kirkendall plane was found at  $x_0 = 18.8 \mu\text{m}$  which corresponds exactly with the experimental value (Fig. 3.11).

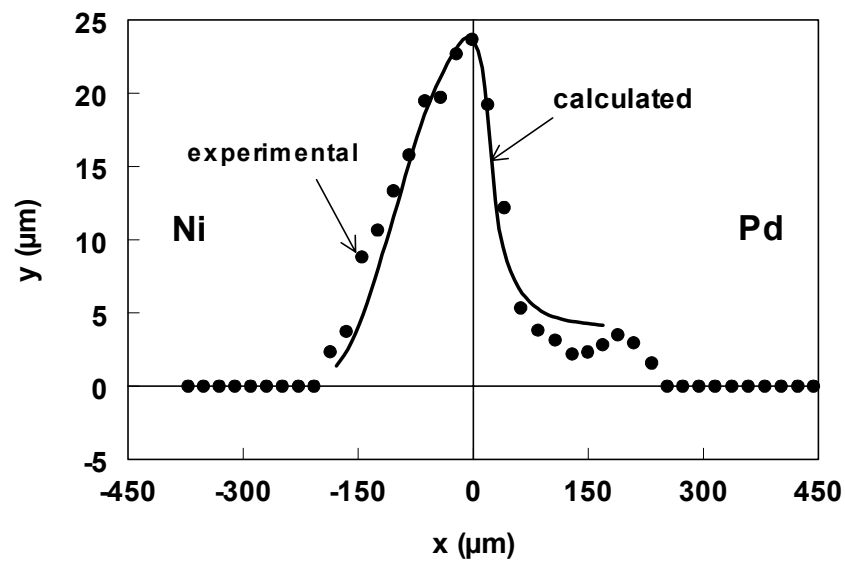


Figure A4.1: The Kirkendall displacement curve of the Ni/Pd multi-foil diffusion couple (1100 °C; 121 h). The dots represent the experimental data (Fig. 3.11) whereas the solid line corresponds to the displacement curve calculated from the velocity curve (Fig. 3.12) by applying the numerical program.



## Chapter 5

### Diffusion in multi-phase systems<sup>1</sup>

#### 5.1 Introduction

The second part of this thesis will be devoted to diffusion phenomena and manifestations of the Kirkendall effect in multi-phase systems that mainly consist of line-compounds, i.e. compounds exhibiting a narrow homogeneity range. The Co-Si system was chosen for studying because of its relatively simple nature and the availability of the thermodynamics on the Co-silicides. Fig. 5.1 shows the phase diagram of the Co-Si system [1].

The phases relevant for the present study are: (1) the Co-rich, fcc terminal solid solution,  $\alpha$ -Co; (2) the Co-rich, cph terminal solid solution,  $\epsilon$ -Co, (3) the orthorhombic  $\text{Co}_2\text{Si}$  phase, C23 structure, (4) the cubic  $\text{CoSi}$  phase, B20 structure, (5) the cubic  $\text{CoSi}_2$  phase, C1 structure, and finally (6) Si with a cubic A4 (diamond) structure. The high-temperature  $\alpha$ - $\text{Co}_3\text{Si}$  phase and  $\beta$ - $\text{Co}_2\text{Si}$  phase were not studied in the present investigations. In the following, we will see that the structures of the Co-Si phases will greatly influence the diffusion properties of the

---

<sup>1</sup> The contents of Chapter 5 has been published as a paper: M.J.H. van Dal, D.G.M.M. Huibers, A.A. Kodentsov and F.J.J. van Loo, *Intermetallics* **9** (2001) 409.



diffusing species Co and Si. It will be shown (see Chapter 6) that this will lead to quite peculiar manifestations of the Kirkendall effect.

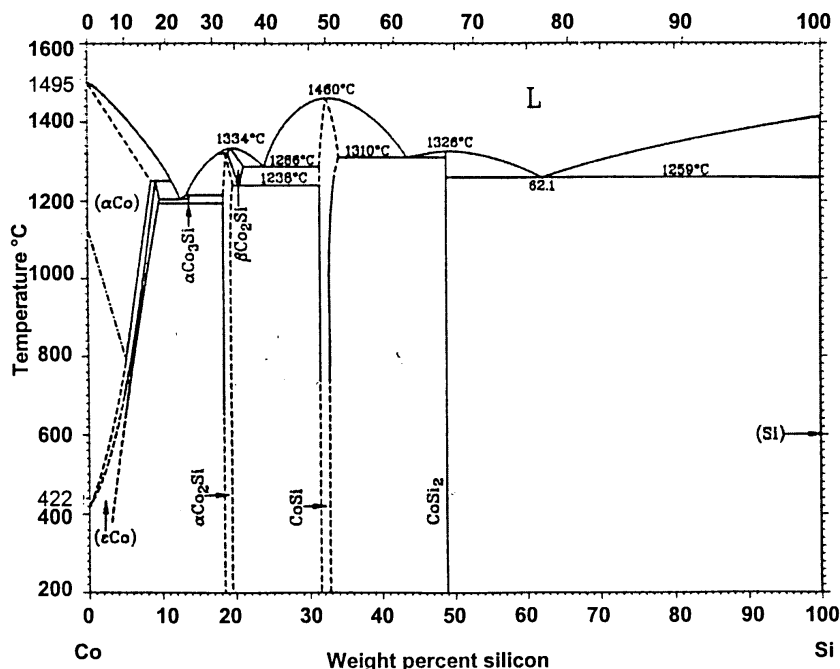


Figure 5.1: The Co-Si phase diagram [1].

An increasing interest exists in Co-Si intermetallics both from a scientific and a technological point of view. Cobalt silicides (particularly CoSi<sub>2</sub>) attract much attention because of their possible application in Very Large Scale Integrated (VLSI) technology as an interconnect material [2]. In view of the intimate relationship between microstructure and properties of the contacts, understanding (and control) of the silicide formation is paramount to obtain desirable metallization. More recently, the role of silicides in joining technology and composites has also become apparent: if one tries to connect Si-containing ceramics (e.g. SiC or Si<sub>3</sub>N<sub>4</sub>) to cobalt or its alloys by solid state bonding, the silicides are often a reaction product.

It should be mentioned right away that the majority of the investigations up to now were carried out using diffusion couples in which one of the component elements (usually Co) was limited in material supply, i.e. in thin-film form. With such sample configuration, the interpretation of the experimental results is rather difficult; interdiffusion in thin films does not always have the general characteristics of bulk diffusion [3,4]. The early stage of

interaction can include the presence of non-equilibrium phases, the absence of equilibrium phases, non-equilibrium and time-dependent interface compositions. High fluxes of components as the result of extremely steep concentration gradients and a diffusion flux, which can be dominated by grain boundary or other extended defect mechanisms, may affect the reaction behaviour. In addition, the description of multi-phase diffusion in thin films may further be complicated by surface phenomena, epitaxial relations, induced stresses and the anisotropy associated with single-crystal substrates.

In this respect, diffusion properties of intermetallic phases are easy to investigate by microscopical examination of sectioned bulk diffusion couples. There have been sporadic attempts to rationalise interactions in the Co-Si system using this type of diffusion technique [5,6]. The authors addressed a broad range of issues involving reaction kinetics by analysing multiple product layers grown from pure cobalt and silicon end-members. However, the data derived from these experiments are not always suitable to evaluate diffusion parameters and species mobilities in the cobalt silicides.

The approach that has been chosen in the present work is to examine bulk semi-infinite diffusion couples in which one single-phased layer of intermetallic compound (silicide) is diffusion-grown from its saturated adjacent phases. The parabolic growth constant determined in this way measures a unique property of a given phase that is independent of the adjacent phases [7]. This provides a framework to determine all important diffusion parameters of the intermetallic phase in question if also the thermodynamic data are known.

The primary objective here is to provide information on the relative mobilities of species in the Co-Si intermetallics by the application of incremental diffusion couples and to present a quantitative analysis of the interrelation between the thermodynamics and the growth kinetics of the cobalt silicides.

Before we start to illustrate specific cases of intermetallic phase formation in the Co-Si system, we will give some details about the theoretical analysis and the thermodynamic information needed to obtain diffusion parameters of the Co-silicides.

## 5.2 Relations between the thermodynamics and the growth kinetics of binary line-compounds

Let us consider the diffusion-controlled growth of an intermetallic compound  $\gamma$  between the adjacent  $\alpha$  and  $\beta$  phases in the A-B binary system (Fig. 5.2). Suppose that all these phases have a narrow homogeneity range, i.e. have virtually constant composition with mole fractions as  $N_A(\alpha) > N_A(\gamma) > N_A(\beta)$ . Despite the very small concentration gradient within the growing  $\gamma$  phase layer there may be, however, a rather high activity gradient providing the necessary driving force for diffusion.

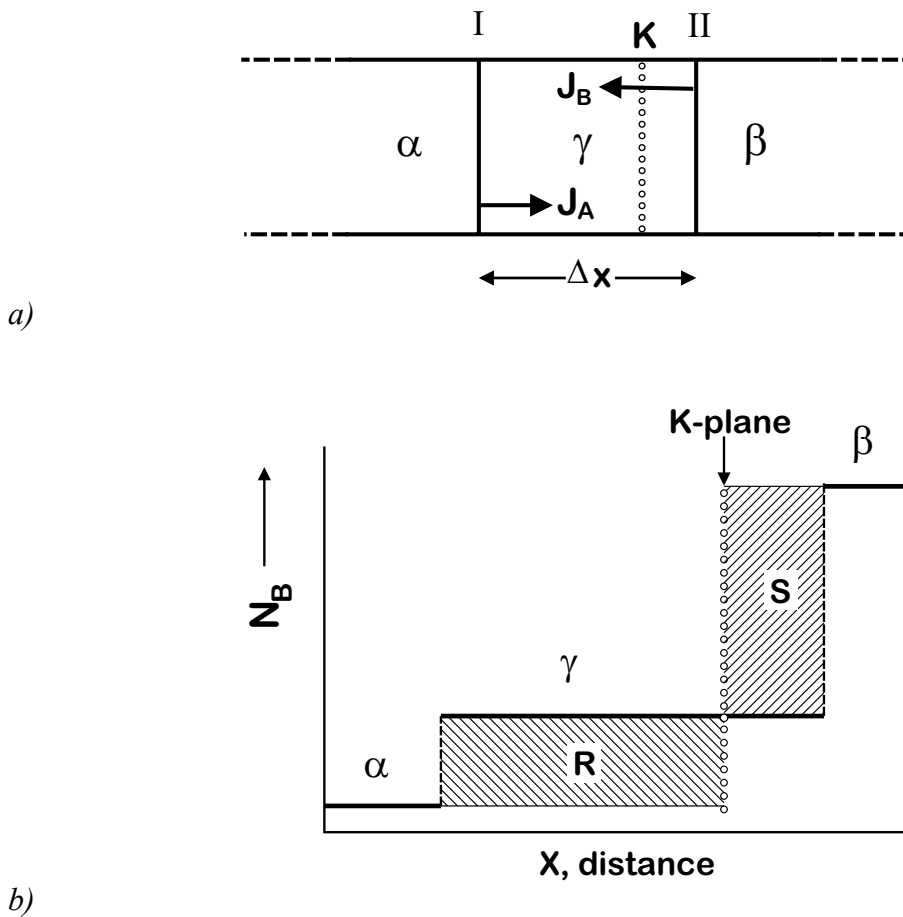


Figure 5.2: a) A hypothetical reaction couple of the binary A-B system with a product layer of the  $\gamma$ -phase (line compound) growing between the line compounds  $\alpha$  and  $\beta$  (the letter K indicates the position of the Kirkendall plane); b) corresponding distribution of component B across the diffusion zone.

The analysis adopted in the present paper is based upon the assumption that the intermediate silicide phases  $\text{Co}_2\text{Si}$ ,  $\text{CoSi}$  and  $\text{CoSi}_2$  are stoichiometric. That is true for  $\text{CoSi}_2$  and it is a very good approximation for  $\text{Co}_2\text{Si}$  and  $\text{CoSi}$ , which exhibit in the temperature range studied narrow homogeneity ranges of 32.5-33.5 at.% and 49.0-50.5 at.% of Si, respectively [1]. Further local equilibrium is assumed in all regions throughout the diffusion zone.

It may be recalled that a fundamental quantity reflecting the interplay between thermodynamics and mobilities of the species involved in the interaction is the intrinsic diffusion coefficient,  $D_i$ , of a component  $i$  in the intermetallic layer. This coefficient is directly related to the atom flux with respect to the position of fiducial markers placed in the diffusion zone. The markers introduced at the original interface at  $t = 0$  define the so-called Kirkendall plane, a convenient plane of reference. In the diffusion couple considered here, the ratio of intrinsic diffusivities  $D_A/D_B$  in the  $\gamma$  intermetallic can be found as (Eq. 3.14) [8]:

$$\frac{D_A}{D_B} = \frac{V_A}{V_B} \left[ \frac{N_A^+ \cdot R - N_A^- \cdot S}{-N_B^+ \cdot R + N_B^- \cdot S} \right], \quad (5.1)$$

where  $R$  and  $S$  equal the hatched areas in Fig. 5.2b,  $N_i$  is the molar fraction and  $V_i$  is the partial molar volume of the component  $i$ . The superscripts + and – refer to the mole fraction of component  $i$  in the end-members of the diffusion couple. In this case,  $N_i^+ = N_i(\beta)$  and  $N_i^- = N_i(\alpha)$ . The molar volume  $V_m$  in the  $\gamma$ -layer is supposed to be constant over its (negligible) homogeneity range.

It should be remarked that for line-compounds, the values of partial molar volumes are generally not available. One could circumvent this problem by taking  $D_A V_B$  and  $D_B V_A$  as material constants, which can be determined.

The intrinsic diffusion coefficients are related to the tracer diffusion coefficients  $D_i^*$  in the homogeneous phase of the same composition by Eq. (3.22):

$$D_B = D_B^* \cdot \frac{V_m}{V_A} \frac{d \ln a_B}{d \ln N_B},$$

with  $\left[ \frac{d \ln a_B}{d \ln N_B} \right] = \left[ \frac{d \ln a_A}{d \ln N_A} \right]$  being the thermodynamic factor ( $a_i$  is the chemical activity of component  $i$  with pure element  $i$  under the experimental conditions as the reference state,  $N_i$  is the mole fraction and  $V_m$  is the molar volume in  $\text{m}^3$  per mole of atoms). The vacancy wind factor associated with asymmetric availability of vacancies to the diffusing atoms (or Manning's correction) is not added to Eq. (3.22) [9]. We will express our ideas on the vacancy wind effect later on in section 5.7.

Substituting Eq. (3.22) in Fick's first law we obtain the flux equations:

$$J_B = -D_B^* \cdot \frac{V_m}{V_A} \frac{d \ln a_B}{d \ln N_B} \cdot \frac{\partial C_B}{\partial x} \quad (5.2a)$$

and

$$J_A = -D_A^* \cdot \frac{V_m}{V_B} \frac{d \ln a_A}{d \ln N_A} \cdot \frac{\partial C_A}{\partial x} = D_A^* \cdot \frac{V_m}{V_A} \frac{d \ln a_B}{d \ln N_B} \cdot \frac{\partial C_B}{\partial x} \quad (5.2b)$$

The flux equations (5.2a) and (5.2b) can be integrated using  $dC_A = (V_B / V_m^2) dN_A$  and  $dC_B = (V_A / V_m^2) dN_B$ :

$$J_A \cdot \Delta x = -D_A^* \cdot \frac{N_A}{V_m} (\ln a_A^{\text{II}} - \ln a_A^{\text{I}}) \quad (5.3a)$$

$$J_B \cdot \Delta x = -D_B^* \cdot \frac{N_B}{V_m} (\ln a_B^{\text{I}} - \ln a_B^{\text{II}}), \quad (5.3b)$$

where superscripts I and II refer to the phase boundaries (Fig. 5.2a).

Equations (5.3a) and (5.3b) can be written in terms of change in Gibbs free energy, i.e.  $\Delta_r G_A^\theta = RT \ln a_A^{\text{II}} - RT \ln a_A^{\text{I}}$  and  $\Delta_r G_B^\theta = RT \ln a_B^{\text{I}} - RT \ln a_B^{\text{II}}$  [10,11]:

$$J_A \cdot \Delta x = -D_A^* \cdot \frac{N_A(\gamma)}{V_m(\gamma)} \cdot \frac{\Delta_r G_A^0}{RT} \quad (5.4a)$$

and

$$J_B \cdot \Delta x = -D_B^* \cdot \frac{N_B(\gamma)}{V_m(\gamma)} \cdot \frac{\Delta_r G_B^0}{RT}, \quad (5.4b)$$

with  $V_m(\gamma)$  being the molar volume of the growing phase  $\gamma$ . The values of  $\Delta_r G_A^0$  and  $\Delta_r G_B^0$  can be visualised with the help of the thermodynamic stability diagram of the A-B system using the common tangent construction. This procedure is shown in Fig. 5.3.

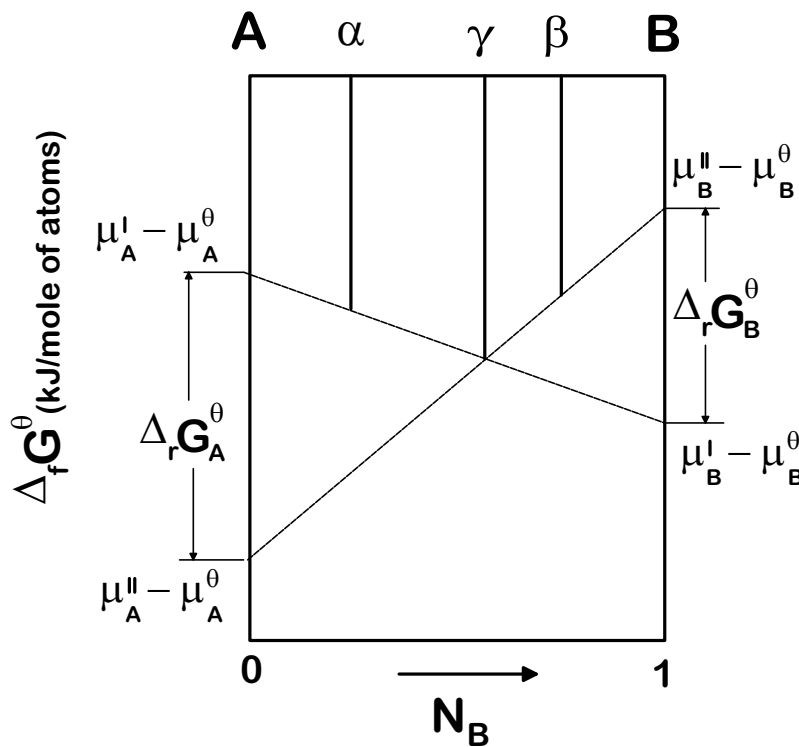


Figure 5.3: Stability diagram of the A-B system with three line compounds  $\alpha$ ,  $\gamma$  and  $\beta$ .  $\Delta_r G_A^0$  and  $\Delta_r G_B^0$  indicate the change of the Gibbs free energy during the isothermal formation of the  $\gamma$ -phase in the  $\alpha/\beta$  couple per moving A- and B-atom, respectively.

It can be seen that, for example,  $\Delta_f G_A^0$ , the Gibbs energy of reaction per moving atom A, is equal (per definition) to  $\Delta\mu_A$ , which is the difference of the intersections of the common tangents to the  $\Delta_f G^0$  “curves” of the coexisting phases on the ordinate at  $N_B = 0$ .

Following Wagner [7], the diffusion-controlled growth of the line-compound  $\gamma$  in between phases  $\alpha$  and  $\beta$  coexisting with  $\gamma$  in the binary A-B system can be described by the parabolic rate constant:

$$k_p = \frac{(\Delta x)^2}{2t} \quad (5.5)$$

where  $\Delta x$  is the reaction layer thickness and  $t$  is the annealing time.

On the other hand, when phases with a very narrow region of homogeneity are formed during solid-state reaction, the concept of the integrated diffusion coefficient  $\tilde{D}_{\text{int}}$  can be used to describe the redistribution of the elements across the interaction zone [7]. This material constant is defined for a line-compound as the interdiffusion coefficient  $\tilde{D}$  in this phase integrated over its (unknown) homogeneity limits  $N'$  and  $N''$  ( $N$  is the molar fraction):

$$\tilde{D}_{\text{int}} = \int_{N'}^{N''} \tilde{D} dN. \quad (5.6)$$

In the case of a system having only phases with a narrow region of homogeneity, the integrated diffusion coefficient  $\tilde{D}_{\text{int}}^j$  of phase  $j$  can be written as:

$$D_{\text{int}}^j = (N_i^j - N_i^-) \cdot \frac{(N_i^+ - N_i^j)}{N_i^+ - N_i^-} \cdot \frac{(\Delta x^j)^2}{2t} + \frac{\Delta x^j}{2t} \cdot \frac{(N_i^+ - N_i^j) \sum_{v=2}^{v=j-1} \frac{V_m^j}{V_m^v} (N_i^v - N_i^-) \Delta x^v + (N_i^j - N_i^-) \sum_{v=j+1}^{v=n-1} \frac{V_m^j}{V_m^v} (N_i^+ - N_i^v) \Delta x^v}{N_i^+ - N_i^-}. \quad (5.7)$$

$N^j$  is the mole fraction of the components in phase  $j$ , the superscript  $\nu$  denotes the serial number of the phase. The numbers 1 and  $n$  refer to the end-members. Again, the superscripts  $+$  and  $-$  pertain to the mole fraction of that component in the end-members of the diffusion couple.

If, however, we assume that the molar volume does not change from one phase to the other, Eq. (5.7) takes the form:

$$\tilde{D}_{\text{int}}^{\gamma} = \left[ \frac{a \cdot b}{a + b} \right] \cdot \frac{(\Delta x^{\gamma})^2}{2t} + \frac{\Delta x^{\gamma}}{2t} \cdot \left[ \frac{b \cdot P + a \cdot Q}{a + b} \right] \quad (5.8)$$

with  $P$  and  $Q$  equal the hatched areas in Fig. 5.4 and  $a = N_{\text{B}}^{\gamma} - N_{\text{B}}^{-}$  and  $b = N_{\text{B}}^{+} - N_{\text{B}}^{\gamma}$ , respectively. In the same way the integrated diffusion coefficients for the phases  $\alpha$  and  $\beta$  can be found.

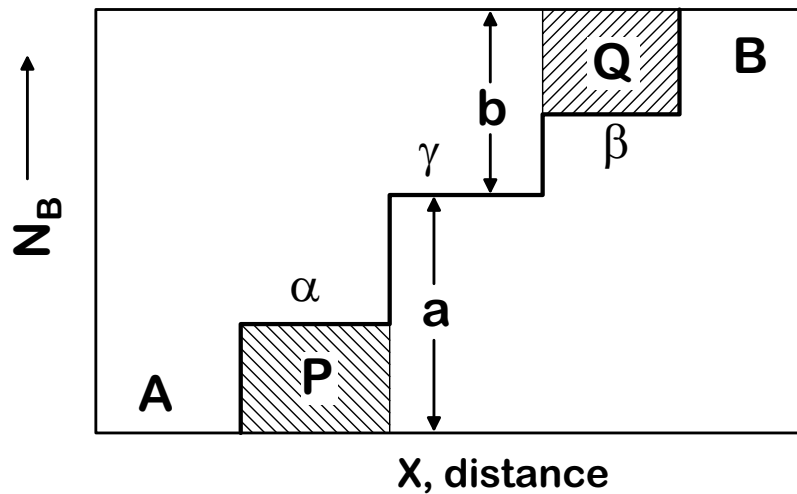


Figure 5.4: Schematic concentration profile of a diffusion couple A/B showing the formation of three line-compounds ( $\alpha$ ,  $\gamma$  and  $\beta$ ) and no terminal solid solutions.

In binary reaction couple where only one phase  $j$  grows between its saturated end-members, the second term in Eq. (5.7) is zero and leads to the simple expression:

$$\tilde{D}_{\text{int}}^j = (N_i^j - N_i^-) \cdot \frac{(N_i^+ - N_i^j)}{N_i^+ - N_i^-} \cdot \frac{(\Delta x^j)^2}{2t} \quad (5.9)$$



One immediately sees that Eq. (5.9) does not depend on the molar volumes of the phases, which can be an advantage for analysing systems where such information is not available.

Since the integrated diffusion coefficient is a material constant, its value does not depend on the starting materials of the reaction couple. This means that the values of  $\tilde{D}_{\text{int}}^{\gamma}$  in the  $\gamma$ -phase (Fig. 5.4) will be the same in an A/B and an  $\alpha/\beta$  incremental diffusion couple.

As shown by Gülpen *et al.* [10,11], combining Eqs. (5.4), (5.6) and Darken's equation (4.3) leads to a general expression for the integrated diffusion coefficient in the  $\gamma$  compound:

$$\tilde{D}_{\text{int}}^{\gamma} = -(N_{\text{B}} \cdot D_{\text{A}}^* + N_{\text{A}} \cdot D_{\text{B}}^*) \cdot \frac{N_{\text{A}} \cdot \Delta_{\text{r}}G_{\text{A}}^{\theta}}{RT}. \quad (5.10)$$

It should be noticed that the term  $N_{\text{A}} \cdot \Delta_{\text{r}}G_{\text{A}}^{\theta}$  equals  $N_{\text{B}} \cdot \Delta_{\text{r}}G_{\text{B}}^{\theta}$ , with  $\Delta_{\text{r}}G_{\text{B}}^{\theta}$  being the Gibbs energy of the net reaction in the case one B atom moves from the interface II to I (Fig. 5.2a). If phase  $\gamma$  grows directly in between pure A and B there is a direct relation between the measured  $\tilde{D}_{\text{int}}$  and the Gibbs energy of formation of the compound,  $\Delta_{\text{r}}G^{\theta}(\gamma)$  as can be appreciated from the stability diagram (Fig. 5.3):

$$\tilde{D}_{\text{int}}(\gamma) = -(N_{\text{B}} \cdot D_{\text{A}}^* + N_{\text{A}} \cdot D_{\text{B}}^*) \cdot \frac{\Delta_{\text{r}}G^{\theta}(\gamma)}{RT}. \quad (5.11)$$

At this point, it is appropriate to consider the pertinent thermodynamic information on Co-silicides available in the literature.

### 5.3 Thermodynamic properties of the Co-silicides

The thermodynamics of the Co-Si intermetallics have been reviewed by Chart [12], Schlesinger [13] and Choi [14]. The most recent review [15] is limited to  $\text{CoSi}_2$ .

The high-temperature heat capacity of  $\text{Co}_2\text{Si}$  has been measured by Frolov *et al.* [16]. No low-temperature heat capacity data for this compound are found. Both high- and low-temperature heat capacities of  $\text{CoSi}$  and  $\text{CoSi}_2$  phases have been determined by Kalishevich *et al.* [17-19]. All these data were obtained by adiabatic calorimetry.

The first attempt to measure the enthalpies of formation of Co-Si intermetallics was made at the end of the thirties by Oelsen *et al.* [20,21] using a direct reaction calorimetry technique. Recently, a very extensive study of vaporisation thermodynamics of the Co-Si binary system has been performed by Lexa *et al.* [22,23]. Both reactive and simple Knudsen effusion mass-spectrometry have been used. The agreement of the reported values of formation enthalpies,  $\Delta_f H_{298}^\theta$ , with the direct calorimetry measurements is very good. The differences do not exceed 3 kJ/mole of atoms, whereas the uncertainties of the techniques are in the order of  $\pm 4.0$  kJ/mole of atoms and  $\pm 2.0$  kJ/mole of atoms, respectively.

The assessed data of Refs. [12,15] are very close to the values obtained in the experiments, which is not surprising since both assessments were based largely on information published by Oelsen *et al.* [20]. The agreement between the experimental measurements and modelled results of Machlin [24] for  $\text{CoSi}$  and  $\text{CoSi}_2$ , Pasturel *et al.* [25] for  $\text{CoSi}$  and  $\text{CoSi}_2$  and Niessen *et al.* [26] for  $\text{Co}_2\text{Si}$  and  $\text{CoSi}$  is acceptable. However, the values of standard formation enthalpies estimated by Pasturel *et al.* for  $\text{Co}_2\text{Si}$  [25] and by Niessen *et al.* [26] for  $\text{CoSi}_2$  are quite different from those determined experimentally. This indicates that, although yielding reasonable results in some cases, the various models used for predicting thermodynamic stability of the Co-silicides are still in need of improvement.

The thermodynamic information adopted in the following discussion is mainly based on the work of Lexa *et al.* [22]. The standard formation enthalpies of Co-Si intermetallic phases at 298 K were obtained by combining these experimental results with available heat capacity and estimated standard entropy values [17-19]. The thermodynamic parameters for Co-silicides used for calculating Gibbs free energy changes of the solid-state reactions analysed in the present study are summarised in Table 5.1.

With respect to the thermodynamic data listed in Table 5.1, one thing should be noted. In the absence of low-temperature heat capacity data for  $\text{Co}_2\text{Si}$ , the value of  $S_{298}^{\theta}$  for this phase was estimated by linear interpolation on a mole of atoms basis between the values for  $\text{CoSi}$  [22] and solid  $\text{Co}$ , with the latter taken from JANAF Tables [27].

Table 5.1

Heat capacity parameters<sup>\*)</sup>, standard entropies,  $S_{298}^{\theta}$  (J/mol·K) and formation enthalpies,  $\Delta_f H_{298}^{\theta}$  (kJ/mole of atoms) of Co-silicides adopted in the present study taken from Ref. [22].

Intermetallic compounds			
	$\text{Co}_2\text{Si}$	$\text{CoSi}$	$\text{CoSi}_2$
A	70.785	49.16	70.86
$B \cdot 10^3$	27.138	12.1	18.66
$C \cdot 10^{-5}$	7.32900	7.5400	9.9300
$S_{298}^{\theta}$	$73.3 \pm 6.0$	$43.2 \pm 6.0$	$64.2 \pm 6.0$
$\Delta_f H_{298}^{\theta}$	$-41.0 \pm 2.0$	$-47.3 \pm 2.0$	$-32.9 \pm 2.0$

$$*) c_p = A + BT - C/T^2$$

#### 5.4 Diffusion in the $\text{CoSi}_2$ intermetallic compound

Diffusion-controlled growth of C1-type  $\text{CoSi}_2$  intermetallic was studied over the temperature range 1000-1217°C in incremental couples based on pure silicon and an equilibrated two-phase alloy with a nominal composition  $\text{Co}_{48}\text{Si}_{52}$ . This alloy consists of a  $\text{CoSi}$ -matrix phase, which is in thermodynamic equilibrium with  $\text{CoSi}_2$ -precipitates. The use of the two-phase material as a constituent of the reaction couples ensures that the composition of the “ $\text{CoSi}$ -reactant” within the end-member corresponds to the phase boundary composition at the Si-rich side of its homogeneity region [1]. In such couples, the  $\text{CoSi}_2$ -intermetallic layer grows

from the saturated adjacent phases, given the negligible solid-state solubility of Co in silicon. The incorporation of  $\text{CoSi}_2$ -precipitates in the growing  $\text{CoSi}_2$ -layer is automatically taken into account in our method of analysis.

Fig. 5.5 shows a representative example of the diffusion zone morphology developed in the  $\text{Co}_{48}\text{Si}_{52}/\text{Si}$  couples after interaction in vacuum at  $1186^\circ\text{C}$ . The two-phase structure of the  $\text{Co}_{48}\text{Si}_{52}$ -alloy is clearly visible on this micrograph. The Kirkendall plane is revealed inside the  $\text{CoSi}_2$ -layer by a row of  $\text{ThO}_2$ -particles introduced at the original contact surface of the couples prior to annealing as inert markers. From the position of the markers, the ratio of intrinsic diffusivities  $D_{\text{Si}}/D_{\text{Co}}$  in the  $\text{CoSi}_2$  intermetallic phase was determined over the temperature range studied by applying Eq. (5.1). These results are presented in Table 5.2.

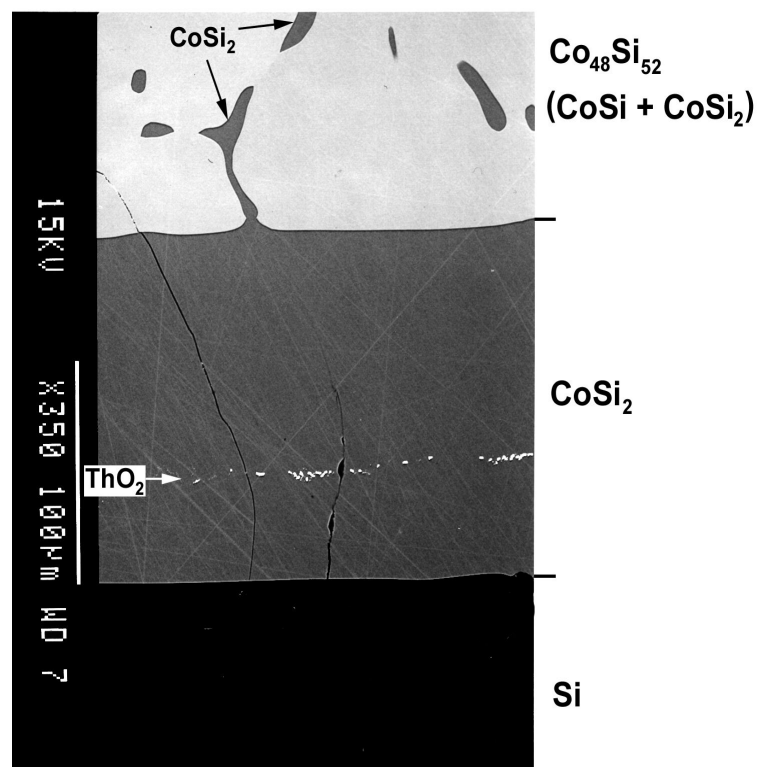


Figure 5.5: BEI of a diffusion zone developed between Si and a two-phase ( $\text{CoSi} + \text{CoSi}_2$ ) alloy with a nominal composition  $\text{Co}_{48}\text{Si}_{52}$  after annealing in vacuum at  $1186^\circ\text{C}$  for 100 h. The Kirkendall plane is revealed within the  $\text{CoSi}_2$  product layer by a row of  $\text{ThO}_2$ -particles used as inert markers.

It was found that the reaction product thickness increased parabolically with time indicating a diffusion-controlled interaction. Using Eq. (5.9), the integrated diffusion coefficient in the  $\text{CoSi}_2$  phase was calculated for different temperatures. The computed values are listed in Table 5.2 and plotted in Fig. 5.6 as a function of reciprocal temperature. One can notice from the graph that the temperature dependence of the integrated diffusion coefficient in the  $\text{CoSi}_2$  intermetallic compound cannot be described by a simple Arrhenius relation in the entire temperature range studied.

Table 5.2

*Ratio of intrinsic diffusivities of Si and Co,  $D_{\text{Si}}/D_{\text{Co}}$ , the integrated diffusion coefficient,  $\tilde{D}_{\text{int}}$ , and the tracer diffusion coefficients of Si and Co,  $D_{\text{Si}}^*$  and  $D_{\text{Co}}^*$ , in the  $\text{CoSi}_2$  compound at various temperatures between 1000-1217 °C as determined in the present work.*

$t$ (°C)	$D_{\text{Si}}/D_{\text{Co}}$	$\tilde{D}_{\text{int}}$ ( $10^{-15} \text{ m}^2/\text{s}$ )	$D_{\text{Si}}^*$ ( $10^{-15} \text{ m}^2/\text{s}$ )	$D_{\text{Co}}^*$ ( $10^{-15} \text{ m}^2/\text{s}$ )
1000	2.3	0.27	0.90	0.39
1048	1.7	0.42	1.24	0.74
1100	1.6	0.78	2.25	1.41
1127	1.0	1.36	2.95	3.01
1156	0.84	2.00	3.91	4.66
1186	1.0	3.31	7.35	7.35
1217	0.6	4.97	7.59	12.9

It should be mentioned that, in general, the temperature dependence of the  $\tilde{D}_{\text{int}}$  does not necessarily follow the Arrhenius law because the homogeneity region of a phase, although very narrow, may also vary with the temperature. Also  $D_{\text{Si}}$  and  $D_{\text{Co}}$  can vary differently with temperature, leading to a non-linear Arrhenius behaviour for  $\tilde{D}_{\text{int}}$ . This can make the relation between  $\tilde{D}_{\text{int}}$  and  $T$  somewhat more complicated. In the case considered here, however, the Arrhenius plot for the integrated diffusion coefficient in  $\text{CoSi}_2$ -intermetallic exhibits a

discernible curvature in the low-temperature domain. This may suggest that besides volume (lattice) diffusion (high temperature part of the graph) also some form of short-circuit diffusion (with a smaller activation energy) contributes to the mass transport at low temperature.

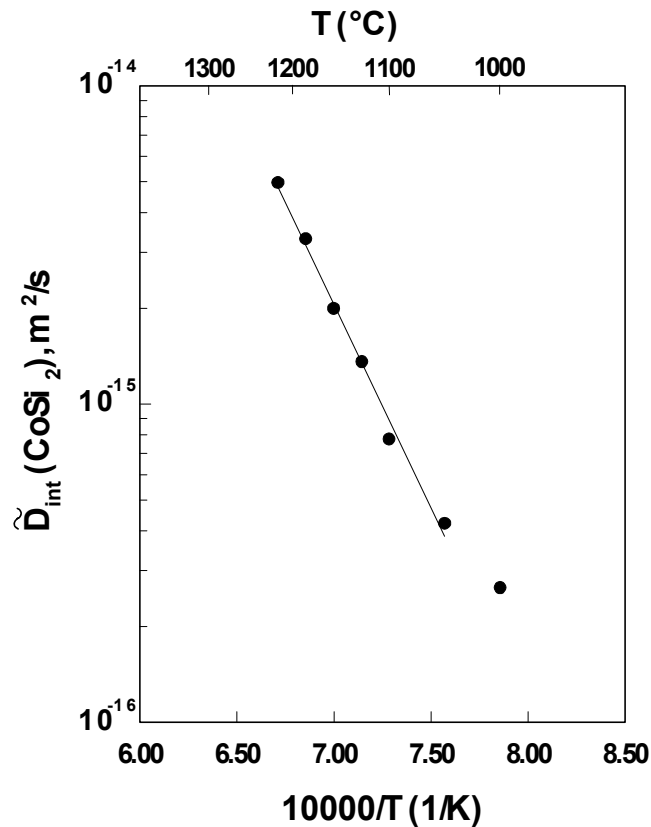
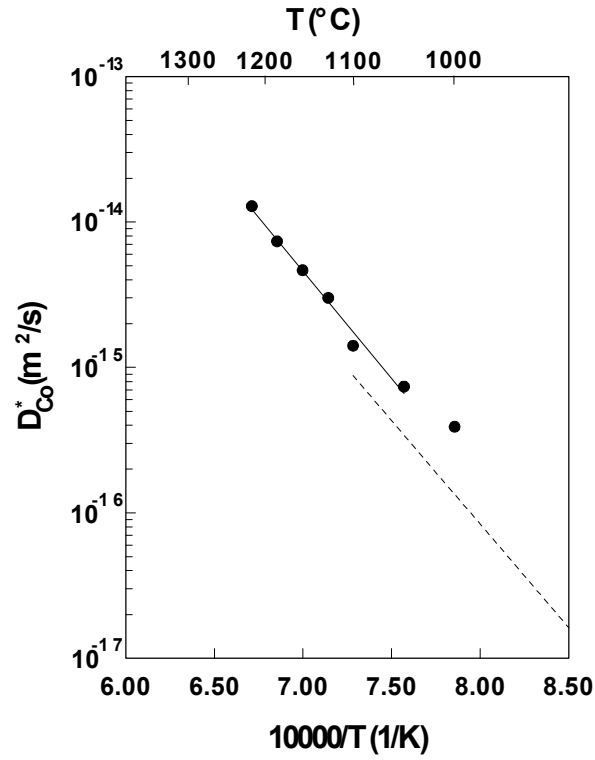


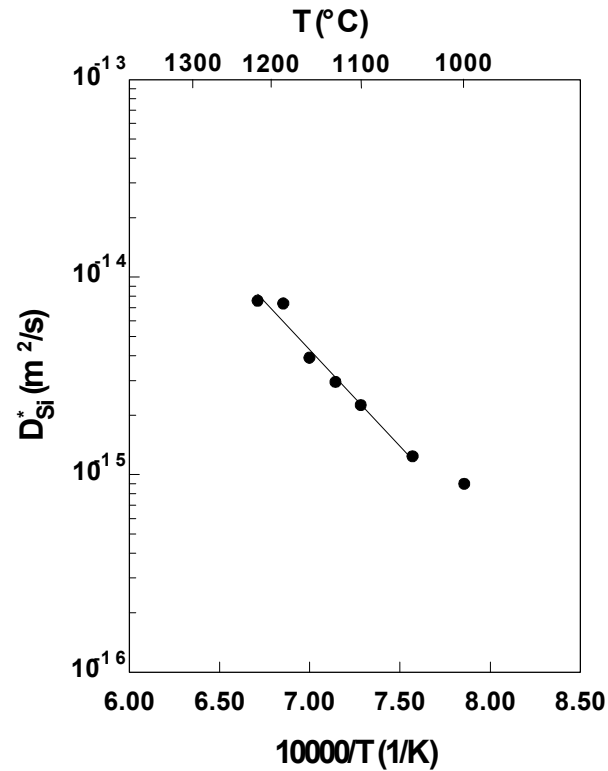
Figure 5.6: The integrated diffusion coefficient in the  $\text{CoSi}_2$ -phase as a function of the reciprocal temperature.

As seen, a reasonably good straight-line fit is obtained for  $\tilde{D}_{\text{int}}(\text{CoSi}_2)$  in the temperature interval 1048-1217°C with a slope that yields an apparent activation energy of approximately 245 kJ/mole (or  $\sim 2.6$  eV).

Further, the tracer diffusion coefficients of the components ( $D_{\text{Co}}^*$  and  $D_{\text{Si}}^*$ ) in  $\text{CoSi}_2$  intermetallic were calculated with Eq. (5.10) at various temperatures using the corresponding  $\tilde{D}_{\text{int}}(\text{CoSi}_2)$ -values in combination with the experimentally found ratios of intrinsic diffusivities  $D_{\text{Si}}/D_{\text{Co}} = D_{\text{Si}}^*/D_{\text{Co}}^*$  and thermodynamic parameters listed in Table 5.1. The results so obtained are presented in Table 5.2 and displayed graphically in Fig. 5.7 in Arrhenius coordinates.



a)



b)

Figure 5.7: Arrhenius plots of the tracer diffusion coefficients: a) of Co and b) of Si in CoSi<sub>2</sub>-intermetallic as determined in the present study. The results of the self-diffusion measurements with <sup>60</sup>Co-radioisotope of Ref. [28] (dashed line in (a)) are given for comparison.

It can be seen that in the temperature range 1048 – 1217 °C the computed tracer diffusivity data are consistent with the customary Arrhenius relationship. The representative lines drawn in Fig. 5.7a and 5.7b may be expressed by the following equations:

$$D_{\text{Co}}^* = 9.8 \cdot 10^{-5} \exp\left(\frac{-283000}{RT}\right) \text{ m}^2/\text{s} \quad (5.12a)$$

$$D_{\text{Si}}^* = 2.8 \cdot 10^{-8} \exp\left(\frac{-186000}{RT}\right) \text{ m}^2/\text{s}, \quad (5.12b)$$

with  $T$  being the absolute temperature and  $R$  is the gas constant (8.3143 J/mol·K). For comparison, the results of self-diffusion of Co obtained for  $^{60}\text{Co}$ -radioisotope tracers determined by Barge *et al.* [28] are included. Although our values seem to be slightly higher (about a factor of 2) than the results of Barge *et al.*, there is a good agreement between the two sets of data (especially the activation energy). Possible error sources of the present analysis will be discussed in section 5.7.

At lower temperatures, the plots slightly deviate from a straight line exhibiting a smaller slope (i.e. smaller activation energies for diffusion) as was found for the integrated diffusion coefficient in the  $\text{CoSi}_2$  phase discussed before. Probably, it can be linked to the influence of short-circuit diffusion on the growth kinetics.

### 5.5 Growth of the B20-type intermetallic CoSi in the $\text{CoSi}_2/\text{Co}_2\text{Si}$ diffusion couples

The formation of the CoSi phase in the reaction between  $\text{CoSi}_2$  and  $\text{Co}_2\text{Si}$  compounds was investigated over the temperature range 914-1217°C. A typical microstructure of the CoSi-reaction product developed in the diffusion zone is shown Fig. 5.8a.

The Kirkendall plane was found inside the intermetallic product layer as a row of  $\text{ThO}_2$ -particles (markers) exhibiting a “white” contrast on the back-scattered electron micrograph. It can be seen that the morphology of the growing phase layer is quite different on either side of the Kirkendall plane. On the Co-rich side of the reaction zone, grains of cubic CoSi are



relatively large and have a columnar shape, whereas the Si-rich side favours smaller grains of more or less columnar morphology. This phenomenon is related to the differences in nucleation of the CoSi-grains at the reaction interfaces. Since the differently nucleated grains of the product phase meet at the Kirkendall plane, this plane can readily be seen even without the presence of any inert markers.

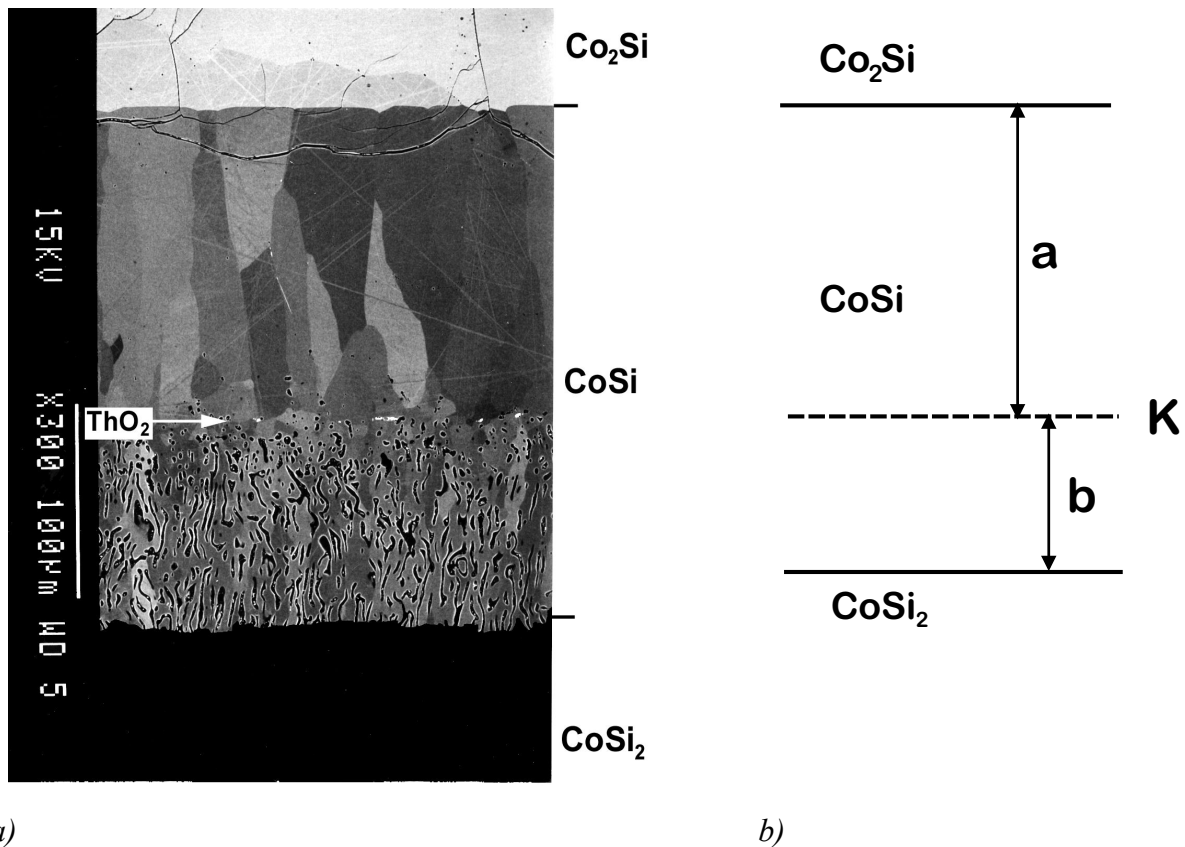


Figure 5.8: a) BEI of a  $\text{Co}_2\text{Si}/\text{CoSi}_2$  diffusion couple after reaction at  $1000^\circ\text{C}$  for 49 h in vacuum. The Kirkendall plane is revealed by the  $\text{ThO}_2$ -markers exhibiting a white contrast on the micrograph; b) schematic situation if 23 % pore formation is taken into account.

Another important aspect of the interaction in the  $\text{CoSi}_2/\text{Co}_2\text{Si}$  couples can be seen from Fig. 5.8a. The reaction between  $\text{CoSi}_2$ - and  $\text{Co}_2\text{Si}$ -compounds is accompanied by the formation of numerous pores (voids) in the part of the  $\text{CoSi}$ -product layer next to the  $\text{CoSi}_2$  end-member. The appearance of the continuous heavily voided band within the growing phase layer provokes curiosity since this is certainly not a usual situation. The observed phenomenon might be attributed to the net volume change during the diffusion interaction in these couples.

The molar volume of the  $\text{Co}_2\text{Si}$ ,  $\text{CoSi}$  and  $\text{CoSi}_2$  are 6.65, 6.62 and 7.75  $\text{cm}^3/\text{mole}$  of atoms, respectively [1,29]. This means that a significant shrinking of the reaction couple takes place upon the formation of  $\text{CoSi}$ -intermetallic from its adjoining phases.

Given the rather poor mechanical characteristics of the Co-silicides, it is conceivable that the volume difference is not healed through plastic deformation, but pertains as pores. It is interesting that the pore formation occurs only in the part of the  $\text{CoSi}$ -reaction layer, which is contiguous with the  $\text{CoSi}_2$  end-member. An explanation for this morphological feature will be discussed later on.

It is important to realise that the theoretical treatment introduced earlier in this paper is based on a presumption that the total volume remains constant and that no voids or changes in the local cross-section of the diffusion couple develop. Therefore, in the case at hand, the kinetic data derived directly from diffusion couple experiments had to be corrected by taking into account the porosity of the  $\text{CoSi}$ -product layer. To this end, a sufficiently large number of randomly selected cross-sections of the  $\text{CoSi}$ -layer were subjected to an areal analysis using an image processing software (e.g. Image Pro Plus for Windows). In this manner, an average porosity value of this part of the product layer (i.e. the part of the  $\text{CoSi}$  layer between the Kirkendall plane and the  $\text{CoSi}/\text{CoSi}_2$  phase boundary) was estimated as about 23( $\pm$ 2)% relative for all diffusion couples annealed in the temperature interval 914-1217°C. In all further calculations, the thickness measurements have been corrected for this volume effect, see Fig. 5.8b.

As an example, three sets of corrected data at different temperatures are shown in Fig. 5.9. The square of the  $\text{CoSi}$ -layer thickness in the  $\text{CoSi}_2/\text{Co}_2\text{Si}$  reaction couple increases linearly with time, which is indicative for a diffusion-limited kinetics.

The corrected results of the layer thickness measurements were also used to determine the integrated diffusion coefficient of  $\text{CoSi}$ ,  $\tilde{D}_{\text{int}}(\text{CoSi})$ , at different temperatures. The values computed with Eq. (5.9) are given in Table 5.3. If these data are plotted in Arrhenius coordinates, an essentially straight line is obtained (Fig. 5.10).

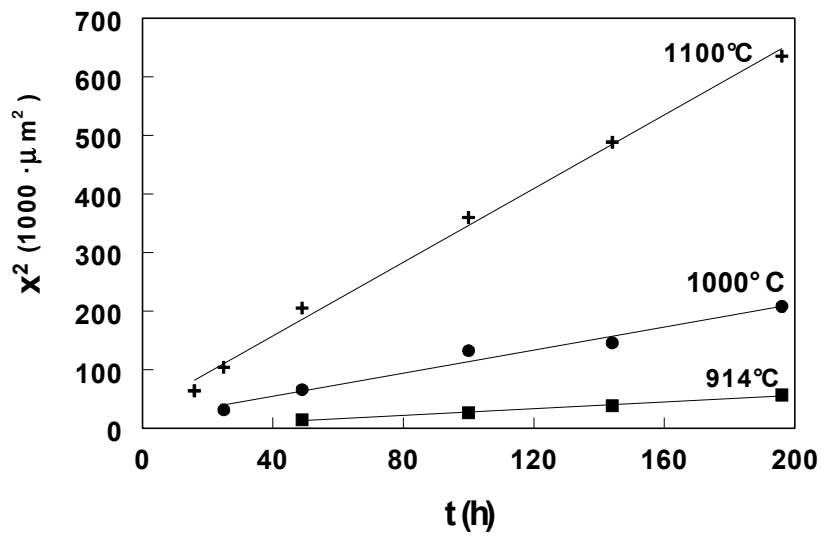


Figure 5.9: Parabolic growth of the CoSi-intermetallic layer in  $\text{Co}_2\text{Si}/\text{CoSi}_2$  diffusion couples.

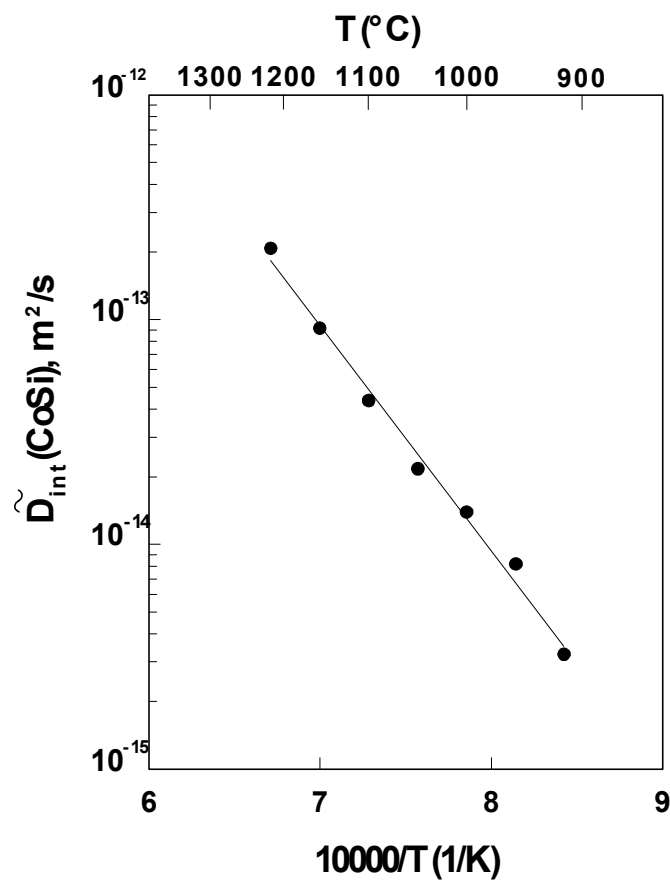


Figure 5.10: Arrhenius diagram of the integrated diffusion coefficient in the CoSi-phase.

From the graph, the apparent activation energy of about 192 kJ/mol ( $\sim 2.0$  eV) and the pre-exponential factor of  $\sim 9.7 \cdot 10^{-7}$  m<sup>2</sup>/s were found.

For each analysed CoSi<sub>2</sub>/Co<sub>2</sub>Si-couple, the ratio of intrinsic diffusivities of the components in the CoSi-phase,  $D_{\text{Si}}/D_{\text{Co}} = D_{\text{Si}}^*/D_{\text{Co}}^*$ , was deduced from the observed location of the Kirkendall plane by applying Eq. (5.1) (see also construction in Fig. 5.2b). The pore formation within the reaction product layer was taken into account. The results are summarised in Table 5.3.

As seen from the table, the values of the  $D_{\text{Si}}/D_{\text{Co}} = D_{\text{Si}}^*/D_{\text{Co}}^*$  ratio found in our experiments are ranging from 20 to, in principle, infinite. In fact the message here is simple: when one of the components is by far the fastest diffusing species in the product layer, the value of the ratio of their intrinsic diffusivities in this phase is very sensitive to small errors in determining the Kirkendall plane position. Bastin *et al.* [30] pointed out that the accuracy of the measured position of the Kirkendall plane is not enough to differentiate between values of 10 and infinite for the ratio of the intrinsic diffusion coefficients. In Fig. 5.8b this is reflected by the ratio a : b, which equals 2 : 1 in accordance with the exclusive diffusion of Si atoms.

Table 5.3:

*Ratio of intrinsic diffusivities of Si and Co,  $D_{\text{Si}}/D_{\text{Co}}$ , the integrated diffusion coefficient,  $\tilde{D}_{\text{int}}$  and the tracer diffusion coefficient of Si,  $D_{\text{Si}}^*$ , in the CoSi compound at various temperatures between 914 - 1217 °C as determined in the present work.*

t (°C)	$D_{\text{Si}}/D_{\text{Co}}$	$\tilde{D}_{\text{int}}$ (10 <sup>-15</sup> m <sup>2</sup> /s)	$D_{\text{Si}}^*$ (10 <sup>-15</sup> m <sup>2</sup> /s)
914	20 - ∞	3.24	1.49
955	69	8.19	6.57
1000	48 - ∞	13.9	11.7
1048	87	21.7	19.1
1100	20 - ∞	43.6	40.5
1156	∞	91.7	89.8
1217	∞	208	216

The present investigation proves that at 914-1217°C silicon is by far the most (or even virtually the only) mobile species in the B20-type CoSi intermetallic, i.e.  $D_{\text{Si}}^* \gg D_{\text{Co}}^*$ . This may also explain why the porosity appeared only in the part of the diffusion-grown CoSi-layer, which is contiguous with CoSi<sub>2</sub> end-member. Since Si is virtually the only mobile species in the CoSi-intermetallic, the Kirkendall effect-induced pore formation takes place exclusively at the “CoSi<sub>2</sub>-side” of the reaction product, which loses half its Si-content. If no plastic relaxation would occur, this would lead to a porosity of 43 %. (This values has been determined taking the maximum porosity as  $(3 \cdot V_{\text{m}}(\text{CoSi}_2) - 2 \cdot V_{\text{m}}(\text{CoSi})) / 3 \cdot V_{\text{m}}(\text{CoSi}_2)$  and the molar volumes of CoSi<sub>2</sub>  $V_{\text{m}}(\text{CoSi}_2) = 7.75 \cdot 10^{-6} \text{ m}^3/\text{mole}$  of atoms and CoSi  $V_{\text{m}}(\text{CoSi}) = 6.62 \cdot 10^{-6} \text{ m}^3/\text{mole}$  of atoms [1,29]).

No tracer diffusion data for the CoSi-phase are available. There is, however, one report due to Salamon and Mehrer [31] about self-diffusion in the isomorphous compound FeSi, which has the same B20-crystal structure as CoSi. The authors show that Si diffuses much faster in this phase, which is in line with our results on CoSi.

Now, using the data on the integrated diffusion coefficient,  $\tilde{D}_{\text{int}}(\text{CoSi})$ , and the thermodynamic parameters given in Table 5.1, the corresponding values of tracer diffusion coefficients of silicon,  $D_{\text{Si}}^*$ , in the CoSi ordered phase can be obtained with Eq. (5.10). The results so estimated for the temperature interval 914-1217°C are listed in Table 5.3.

The same set of computed values is also presented graphically in Fig. 5.11 as a function of the reciprocal temperature. In this case, least-squares fit of an Arrhenius equation yields for tracer diffusion of silicon in the CoSi intermetallic:

$$D_{\text{Si}}^* = 3.2 \cdot 10^{-6} \exp\left(\frac{-206000}{RT}\right) \text{ m}^2/\text{s} . \quad (5.13)$$

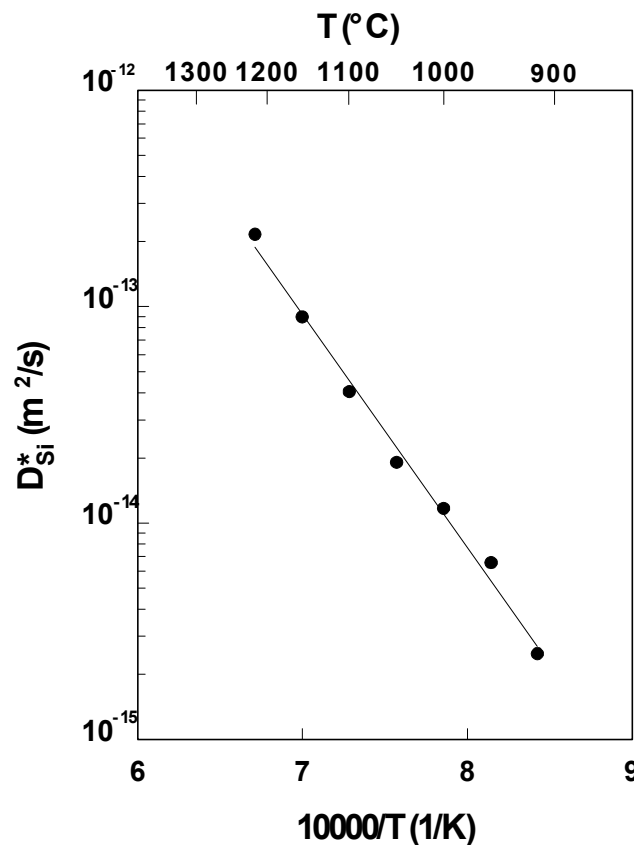


Figure 5.11: Arrhenius plot of the tracer diffusivity of Si in the CoSi-phase obtained in the present investigation.

### 5.6 Relative mobilities of species in the C23-type intermetallic Co<sub>2</sub>Si at 1100°C

Discussion in this section on the Co<sub>2</sub>Si-intermetallic growth in the incremental couples is confined to the diffusion interaction at 1100°C. Two-phase alloys with nominal composition Co<sub>52</sub>Si<sub>48</sub> and Co<sub>81</sub>Si<sub>19</sub> were used as end-members of the diffusion couples. The former alloy after equilibration at this temperature consists of a CoSi-matrix and Co<sub>2</sub>Si-precipitates, and the latter composition corresponds to the material that contains a hexagonal ε-Co(Si)-matrix phase and Co<sub>2</sub>Si-inclusions. Apparently, both of the alloy matrices are saturated with respect to Co<sub>2</sub>Si. The two-phase morphology of the initial couple halves is easy to see in Fig. 5.12, which shows a typical microstructure of the diffusion zone after interaction at 1100°C in vacuum. The Kirkendall plane was revealed by a row of ThO<sub>2</sub>-inclusions (markers) and by different appearance of grains within the Co<sub>2</sub>Si-product layer. As in the cases described before, the ratio of intrinsic diffusivities of the components in the Co<sub>2</sub>Si-phase,  $D_{\text{Si}}/D_{\text{Co}}$ , was

estimated from the position of the Kirkendall markers inside the phase layer using Eq. (5.1). It was found that at 1100 °C cobalt diffusion in orthorhombic  $\text{Co}_2\text{Si}$  is about 10 times faster than that of Si.

The growth of the intermetallic layer obeys the parabolic law underlying a diffusion-controlled process. On the basis of the thickness measurements, the integrated diffusion coefficient at 1100 °C in the  $\text{Co}_2\text{Si}$ ,  $\tilde{D}_{\text{int}}(\text{Co}_2\text{Si})$ , of  $\sim 2.13 \cdot 10^{-14} \text{ m}^2/\text{s}$  was obtained with Eq. (5.9).

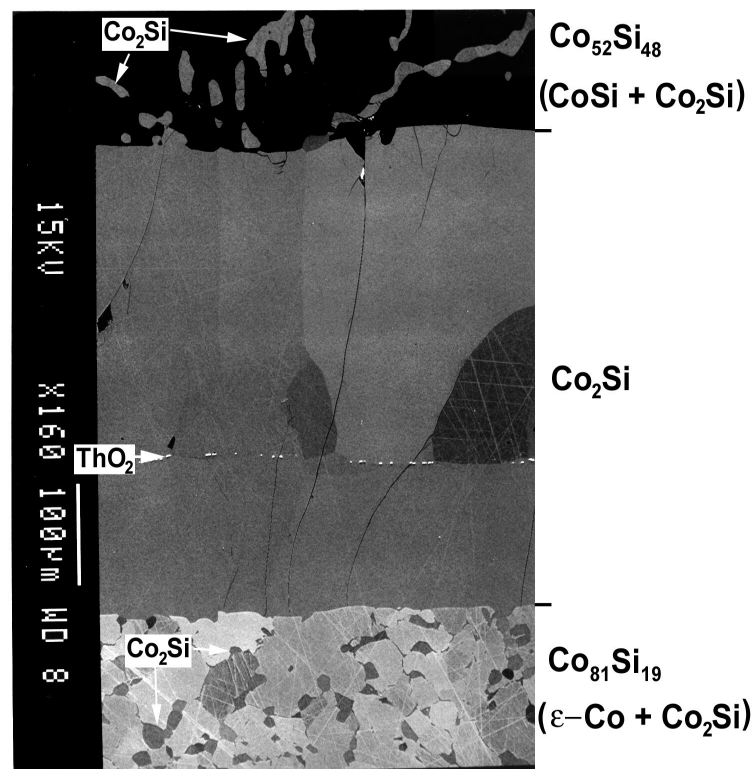


Figure 5.12: BEI showing the growth of the  $\text{Co}_2\text{Si}$ -intermetallic in an annealed  $\text{Co}_{52}\text{Si}_{48}/\text{Co}_{81}\text{Si}_{19}$  diffusion couple (1100 °C; 100 h; vacuum). The two-phase structure of the initial end-members is clearly visible. The Kirkendall plane appears as a straight row of the  $\text{ThO}_2$ -particles used as inert markers.

Unfortunately, no thermodynamic information on the  $\epsilon$ -Co(Si) phase is available in the literature. Therefore, absolute values of the tracer diffusivities  $D_{\text{Co}}^*$  and  $D_{\text{Si}}^*$  could not be deduced from the diffusion couple experiments.

### 5.7 Deficiencies of the proposed analysis

From a theoretical as well as a practical point of view, it is interesting to have means that enable us to obtain tracer diffusivities (atomic mobilities) of species in an ordered phase (intermetallic compound) using just data that are relatively easily attainable in experiments (like growth constants or integrated diffusion coefficients and thermodynamical information). Such a technique has an obvious advantage. It is not necessary to produce intermetallics in their pure form and apply radioactive tracers, that can be not only very tedious and time-consuming, but frequently it is not possible at all. The latter can be due to the lack of a relevant radioactive tracer or to technical difficulties in preparing of single-phased intermetallic alloys.

However, judicious cautions should be exercised in applying the proposed general deductions in evaluating diffusion transport during the Co-silicide formation. In this respect, several points are to be noted.

The first problem that may arise is the reliability of the thermodynamic information that can be found in the literature or in various databanks. It is important to emphasise that the accuracy in calculating Gibbs energy change  $\Delta_r G_i^0$  (per one moving  $i$ -atom) cannot be expected to be very high. Apparently, this is because of the change in Gibbs energy in the net reactions per one moving atom is sensitively dependent on the Gibbs energies of formation of the Co-silicides as can be appreciated from Fig. 5.3.

Secondly, the term  $V_A/V_B$  in the  $D_A/D_B$  ratio (Eq. 5.1) can be determined only if the variation of the molar volume of the phase within the homogeneity region is known. Especially for phases with a very narrow region of homogeneity this relation is commonly unknown and there is no simple experiment to obtain it. If this term is assumed to be equal to unity then it implies that the molar volume is constant over the very small homogeneity range. At first



sight, this seems to be a reasonable assumption. However, one has to realise that even a small deviation from a constant volume may affect the  $V_A/V_B$ -ratio considerably because the change in atomic fraction from one compositional limit of the stability region to the other is very small, too.

Another aspect that might cause uneasiness in determining the ratio of the intrinsic diffusion coefficients in the silicide phases regards the Kirkendall plane location within a product phase layer. As already stated, very great accuracy in measuring the position of the Kirkendall plane is required to get reliable values for this ratio, especially when this is larger than about 10.

Thirdly, in the analysis employed in the present paper the vacancy wind factor is not taken into account. This becomes important only if one wants to correlate intrinsic and tracer diffusion coefficients (Eq. (3.22)). It should be remembered that this term was introduced by Manning [9] on the basis of his random-alloy model. It is not clear for now whether and how the Manning's approach can be applied to ordered alloys, particularly to the B20(CoSi)- and C1(CoSi<sub>2</sub>)-structures studied here. Apart from theoretical studies [9] (see, for example, [32,33]), it should be remarked here that to the author's knowledge no consistent experimental data on the vacancy wind factor have been published.

Finally, it should be stressed that in the foregoing discussion we tacitly assumed that the initial end-members of the couple (reactants) and products are monocrystalline materials. Obviously, this is not the case here. Diffusion along grain boundaries, being commonly orders of magnitude faster than through the bulk of the crystal, may play a definite role (especially at low homologous temperatures) in the overall mass transport within the reaction zone. It is possible that the tracer diffusion coefficients obtained with Eq. (5.10) are effective ones, which comprise lattice and grain boundary diffusivities. However, at relatively high temperatures used in the present study, the contribution of diffusion along grain boundaries to reactive growth is not expected to be significant, providing the grains within the product layers are sufficiently large.

It should be added here that crystals of the new phase in the reaction layer can grow with their "fast growth direction" parallel to the direction of diffusion fluxes. In such situation, higher tracer diffusion coefficients are sometimes found using the results of the diffusion couple

experiments than from the experiments with radioactive tracers, where crystallographic orientation of grains is random [11].

All these factors play a role if for the growth of the  $\text{CoSi}_2$ -product layer one wants to account for the difference of about a factor of 2 between our results and self-diffusion data of Barge *et al.* [28] (Fig. 5.7a), although the uncertainties in the measurements using radiotracers can also be substantial.

## References

1. K. Ishida, T. Nishizawa and M.E. Schlesinger, *J. Phase Equilibria* **12** (1991) 578.
2. S.P. Murarka, *Silicides for VSLI Applications*. Orlando: Academic Press Inc., (1983).
3. R.W. Balluffi and J.M. Blakeley, *Thin Solid Films* **25** (1975) 363.
4. J. Philibert, *Applied Surface Science* **53** (1991) 74.
5. C.-H. Jan, C.-P. Chen and Y.A. Chang, *J. Appl. Phys.* **73** (1993) 1168.
6. T. Barge, P. Gas and F.M. d'Heurle, *J. Mater. Res.* **10** (1995) 1134.
7. C. Wagner, *Acta Metall.* **17** (1969) 99.
8. F.J.J. van Loo, *Prog. Solid St. Chem* **20** (1990) 47.
9. J.R. Manning, *Acta Metall.* **15** (1967) 817.
10. J.H. Gülpen, Reactive phase formation in the Ni-Si system. Ph.D. thesis, Eindhoven University of Technology, (1995).
11. J.H. Gülpen, A.A. Kodentsov and F.J.J. van Loo, In: P. Nash *et al*, ed. *Applications of Thermodynamics in the Synthesis and Processing of Materials*. USA: TMS, (1995) p. 127.
12. T.G. Chart, *High Temp.- High Press.* **5** (1973) 241.
13. M.E. Schlesinger, *Chem. Rev.* **90** (1990) 607.
14. S.-D. Choi, *CALPHAD* **16** (1992) 151.
15. M.S. Chandrasekharaiah and J.L. Margrave, *J. Phys. Chem. Ref. Data* **22** (1993) 1459.
16. A.A. Frolov, Y.V. Putintsev, F.A. Sidorenko, P.V. Geld and R.P. Krentsis, *Inorg. Mater.* **8** (1972) 408.
17. G.I. Kalishevich, P.V. Geld and R.P. Krentsis, *High. Temp.* **2** (1964) 11.
18. G.I. Kalishevich, P.V. Geld and Y.V. Putintsev, *High Temp.* **6** (1968) 959.
19. G.I. Kalishevich, P.V. Geld and R.P. Krentsis, *Russ. J. Phys. Chem.* **42** (1968) 675.
20. W. Oelsen and H.O. von Samson Himmelstjerna, *Mitt. Kaiser Wilhelm Institut Eisenforsch.* **18** (1936) 131.
21. W. Oelsen and W. Middel, *Mitt. Kaiser Wilhelm Institut Eisenforsch.* **19** (1937) 1.
22. D. Lexa, R.J. Kematich and C.E. Myers, *Chem. Mater.* **8** (1996) 2636.
23. D. Lexa, R.J. Kematich and C.E. Myers, *Metall. Mater. Trans. A* **28A** (1997) 909.
24. E.S. Machlin, *CALPHAD* **5** (1981) 1.
25. A. Pasturel, P. Hicter and F. Cyrot-Lackmann, *Physica B + C* **124** (1984) 247.
26. A.K. Niessen, A.R. Miedema, F.R. de Boer and R. Boom, *Physica B* **151** (1988) 401.

27. M.W. Chase Jr, C.A. Davies, J.R. Downey, D.J. Frurip, R.A. McDonald and N. Syverud, JANAF Thermodynamic Tables. Washington DC: American Chemical Society, (1986).
28. T. Barge, S. Poize, J. Bernardini and P. Gas, *Applied Surface Science* **53** (1991) 180.
29. P. Villarsa and L.D. Calvert, Pearson's Handbook of Crystallographic Data. Metals Park, Ohio: American Society for Metals, (1985).
30. G.F. Bastin and G.D. Rieck, *Metall. Trans.* **5** (1974) 1817.
31. M. Salamon and H. Mehrer, *Phil. Mag. A* **79** (1999) 2137.
32. I.V. Belova and G.E. Murch, *Phil. Mag. A* **75** (1997) 1715.
33. I.V. Belova and G.E. Murch, *Phil. Mag. A* **78** (1998) 1085.



## Chapter 6

### Manifestations of the Kirkendall effect accompanying reactive diffusion<sup>1</sup>

#### 6.1 Introduction

In the foregoing chapter we have reported upon the formation of cobalt silicides in bulk incremental couples and the relative mobilities of species in the intermetallic compounds. This chapter deals with the Kirkendall effect accompanying the diffusion-controlled growth of the Co-Si intermetallics.

As we have seen, the results of our experimental studies on single-phase systems demonstrated that the Kirkendall plane need not be unique. Multiple planes can emerge within a diffusion zone, and, sometimes, the Kirkendall plane transforms in a spreading crowd of markers. A phenomenological approach was introduced to explain the behaviour of inert markers within the diffusion zone (see Chapter 4).

---

<sup>1</sup> Parts of this chapter are published as papers:

M.J.H. van Dal, A.A. Kodentsov and F.J.J. van Loo, *Intermetallics* **9** (2001) 451.

M.J.H. van Dal, A.A. Kodentsov and F.J.J. van Loo, *Solid State Phenomena* **72** (2000) 111.

In multi-phase silicide systems, we have observed the same peculiar diffusion phenomenon. Given the relative simplicity of phase relations in the Co-Si system and availability of diffusion data (obtained in the previous chapter), it is interesting to verify the proposed ideas by analysing Kirkendall-markers movement during Co-Si intermetallic growth in bulk diffusion couples.

In the ensuing discussion we shall look at the migration of “inert markers” from a general standpoint and show explicitly how the behaviour of the macroscopic inclusions inside interdiffusion zones can be rationalised by using the Kirkendall velocity concept. This treatment is phenomenological, i.e. all parameters are defined in such a way that they can be measured or estimated by independent methods. No attempts will be made to elucidate diffusion mechanisms in cobalt silicides.

## 6.2 On migration of inert markers upon interdiffusion in a binary multi-phase system

The Kirkendall-effect induced migration of fiducial markers (e.g. inert particles) inside a reaction zone of a semi-infinite diffusion couple can be best described in terms of the Kirkendall velocity plot. This graph displays the marker velocities at each location throughout the entire interaction zone relative to the laboratory-fixed (Matano) frame of reference. The theoretical analysis of marker movement during interdiffusion has already been discussed (Chapter 4). Reproduction of the expressions is presented here only to the extent necessary to facilitate discussion.

For an A/B diffusion couple, the marker velocity  $v$  is determined by the difference in the intrinsic diffusivities of the components and the concentration gradients developing upon interdiffusion in the reaction zone (Eq. 3.10):

$$v = V_A (D_A - D_B) \frac{\partial C_A}{\partial x} = \frac{V_A V_B}{V_m^2} (D_A - D_B) \frac{\partial N_A}{\partial x}.$$

In a diffusion-controlled interaction, the Kirkendall plane, i.e. the plane of constant composition marked by the inert particles originally situated at the interface between the

couple halves, moves parabolically in time with respect to the Matano frame of reference with a velocity  $v = x_K/2t$ . In the last formula,  $x_K$  is at each moment the distance between the Kirkendall and Matano plane ( $x = 0$ ), and  $t$  is the reaction time. The location (and velocity) of the Kirkendall plane is found as the intersection of the velocity plot and the straight line  $v = x/2t$ .

In our theoretical analysis, we treat the Co-Si intermetallics as line-compounds and use the concept of the integrated diffusion coefficient to describe the redistribution of the elements across the interaction zone (Eq. (5.6)):

$$\tilde{D}_{\text{int}} = \int_{N'}^{N''} \tilde{D} dN.$$

Equation (3.10) together with Eq. (5.6) and the usual Darken expression for interdiffusivity (Eq. (3.12)):

$$\tilde{D} = \frac{V_A N_A}{V_m} D_B + \frac{V_B N_B}{V_m} D_A$$

give a general expression for the marker velocity in a line-compound:

$$v = \frac{V_B}{V_m} \cdot \frac{\left(\frac{D_A}{D_B} - 1\right)}{\left(\frac{V_B D_A}{V_A D_B}\right) \cdot N_B + N_A} \cdot \left(\frac{\tilde{D}_{\text{int}}}{\Delta x}\right). \quad (6.1)$$

Here,  $\Delta x$  is the thickness of the phase layer in question.

For sake of simplicity we assume that the partial molar volumes of the components in the phase (which are unknown) are equal. Then, the Kirkendall marker velocity can be written as:



$$v = \frac{\frac{D_A}{D_B} - 1}{\frac{D_A}{D_B} \cdot N_B + N_A} \cdot \left( \frac{\tilde{D}_{\text{int}}}{\Delta x} \right). \quad (6.2)$$

Within a line-compound, the integrated diffusion coefficient and the ratio of the intrinsic diffusivities can be considered constant, hence the Kirkendall velocity has also a constant value. Equation (6.2) is a good and general approximation for constructing the Kirkendall velocity diagrams in the case of a multi-phase diffusion system.

Apparently, if the ratio of the intrinsic diffusivities,  $D_A/D_B$ , approaches to infinity, the marker velocity equals:

$$\lim_{D_A/D_B \rightarrow \infty} (v) = \frac{1}{N_B} \frac{\tilde{D}_{\text{int}}}{\Delta x}, \quad (6.3a)$$

and if  $D_A/D_B$  approximates to zero, then:

$$\lim_{D_A/D_B \rightarrow 0} (v) = \frac{-1}{N_A} \frac{\tilde{D}_{\text{int}}}{\Delta x}. \quad (6.3b)$$

In fact, Eqs. (6.3a) and (6.3b) represent the limits of the marker velocity. Obviously, when the components mobilities are equal (i.e.  $D_A/D_B = 1$ ), the Kirkendall marker velocity is zero.

### 6.3 Kirkendall effect in the multi-phase diffusion couples of the Co-Si system

To focus on the essential points, we will confine the present discussion to one temperature, viz. 1100°C. At this temperature, CoSi was found to be the fastest growing phase in the reaction between cobalt and silicon. Fig. 6.1 shows a representative example of the multi-phase diffusion zone developed in the Co/Si couple after interaction at 1100°C for 100 h. Using the corresponding concentration profile (measured with EPMA) and Eq. (5.7) (taking into account the change in molar volume [1]), the integrated diffusion coefficients in the

silicides  $\text{Co}_2\text{Si}$ ,  $\text{CoSi}$  and  $\text{CoSi}_2$  were found as  $1.8 \cdot 10^{-14} \text{ m}^2/\text{s}$ ,  $4.7 \cdot 10^{-14} \text{ m}^2/\text{s}$  and  $1.1 \cdot 10^{-15} \text{ m}^2/\text{s}$ , respectively. The present results agree well with those measured in the experiments with the incremental diffusion couples (Chapter 5), where the  $\tilde{D}_{\text{int}}$ -values in  $\text{Co}_2\text{Si}$ ,  $\text{CoSi}$  and  $\text{CoSi}_2$  were found as  $2.1 \cdot 10^{-14} \text{ m}^2/\text{s}$ ,  $4.4 \cdot 10^{-14} \text{ m}^2/\text{s}$  and  $0.8 \cdot 10^{-15} \text{ m}^2/\text{s}$ , respectively. The above findings indicate that diffusion is the rate-controlling step for the growth of the intermetallic compounds in these couples.

One can see from the micrograph that the  $\text{ThO}_2$ -markers between the end-members show up in the diffusion zone at two different locations. In other words, two Kirkendall marker planes emerged upon interdiffusion, one in the  $\text{Co}_2\text{Si}$ - and one in the  $\text{CoSi}$ -intermetallic layer.

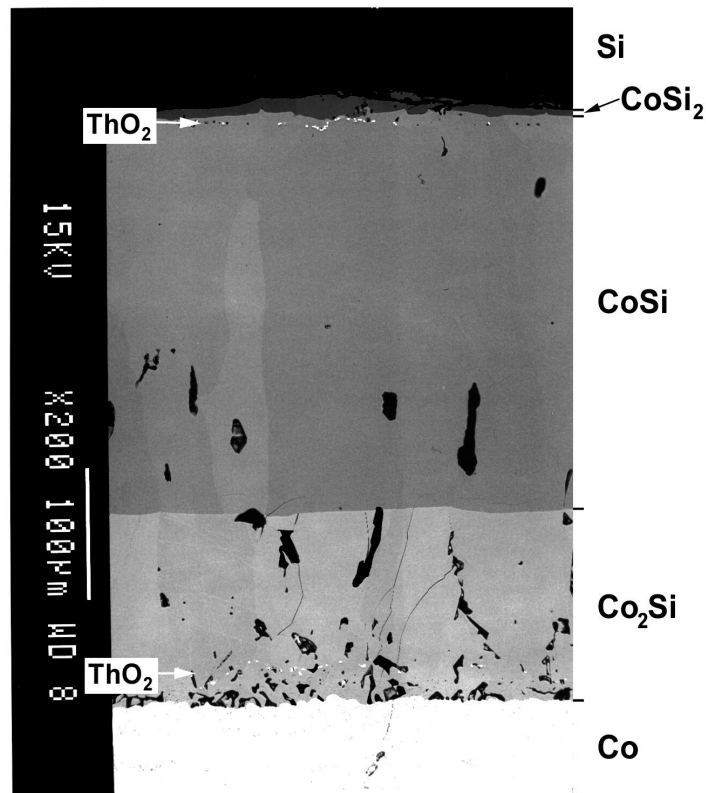


Figure 6.1: BEI of a cross-section of a Co/Si diffusion couple after annealing at  $1100^\circ\text{C}$  in vacuum for 100 h.  $\text{ThO}_2$ -particles were used as inert markers between the initial end-members. Two “Kirkendall planes” emerged upon the interaction.

In order to construct the complete Kirkendall velocity diagram corresponding to the Co/Si diffusion couple, an additional experiment has been performed to be able to estimate the Kirkendall velocity in the (Co,Si)-solid solution. A diffusion couple based on pure Co and an

equilibrated (1100°C) two-phase  $\text{Co}_{68}\text{Si}_{32}$  alloy was examined. The alloy end-member consists of a  $\text{Co}_2\text{Si}$ -matrix and precipitates of the hexagonal  $\epsilon\text{-Co}(\text{Si})$  phase. This two-phase structure is clearly visible in Fig. 6.2 representing the diffusion zone morphology developed after interaction at 1100°C in vacuum for 25 h.

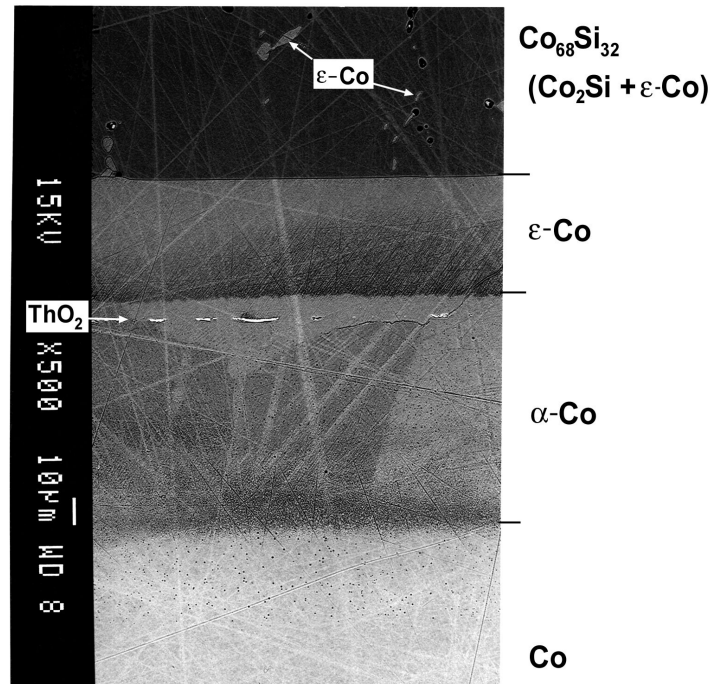


Figure 6.2: BEI of a diffusion zone developed after reaction at 1100°C for 25 h in vacuum between Co and a two-phase ( $\text{Co}_2\text{Si} + \epsilon\text{-Co}$ ) alloy with a nominal composition  $\text{Co}_{68}\text{Si}_{32}$ . The position of the Kirkendall plane is revealed by  $\text{ThO}_2$ -markers.

After etching of the polished cross-section of the  $\text{Co}_{68}\text{Si}_{32}/\text{Co}$  couple, two phases were found, viz. the  $\epsilon\text{-(Co,Si)}$  and the  $\alpha\text{-(Co,Si)}$  solid solutions, which is in accordance with phase diagram (Fig. 5.1). The Kirkendall plane is situated inside the layer of the  $\alpha\text{-(Co,Si)}$ -solid solution and is revealed by the straight row of the  $\text{ThO}_2$ -particles. The Si-concentration at the location of the Kirkendall plane was found (in terms of EPMA) to be approximately 17 at.%. The interdiffusion coefficient and the ratio of intrinsic diffusivities of the components, corresponding to this composition, were determined by subjecting the concentration profile measured across the reaction zone to a conventional Matano-Boltzmann analysis (section 3.1). It turned out that the interdiffusion coefficient  $\tilde{D}$  (17 at.% of Si) was equal to  $4.2 \cdot 10^{-14} \text{ (m}^2/\text{s)}$  and the ratio of the intrinsic diffusivities  $D_{\text{Si}}/D_{\text{Co}}$  (17 at.% of Si) was calculated as 1.5.

In our experiments, we were not able to find the ratio of the intrinsic diffusivities of Si and Co inside the  $\epsilon$ -Co phase. In the case at hand, we have assumed that Si is also the fastest diffusing species in the  $\epsilon$ -(Co,Si) solid solution. In the calculations that follow, Eq. (4.6) is used to determine the Kirkendall velocity at 17 at.% of Si and with this data point the Kirkendall velocity in the (Co,Si)-solid solutions is estimated. This assumption will not influence the main conclusions of this Chapter.

The Kirkendall velocity construction calculated for the annealed (1100°C; 100 h) Co/Si diffusion couple is given in Fig. 6.3 In this diagram,  $x = 0$  refers to the position of the Matano plane, which was deduced from the measured concentration profile of this couple.

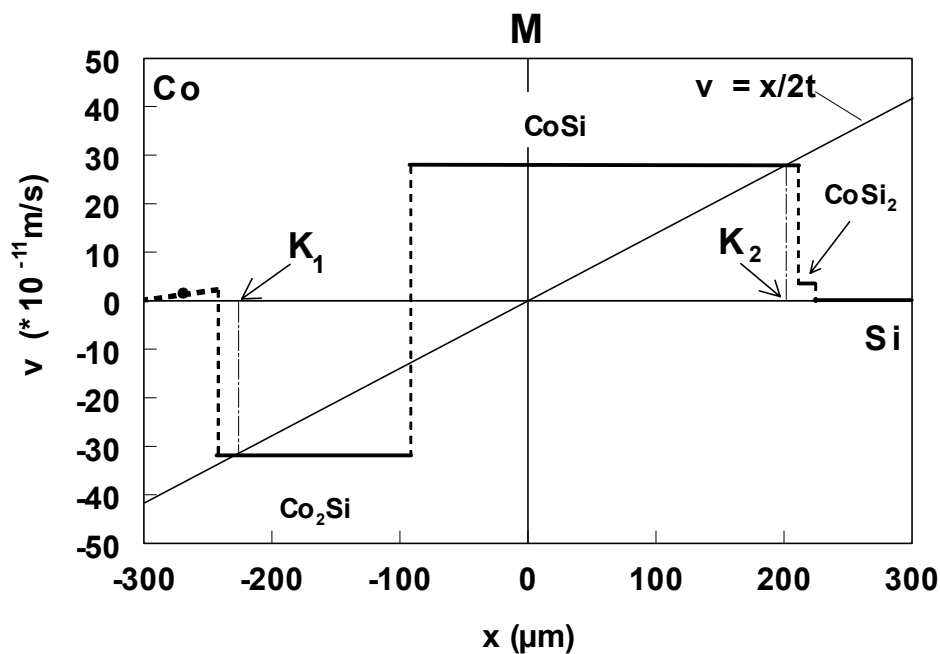


Figure 6.3: The Kirkendall velocity diagram calculated for the annealed (1100°C; 100 h) Co/Si diffusion couple. The straight line  $v = x/2t$  intersects the velocity plot twice, i.e. two Kirkendall marker planes form ( $K_1$  and  $K_2$ ). Note:  $x = 0$  corresponds to the Matano plane, the location of the initial contact surface at  $t = 0$ .

The straight line  $v = x/2t$  intersects the velocity plot at two positions. It means that there are two marker planes moving parabolically in time, i.e. two Kirkendall marker planes should become visible within the interdiffusion zone: one in the CoSi-phase and another in the Co<sub>2</sub>Si-intermetallic layer. Returning to the Fig. 6.1 one sees that, indeed, the theoretical predictions are consistent with the experimental observations.

Another interesting example of the multiple Kirkendall plane formation is provided by the interaction between Co and CoSi<sub>2</sub>-intermetallic. Fig. 6.4 shows the reaction zone of the CoSi<sub>2</sub>/Co diffusion couple after annealing at 1100 °C in vacuum for 100 h.

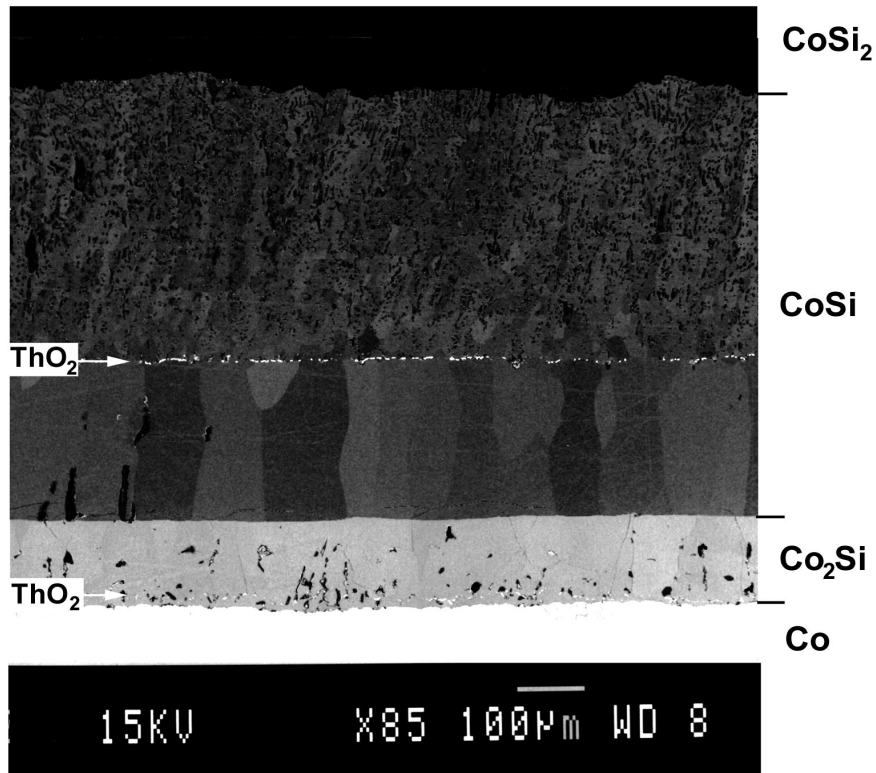
As in the previous case, two separate Kirkendall planes marked by ThO<sub>2</sub>-particles developed in the multi-phase diffusion zone: one inside the Co<sub>2</sub>Si-layer and another within the CoSi-phase.

Metallographic features of the intermetallic layers are very useful here in detecting of the Kirkendall plane location (see also Chapter 4 and 5). The differently nucleated grains of the product phase meet at the Kirkendall plane, and the marker planes inside Co<sub>2</sub>Si- and CoSi-layers can be seen even without the presence of any ThO<sub>2</sub>-particles. Similar to the observations made in the CoSi<sub>2</sub>/Co<sub>2</sub>Si couple, pore formation accompanied the growth of the CoSi layer. Again, this is probably due to the “Kirkendall voiding” as a result of the much higher mobility of Si as compared to Co in this phase.

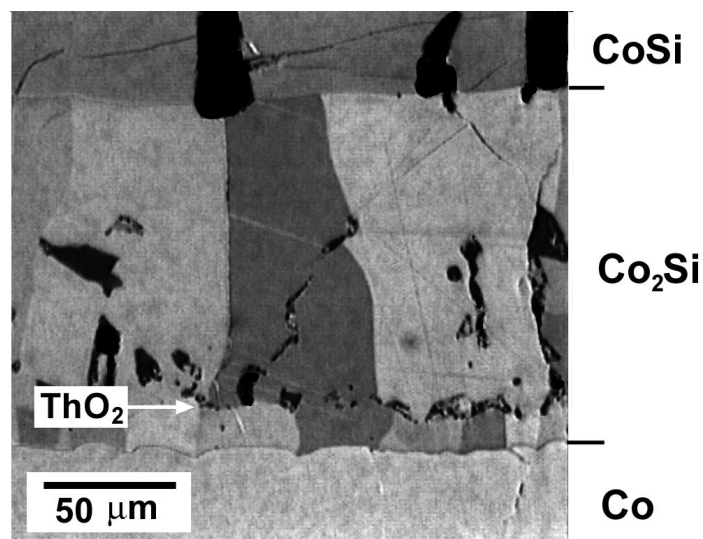
Upon comparing the microstructures of the diffusion zones evolved in the Co/Si and the Co/CoSi<sub>2</sub> couple, a clear difference in the position of the Kirkendall marker plane within the CoSi-product layer can be noticed. In the Co/Si couple this marker plane appears in the CoSi-intermetallic near the CoSi/CoSi<sub>2</sub> interphase interface, while after interaction between CoSi<sub>2</sub> and Co, the corresponding Kirkendall plane was found in the middle part (even closer to the Co<sub>2</sub>Si) of the CoSi-product layer.

This is a direct outcome from the fact that number of the expected Kirkendall marker planes and their locations within the newly formed phase layers are also dependent on the initial difference in component concentration in the end-members. This can be appreciated looking at Fig. 6.5, which represents the marker velocity construction for the annealed (1100 °C; 100 h) CoSi<sub>2</sub>/Co-couple.

Two aspects are to be mentioned here. Firstly, when cobalt disilicide is used instead of Si as initial end-member in the diffusion couple with pure Co, the position of the Matano plane shifts in the direction of the Co-side of the reaction zone. Secondly, in the reaction between



a)



b)

Figure 6.4: a) BEI of the reaction zone between  $\text{Co}$  and  $\text{CoSi}_2$  showing the formation of two Kirkendall marker planes after interdiffusion at  $1100^\circ\text{C}$  for 100 h ( $\text{ThO}_2$ -particles were used as inert markers between the couple halves). b) Optical micrograph of a magnified area of the same diffusion couple using polarised light showing the different morphology on either side of the Kirkendall plane in the orthorhombic  $\text{Co}_2\text{Si}$  intermetallic.

Co and CoSi<sub>2</sub> the CoSi-reaction layer grows faster as compared to the CoSi growth in the case of the Co/Si couple. According to Eq (6.2), the marker velocity  $v$  decreases with increasing product layer thickness,  $\Delta x$ . These two effects influence the positions of the intersection points on the Kirkendall velocity construction and, hence, the locations of the marker planes.

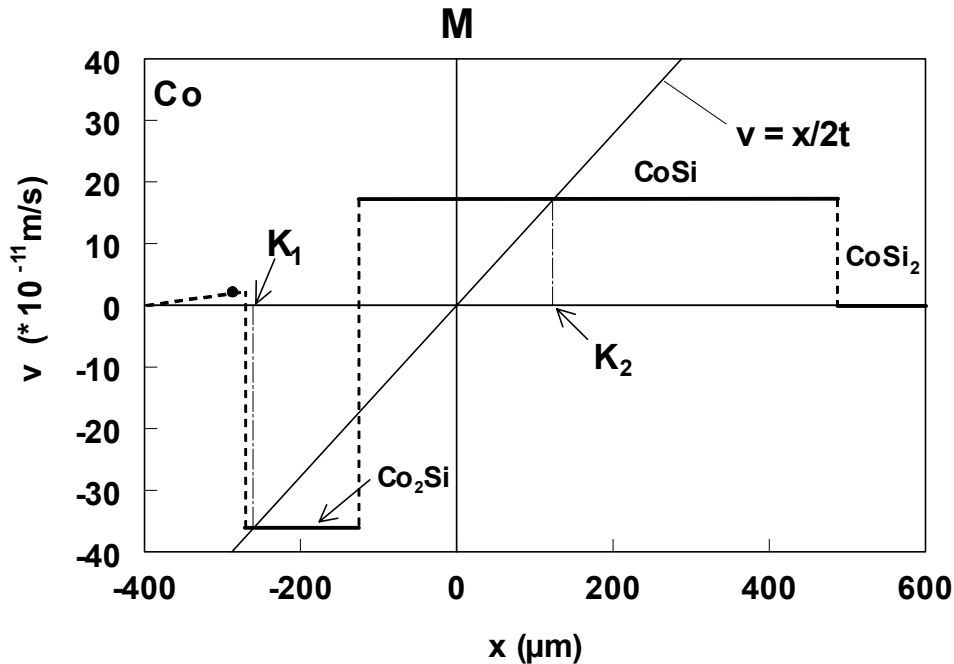
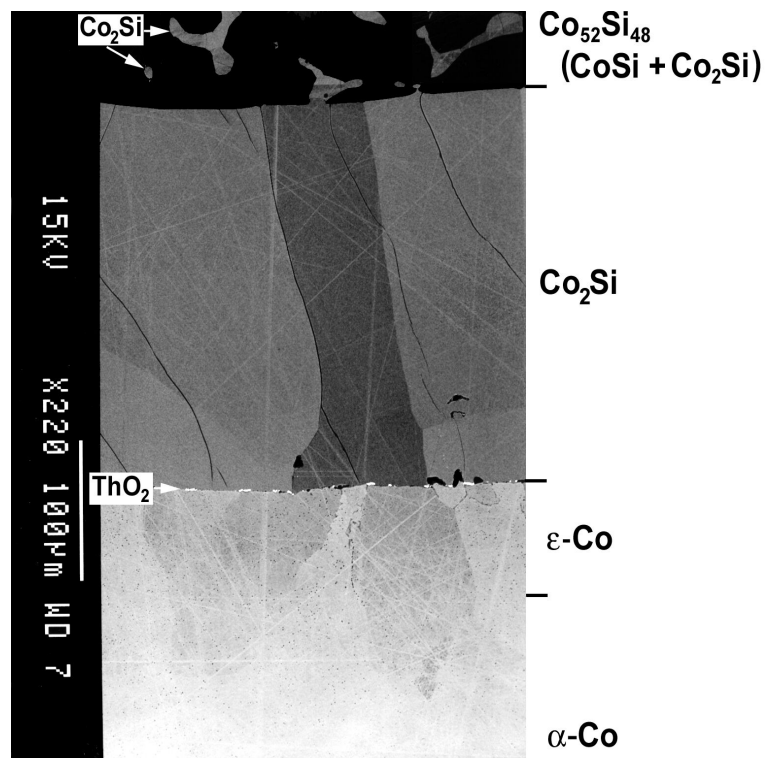


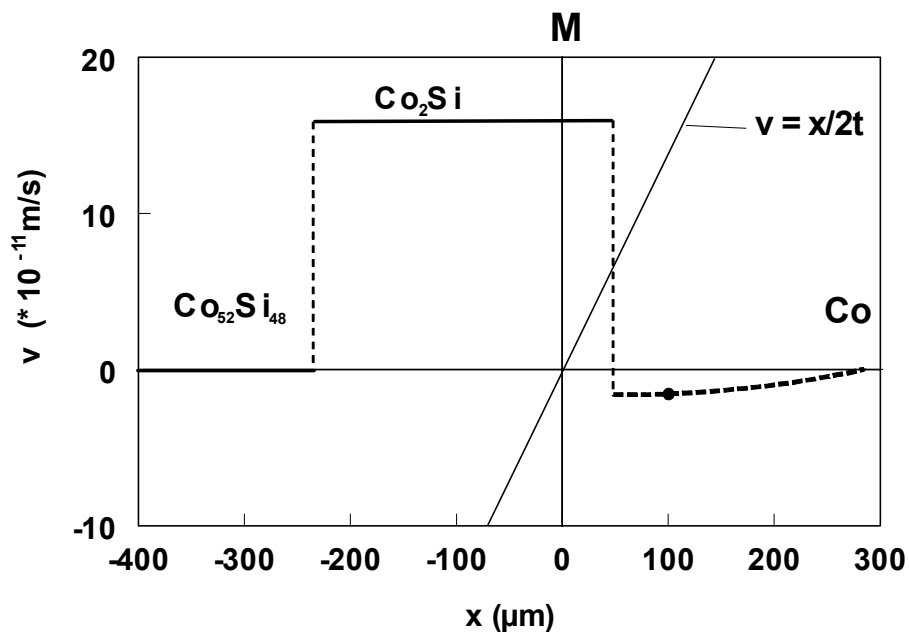
Figure 6.5: The Kirkendall velocity plot corresponding to the Co/CoSi<sub>2</sub> diffusion couple after interdiffusion at 1100 °C for 100 h. (The Matano plane is located at  $x = 0$ ;  $K_1$  and  $K_2$  are positions of the marker planes).

When using the Kirkendall velocity diagrams in describing marker behaviour inside a multi-phase reaction zone another important issue should be clarified. It is possible that the straight line  $v = x/2t$  on the diagram does not intersect the velocity plot in single-phased domains at all. Instead, it can traverse through a finite discontinuity, which corresponds to the interface between the layers.

Such situation occurs, for example, in the case of a diffusion couple based on pure Co and a two-phase Co<sub>52</sub>Si<sub>48</sub> alloy, which, after equilibration at 1100 °C, is composed of CoSi-matrix and Co<sub>2</sub>Si-precipitates. The morphology of the reaction zone developed in this couple after annealing at 1100 °C for 100 h is given in Fig. 6.6 together with the corresponding Kirkendall velocity plot.



a)



b)

Figure 6.6: a) BEI of a reaction zone between Co and a two-phase ( $\text{CoSi} + \text{Co}_2\text{Si}$ ) alloy with a nominal composition  $\text{Co}_{52}\text{Si}_{48}$  after annealing at  $1100^\circ\text{C}$  for 100 h in vacuum.  $\text{ThO}_2$ -particles used as inert markers between the initial end-members exhibit a white contrast on the micrograph; b) the corresponding marker velocity construction (the Matano plane is located at  $x = 0$ ).



One sees that there are no intersection points in the parts of the construction representing the Kirkendall velocity within the single-phased layers (Fig. 6.6b). The line  $v = x/2t$  passes through the discontinuity associated with the  $\epsilon$ -Co/Co<sub>2</sub>Si interface. Obviously, this discontinuity displays an abrupt decrease of Kirkendall velocity from one phase to the other.

At this point, it should be recalled that existence of a Kirkendall marker plane suggests that this well-defined plane in a reaction zone can be considered (from a phenomenological point of view) as an “attractor” for markers, which during interdiffusion accumulates the markers in its vicinity. In general, for a Kirkendall plane to appear as a straight row of markers moving parabolically in time, i.e. to be spatial and temporal stable, the corresponding marker velocity near the location of the Kirkendall plane must have a negative gradient with respect to the position parameter (see Chapter 4).

In this sense, the “Kirkendall marker plane” that is expected to develop in the Co/Co<sub>52</sub>Si<sub>48</sub> diffusion couple (Fig. 6.6) is viewed as a “very stable” one, because the gradient of the velocity can be considered equal to  $-\infty$ . Markers that will end up at that interface will never leave this position. If the phase boundary, corresponding to the Kirkendall plane, is moving with respect to the Matano plane, all particles, pores or other inclusions present in the adjoining end-member, towards which the boundary is moving, will be trapped by that interface upon interaction.

The physical meaning of the last observation is that inert markers, e.g. ThO<sub>2</sub>-particles, placed at the original interface of this couple, cannot go either way. Eventually, the fiducial inclusions have to end up at the  $\epsilon$ -Co/Co<sub>2</sub>Si interface as was found indeed. On the other hand, for the same reasons markers can never end up in an interface where the velocity curve has a gradient  $+\infty$ .

This phenomenon is very important from a general point of view. Very often one finds Kirkendall markers back at phase interfaces. Now we can understand this is because of the large chance to have a crossing point of the velocity plot with the line  $x/2t$ , especially if the difference in Kirkendall velocity in the phases is large. One should realise that in this situation nothing specific can be said about the ratio of the two intrinsic diffusion coefficient in the neighbouring phases. However, using the Kirkendall velocity construction and the limits of

the Kirkendall velocity (Eqs. 6.3a and b) one can make an estimate (in term of a range) of the relative mobilities of the diffusing species in the phase. Such analysis was recently performed by Oberndorff [2].

#### 6.4 The Kirkendall effect in multi-phase Ti/Ni diffusion couple

The appearance of multiple Kirkendall planes in multi-phase systems is by no means restricted to the Co-Si system. During our study on new phenomena concerning the Kirkendall effect, we have encountered similar behaviour in the Ti-Ni system. Actually, the first clear-cut evidence for the existence of plural Kirkendall planes in our studies was found by repeating the Ti/Ni diffusion couple experiment as described by Bastin *et al.* [3,4] which is shown in this thesis in Chapter 1 (Fig. 1.3). However, instead of using tungsten wires to mark the initial contact surface between Ti and Ni, we used the  $\text{ThO}_2$  particles. Fig. 6.7 shows a cross-section of the Ti/Ni diffusion couple, which was annealed at  $850^\circ\text{C}$  for 196 h.

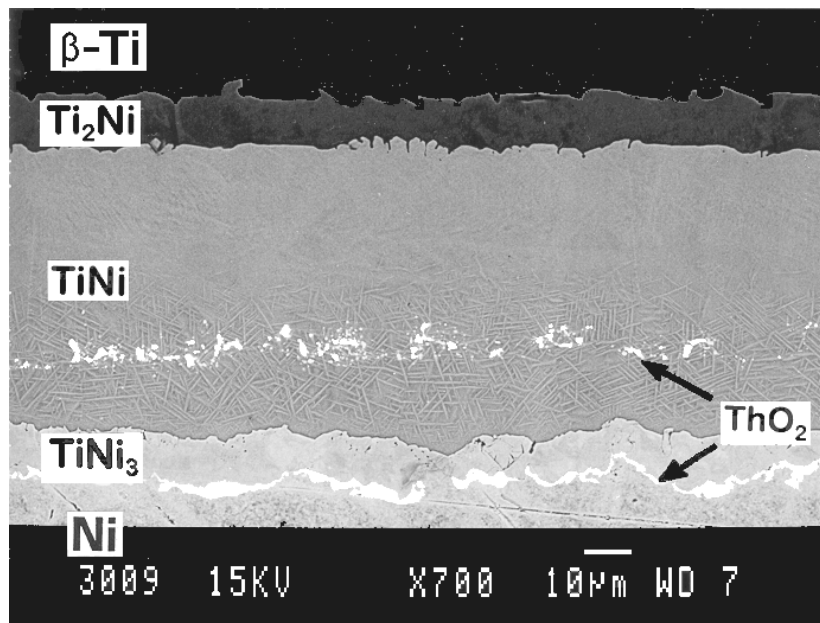


Figure 6.7: BEI of a cross section of a Ti/Ni diffusion couple annealed at  $850^\circ\text{C}$  for 196 h.  $\text{ThO}_2$ -particles were used as inert markers between the initial end-members (the  $\beta$  –  $\text{Ti}_{ss}$  solid solution layer is very thick and the  $\alpha$ -Ti end-member is far away from the intermetallic layers shown in the picture).

Three intermetallic phases are formed:  $\text{TiNi}_3$ ,  $\text{TiNi}$  and  $\text{Ti}_2\text{Ni}$  which is in accordance with the binary phase diagram [5]. One can clearly see that the  $\text{ThO}_2$  particles rearranged inside the interaction zone into two distinct planes. Apparently, two Kirkendall planes emerged.

The corresponding Kirkendall velocity curve was constructed using the data of the work of Bastin [4] (Fig. 6.8). The value of the Kirkendall velocity inside the  $\beta$ -Ti solid solution (where Ni is by far the fastest moving species [3,4]) was estimated to be approximately  $10^{-9}$  m/s and was out of range in Fig. 6.8. The straight line  $v = x/2t$  hits the velocity plot twice. This would lead to a Kirkendall plane in the  $\text{TiNi}$  phase and one in the  $\text{TiNi}_3$  phase, which were found indeed.

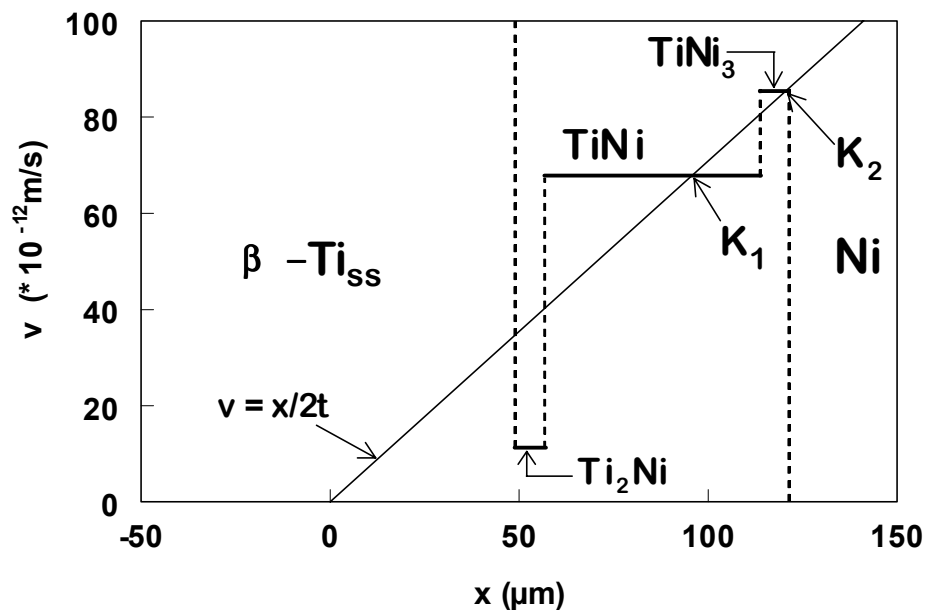


Figure 6.8: The Kirkendall velocity plot corresponding to the Ti/Ni diffusion couple ( $850^\circ\text{C}$ ; 196 h) computed using data of Bastin [4]. Note:  $x = 0$  corresponds to the Matano plane, the location of the initial contact surface at  $t = 0$ . The Kirkendall velocity in the  $\beta - \text{Ti}_{ss}$  phase was estimated as  $10^{-9}$  m/s.

One point should be noticed here. Careful inspection of the Kirkendall plane situated in the  $\text{TiNi}$  phase (Fig. 6.7) reveals a rather significant scattering of particles. It is tempting to say that this effect is related to the stability of the Kirkendall plane. Since the  $\text{TiNi}$  phase has a relatively large homogeneity range at  $850^\circ\text{C}$  (49 – 56 at.% of Ni [5]), this phase may not be regarded as a line compound and, consequently, the concentration gradient developing within

the TiNi phase upon interaction may not be neglected. In this sense a (slightly) positive gradient of the Kirkendall velocity in this phase could occur. This, in turn, would lead to an unstable Kirkendall plane, explaining the observed scattering of Kirkendall markers.

However, one should be cautious in posing such conclusions. Firstly, the concentration dependence of the intrinsic diffusivities of Ni and Ti in the TiNi phase is not known. A complete analysis of the Kirkendall velocity is, therefore, not possible. Secondly, upon cooling the Ti/Ni diffusion couple we observed a martensitic transformation within the TiNi phase (a needle-like structure in Fig. 6.7; see also the cover of this thesis). Such a transformation might influence the position of the small ThO<sub>2</sub> particles as well.

**References**

1. K. Ishida, T. Nishizawa and M.E. Schlesinger, *J. Phase Equilibria* **12** (1991) 578.
2. P.J.T.L. Oberndorff, Lead-free solder systems: Phase relations and microstructures. Ph.D. thesis, Eindhoven, The Netherlands, (2001).
3. G.F. Bastin and G.D. Rieck, *Met. Trans.* **5** (1974) 1817.
4. G.F. Bastin, Diffusie in het systeem Titanium-Nikkel. Ph.D. thesis, Eindhoven, The Netherlands, (1972).
5. J.L. Murray, Ed., Phase diagrams of binary titanium alloys. ASM International, Metals Park, Ohio, (1987) pp. 197-211.

## Chapter 7

### Final considerations and recommendations for future work

No further proof is necessary to demonstrate that, in a diffusion-controlled interaction, the Kirkendall plane, as marked by inert particles placed at the original contact surface of a reaction couple, *need not be unique*. The results of the experimental studies of interdiffusion in binary systems presented in this thesis show that the Kirkendall plane can be multiple, stable and unstable. With a rather simple phenomenological approach the behaviour of inert particles placed at the original contact surface of a diffusion couple can be rationalised and predicted if the pertinent data are available. The Kirkendall velocity curve construction enables us to determine the number of the Kirkendall planes and their positions inside an interaction zone. The latter was a long-standing problem that had not been solved in all but some simplified cases [1-3].

The findings of the present work also raise new questions. For instance, since we only investigated binary systems, one can ask oneself how the Kirkendall effect will manifest itself in ternary (or higher order) systems. Another question is whether it is possible to have *more than two* Kirkendall planes inside an interaction zone. In this Chapter, we would like to discuss these questions and express our ideas of possible consequences of the microstructural stability of the Kirkendall plane not only from a scientific but also from a technological point

of view. It has to be emphasised here that the aspects that follow are sometimes speculative and are not to be interpreted as conclusions from the present work. Instead, it is tried to provide a framework for eventual future work.

### **7.1 Unstable and stable Kirkendall planes: their mechanical consequences.**

The Kirkendall effect and the associated microstructural consequences have a great technological significance. In materials where dissimilar solids are in contact at elevated temperature (e.g. bonded component, composites, coating, thin-film metallizations, etc.), the original interface or Kirkendall plane (often referred to as “welding” interface) is a notoriously problematic feature in hybrid structures because of higher mechanical failure risks at this plane. Obviously, for further development of the material systems suitable for applications it is important to be able to predict (and control) the microstructural features associated with the Kirkendall effect.

In this respect, the case of a *single unstable* Kirkendall plane (e.g. the Fe-Pd diffusion couple discussed in section 4.6) attracts special attention from a mechanical point of view. One may argue whether a diffusion bond exhibiting a single unstable Kirkendall plane possesses a Kirkendall plane as such. After all, inert particles originally marking the initial contact surface are scattered across the interdiffusion zone after interaction, leaving no trace of the exact location of the initial contact interface. Moreover, upon annealing such a joint, the particles will be spread even more. One could say that the system simply “forgets” the original contact surface and no Kirkendall plane is present anymore. This would, in principle, lead to a stronger bond than in systems with (a) stable Kirkendall plane(s).

On the other hand, in the case of a *single, “infinitely” stable* Kirkendall plane as was found in the  $\text{Co}_{52}\text{Si}_{48}/\text{Co}$  diffusion couple discussed in section 6.3, a very weak bond will develop. Such a stable Kirkendall plane, if moving with respect to the Matano plane, will act as a “trap” for debris, pores and other inclusions present in the initial material. The joint will be deteriorating as the annealing proceeds.

In the present work no mechanical tests were performed to verify these ideas. It might be interesting to study the mechanical behaviour of, for instance, diffusion couples of the Au-Zn system as prepared in section 4.4. In these couples, both single, multiple, stable and unstable Kirkendall planes are found within a single phase by varying the composition of the starting end-members.

## 7.2 More than two Kirkendall planes: is it possible?

In Chapter 4 we have demonstrated the Kirkendall velocity curve construction that allows determining the locations and the number of Kirkendall planes inside any interdiffusion zone if the pertinent intrinsic diffusivities are known. The formation of two (stable) Kirkendall planes was predicted and found in the Au-Zn and later also in the Co-Si and Ti-Ni systems. Now we can ask ourselves the following questions. Is it possible to have three (or more) intersection between the line  $v = x/2t$  with the velocity curve so that three (or more) stable Kirkendall planes can be expected inside an interaction zone? And if this is possible how will the microstructure of the interdiffusion zone develop? Or will there be no joining at all in such a situation?

Figure 7.1 shows two hypothetical cases of Kirkendall velocity curves, in which three Kirkendall planes are expected. In Fig. 7.1a, only the stable Kirkendall planes are indicated as “real” Kirkendall planes (indicated by K in Fig. 7.1), i.e. which are visible after interactions according to the analysis described in Chapter 4. It is clear that, theoretically speaking, a diffusion couple in which more than two Kirkendall planes are formed can be envisaged (especially in a multi-phase diffusion couple).

However, no experimental evidences for more than two Kirkendall planes inside an interaction were found in the present work. In this respect, diffusion studies on ternary metallic systems may provide the necessary framework to explore all the possibilities of the Kirkendall effect, because one extra degree of freedom is available to control the direction of the mass flow accompanying interdiffusion. Numerical evaluation of the re-distribution of Kirkendall particles in hypothetical diffusion couples, as done in Ref. [4], might facilitate the choice of promising ternary systems.



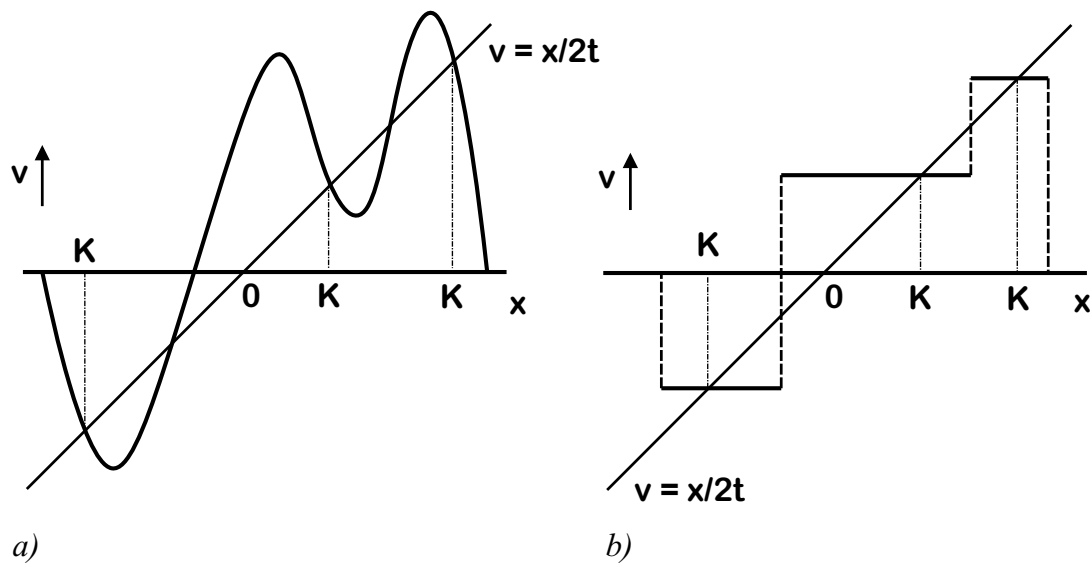


Figure 7.1: Hypothetical velocity curves of a) a single-phase and b) a multi-phase diffusion couple, in which three (stable) Kirkendall planes (indicated with K) are expected.

### 7.3 Periodic layer formation as a manifestation of the Kirkendall effect

In a recent paper, Kodentsov *et al.* [5] classified a new type of morphology that may develop in a ternary system during a solid state reaction: *periodic pattern formation*. The authors explained this phenomena as a manifestation of the Kirkendall effect. Here, we would like to show the relation between the periodic layer formation and our experimental observation of plural Kirkendall planes inside an interaction zone.

Figure 7.2 shows a Pt/SiC diffusion couple annealed at 750 °C for 24 h demonstrating a typical example of periodic pattern formation taken from the work of Kodentsov *et al.* [5]. The reaction zone consists of a Pt<sub>3</sub>Si, Pt<sub>7</sub>Si<sub>3</sub> and a Pt<sub>2</sub>Si layer. Within the Pt<sub>7</sub>Si<sub>3</sub> intermetallic periodic carbon bands are formed and a continuous band of carbon can be seen in the Pt<sub>2</sub>Si.

It is important to mention here that in the Pt<sub>7</sub>Si<sub>3</sub> Pt is the fastest moving species and in Pt<sub>2</sub>Si Si diffuses faster [5]. We have already shown that such a situation may lead to the formation of two Kirkendall planes inside the interaction zone: see, e.g., the Co/Si and Co/CoSi<sub>2</sub> diffusion couple (Chapter 6).

Since Pt is a non-carbide forming metal, carbon is formed as a side product during the reaction between Pt and SiC. The carbon inclusions embedded in the continuous intermetallic matrix may be considered as “inert markers” formed *in situ* inside the reaction zone. These particles experience a different Kirkendall “force” in the different phases. They are directed towards the SiC-side of the couple when they are present in the Pt<sub>2</sub>Si phase and when they are situated in the Pt<sub>7</sub>Si<sub>3</sub> intermetallic they are “pushed” towards the Pt-side of the couple. The opposing forces will eventually “split-up” the carbon bands at (or in the vicinity of) the Pt<sub>2</sub>Si/Pt<sub>7</sub>Si<sub>3</sub> interface. After this “splitting” this process will repeat. However, when the thickness of the Pt<sub>2</sub>Si layer exceeds the thickness of the carbon-containing zone adjacent to the SiC, the formation of the bands is stopped: no graphite is formed anymore in the Pt<sub>7</sub>Si<sub>3</sub> phase.

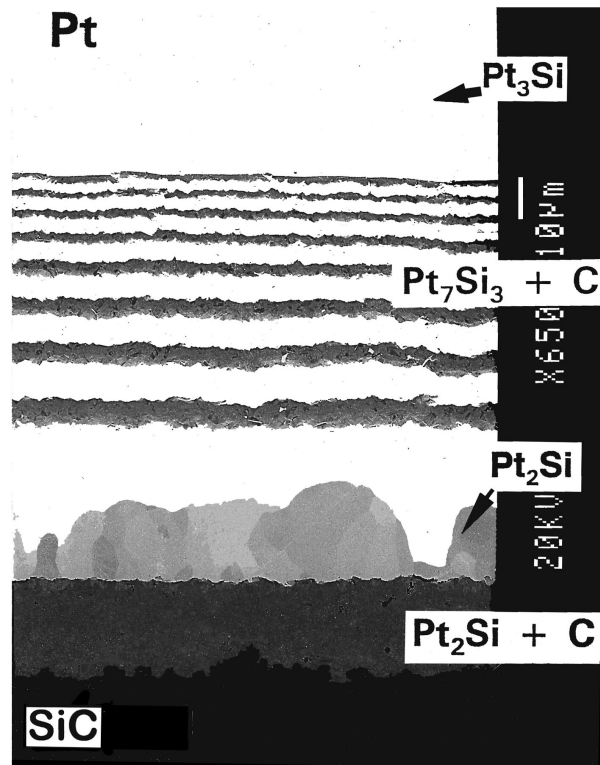


Figure 7.2: BEI of the reaction zone between SiC and Pt after annealing at 750 °C for 24 h in vacuum.

As a conclusion one can say that the Pt<sub>2</sub>Si/Pt<sub>7</sub>Si<sub>3</sub> interface acts as a “separator” of the carbon bands because of the sudden change of the Kirkendall velocity. This is similar to the “splitting” of the Kirkendall plane as observed in the Co/CoSi<sub>2</sub> diffusion couple (see Fig.

6.4a) in which the CoSi/Co<sub>2</sub>Si interface plays the role of “separator” to form two Kirkendall planes out of one original contact surface. In terms of the Kirkendall velocity curve, such an interface would correspond to an intersection with the straight line  $v = x/2t$  at a point where the slope of the Kirkendall velocity is infinitely positive. As it has been stated in section 6.3, inert markers can never end up at such an interface. The continuously forming carbon bands in the Pt/SiC diffusion couple will therefore split up in the vicinity of this interface. Indications of periodic layer formation were also observed in a Co/SiC diffusion couple [6], in which the CoSi/Co<sub>2</sub>Si interface acts as a “separator” for the carbon bands, indeed.

#### 7.4 The influence of the Kirkendall effect on the microstructural evolution in the ternary system Ti-Ni-Cr

The role of the Kirkendall effect on microstructures developing in ternary systems was investigated by incorporating Cr in the Ni end-member of the Ti/Ni diffusion couple (Fig. 6.7). To this end, an alloy consisting of 85 at.% of Ni and 15 at.% of Cr was melted in the arc furnace and this alloy was used as an end-member against pure Ti.

Valuable information on the microstructure of a ternary diffusion couple after heat treatment can be obtained from a ternary phase diagram. In Fig. 7.3, the ternary Ni-Cr-Ti phase diagram at 850 °C taken from Ref. [7] is shown. No ternary phases are present in this system. The mass balance line connecting the two starting materials of the diffusion couple is depicted as a dashed straight line.

Fig. 7.4 shows a BEI of a Ni(+15 at.% Cr)/Ti diffusion couple annealed at 850 °C for 100 h. Next to the three intermetallics: TiNi<sub>3</sub>, TiNi and Ti<sub>2</sub>Ni, as was found in the Ti/Ni diffusion couple (Fig. 6.7), also pure Cr-precipitates were formed. This observation can be appreciated with the help of the concept of the *diffusion path* [8,9]. The diffusion path is a line on a ternary isotherm, representing the locus of the average composition in planes parallel to the original contact surface throughout the diffusion zone. Since no material can be lost or created during reaction, the diffusion path is impelled to cross the mass balance line at least once. The diffusion path, as drawn based on the microstructure of Fig. 7.4, is depicted as a solid/dotted line in Fig. 7.3.

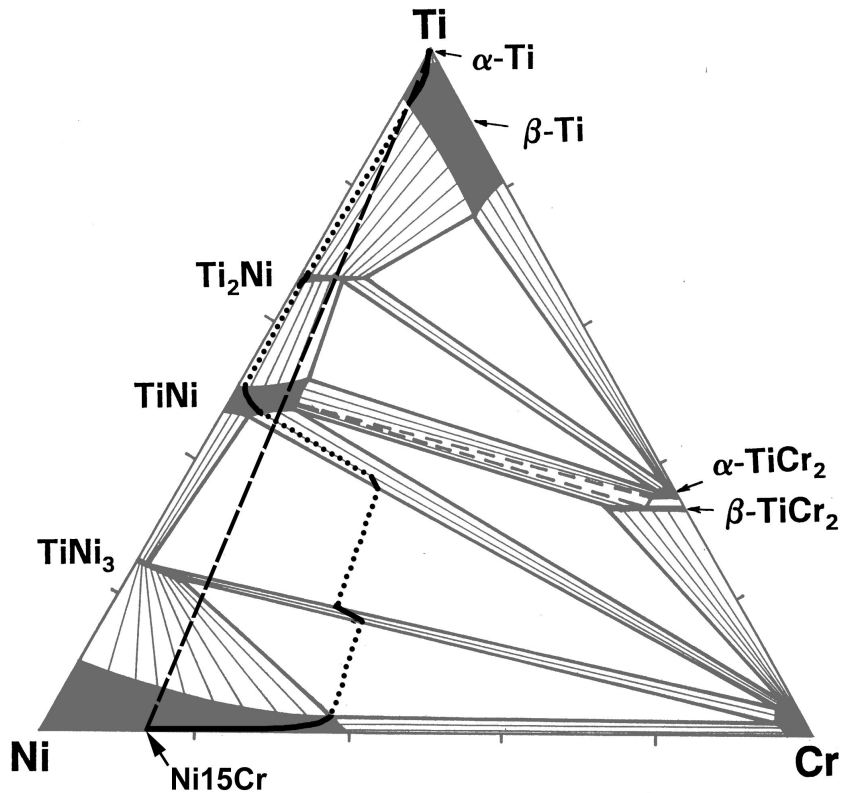


Figure 7.3: Isothermal cross-section through the ternary phase diagram Ni-Cr-Ti at 850 °C [7].

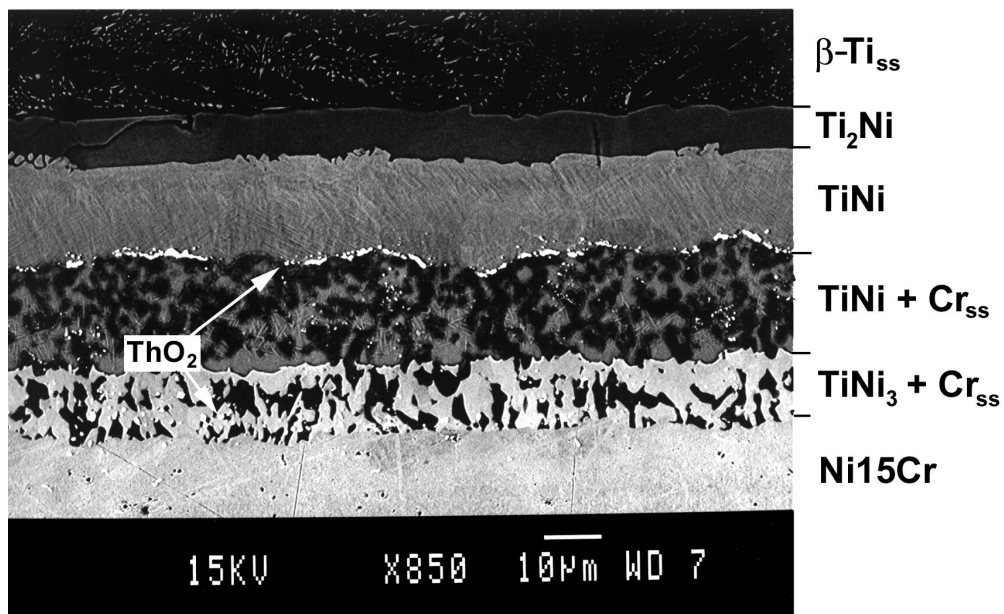


Figure 7.4: BEI of a Ni15Cr/Ti diffusion couple annealed at 850 °C for 100 h.  $\text{ThO}_2$  particles were used to mark the Kirkendall plane. Probably two Kirkendall planes are formed and in between these planes Cr precipitated out.

ThO<sub>2</sub> particles were used to mark the initial contact surface between the two end-members. It may be recalled that in the pure end-member Ti/Ni diffusion couple two Kirkendall planes emerged: one inside the TiNi layer and one in the TiNi<sub>3</sub> compound (near the TiNi<sub>3</sub>/Ni interface). In the Ni<sub>15</sub>Cr/Ti diffusion couple, we observe a slightly different behaviour of the inert ThO<sub>2</sub> particles. One can see clearly the Kirkendall plane in the TiNi phase. However, the one in the TiNi<sub>3</sub> was not found back a row of ThO<sub>2</sub> particles. In fact, the markers are spread all over the diffusion zone between the Kirkendall plane in TiNi and the Ni<sub>15</sub>Cr end-member.

During the reaction between Ti and Ni<sub>15</sub>Cr, Cr is formed as a “side product” and appeared in between the Kirkendall plane in the TiNi phase and the Ni<sub>15</sub>Cr end-member. The reason that the Cr-agglomerates do not exceed the Kirkendall plane in the direction of the Ti-end-member is because the “pure” Cr precipitates as a whole cannot intrinsically diffuse up-hill their own activity gradient. In a sense, the Cr-precipitates can be, just as carbon in the Pt/SiC couple, considered as *in situ* formed “inert” markers, which are immobile and indicate the position the original contact surface. Such observations have also been done in the systems Fe/SiC [10] and Co/SiC [11].

Returning to the ThO<sub>2</sub> particles, it can be concluded that the position of the Cr-precipitates is related to the location of thoria markers. Although the exact mechanism of formation of the interaction zone in this couple is not fully understood, it is clear that the Kirkendall effect plays a prominent role on the microstructural evolution during the interdiffusion between Ni<sub>15</sub>Cr and Ti. Next to the concept of the diffusion path, the analysis shown in this thesis may provide a useful tool in understanding (and predicting) the microstructural evolution in ternary (or higher order) systems.

## References

1. F.J.J. van Loo, G.F. Bastin and J.W.G.A. Vrolijk, *Met. Trans. A* **18A** (1987) 801.
2. Y. Adda and J. Philibert, *La diffusion dans les solides*, Tome I., Press Universitaires de France, Paris, (1966).
3. F.J.J. van Loo, B. Pieraggi and R.A. Rapp, *Acta metall. mater.* **38** (1990) 1769.
4. M.J.H. van Dal and A.M. Gusak, *Proceedings of Metal Physics and Advanced Technologies* **19** (2000) 5.
5. A.A. Kodentsov, M.R. Rijnders and F.J.J. van Loo, *Acta mater.* **46** (1998) 6521.
6. S.L. Markovski, M.J.H. van Dal, M.J.L. Verbeek, A.A. Kodentsov and F.J.J. van Loo, *J. Phase Equilibria* **20** (1999) 373.
7. J.A. van Beek, A.A. Kodentsov and F.J.J. van Loo, *J. Alloy Comp.* **270** (1998) 218.
8. J.S. Kirkaldy and L.C. Brown, *Can. Met. Quat.* **2** (1963) 89.
9. F.J.J. van Loo, *Prog. Solid St. Chem.* **20** (1990) 47.
10. J.H. Gülpen, Reactive phase formation in the Ni-Si system. Ph.D. thesis, Eindhoven University of Technology, (1995).
11. M.R. Rijnders, Periodic layer formation during solid state reactions. Ph.D. thesis, Eindhoven University of Technology, (1996).



## Summary<sup>1</sup>

In 1947, Ernest Kirkendall reported the results of his study on the interdiffusion between Cu and  $\alpha(\text{Cu,Zn})$ -brass [1]. In his experiments he marked the contact interface between Cu and brass, prior to annealing, with inert thin molybdenum wires and observed that this planar array of wires (marker plane, scientifically referred to as the Kirkendall plane and in a technological sense the “welding” plane) shifted with respect to the ends of the diffusion couple. This phenomenon is known since then as the Kirkendall effect. It played a decisive role in the development of the solid-state diffusion theory, as it is seen as the most explicit evidence for the occurrence of a vacancy mechanism in most solid-state diffusion processes. In fact, in a binary system it shows the different independent intrinsic diffusion fluxes of the components A and B [2], which causes swelling of one part and shrinking of the other part of the couple, leading to the marker displacement.

The reason for writing this thesis was the need for a re-examination of some basic concepts involved in the analysis of the marker behaviour. The most important conclusion, emerging from our experimental studies over the last years [3-11], is that in a volume-diffusion controlled interaction the Kirkendall plane *need not be unique* as was tacitly assumed up to now. The experimental evidence was found by using as inert markers very fine agglomerates of  $\text{ThO}_2$ -particles, 0.5-5  $\mu\text{m}$  in size, which were evenly spread at the contact surface of the couple in such a way that the interdiffusion was not hindered and each particle can move individually.

In most cases the  $\text{ThO}_2$ -particles after annealing appeared as a row of markers gathered in a single plane. In some cases, however, we found these particles back in two distinct rows, each moving with a (different) velocity  $v = x/2t$ . In other cases the  $\text{ThO}_2$ -particles were found back not as a straight row, but dispersed in a part of the diffusion couple. In the present thesis we

---

<sup>1</sup> Most part of this summary has been published in a paper:  
M.J.H. van Dal, A.M. Gusak, C. Cserhádi, A.A. Kodentsov and F.J.J. van Loo, *Phys. Rev. Let.* **86** (2001) 3352.



have introduced a new approach that takes care of all these experimental findings and enables us to rationalise (and predict) the different manifestations of the Kirkendall effect.

The formation of two “Kirkendall planes” moving with different velocities was, for instance, observed in a layer of  $\beta'$ -AuZn (B2; CsCl-structure), diffusion-grown during solid state reaction at 500 °C between Au and  $\gamma$ -AuZn<sub>2</sub> (Fig. 1). The Kirkendall planes are revealed by the straight rows of ThO<sub>2</sub>-particles used as markers between the initial end-members.

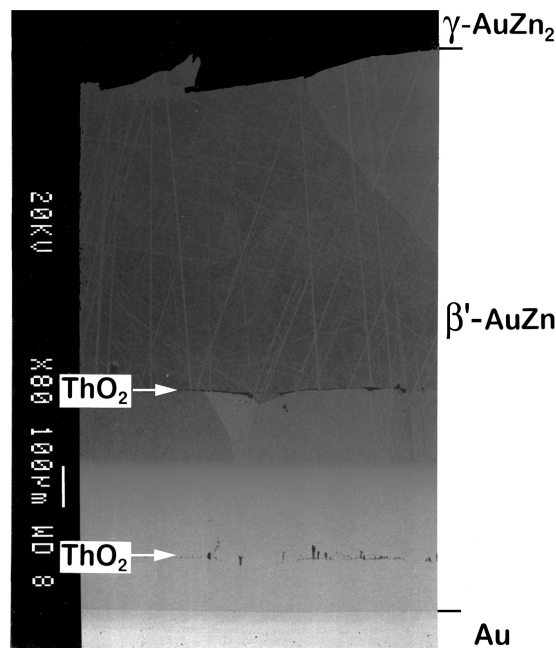


*Figure 1: Back-scattered electron image (BEI) of a Au/Au<sub>36</sub>Zn<sub>64</sub> (“ $\gamma$ -AuZn<sub>2</sub>”) diffusion couple annealed at 500 °C for 17.25 h under flowing argon. After interdiffusion the ThO<sub>2</sub>-markers introduced between the couple halves are clearly visible as two distinct straight rows of inclusions.*

The migration of macroscopic inert inclusions within the zone of interdiffusion can be rationalised in terms of a so-called Kirkendall velocity curve [3,6,12]. This plot displays the velocities of inert particles, placed prior to the annealing at various locations within the anticipated interaction zone, relative to the couple end. In a binary system the Kirkendall velocity,  $v$ , is dependent on the difference in intrinsic diffusivities of the species and can be calculated taking into account the volume changes accompanying interdiffusion [13].

The particles placed at the Kirkendall plane (original contact surface) are the only markers which move parabolically in time with a velocity  $v = x/2t$ . The location (and velocity) of the Kirkendall plane after interdiffusion time  $t$  can be determined from the intersection of the velocity curve and the straight line  $v = x/2t$ .

In the case of the Au/AuZn<sub>2</sub> couple shown in Fig. 1, we note that at 500°C the growing  $\beta'$ -phase exhibits a wide compositional range (38.5 – 56.0 at.% of Zn [14]) and that in the Au-rich part of the homogeneity region Au is the faster diffusing species whereas in the Zn-rich part, Zn-atoms diffuse faster [15]. This means that the velocity plot corresponding to the Au/AuZn<sub>2</sub> diffusion couple resembles the one shown in Fig. 2. The position  $x = 0$  is the location of the original contact surface. It is possible for the line  $v = x/2t$  to intersect the Kirkendall velocity curve up to three times as is shown in the figure. This implies that in such a diffusion couple three “Kirkendall” planes might exist, which move parabolically in time. As a result, the markers originally introduced between the end-members would rearrange during interdiffusion into three distinct parallel rows of inclusions, situated at the positions  $K_1$ ,  $K_2$  and  $K_3$ .

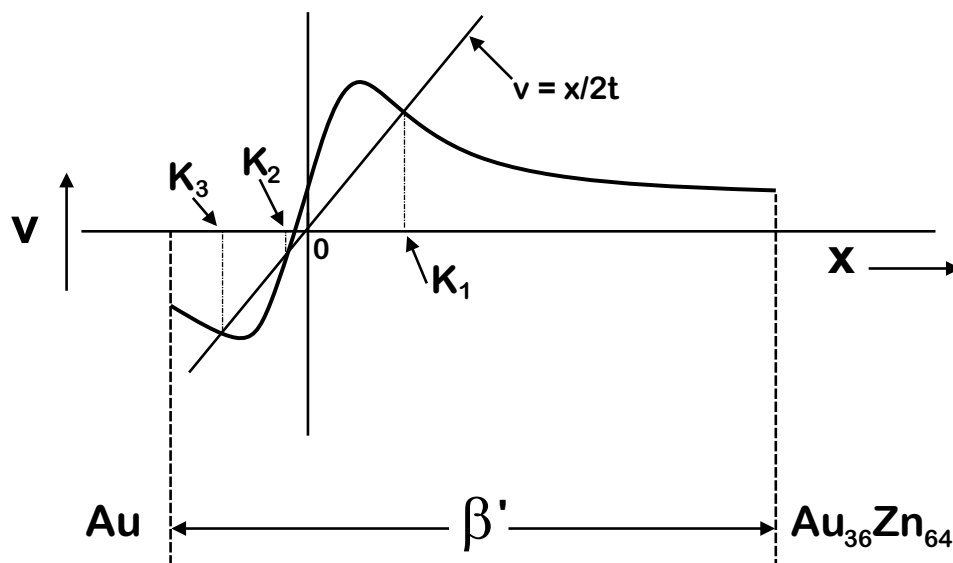


Figure 2: Semi-quantitative Kirkendall velocity corresponding to the  $\beta'$ -AuZn product layer in the annealed (500 °C; 17.25 h; Ar + 5 vol.% H<sub>2</sub>) Au/Au<sub>36</sub>Zn<sub>64</sub> ( $\gamma'$  'AuZn<sub>2</sub>') couple. The position  $x = 0$  corresponds to the original contact surface. Three intersections  $K_1$ ,  $K_2$  and  $K_3$  are found, of which only two correspond to stable Kirkendall planes ( $K_1$  and  $K_3$ ).

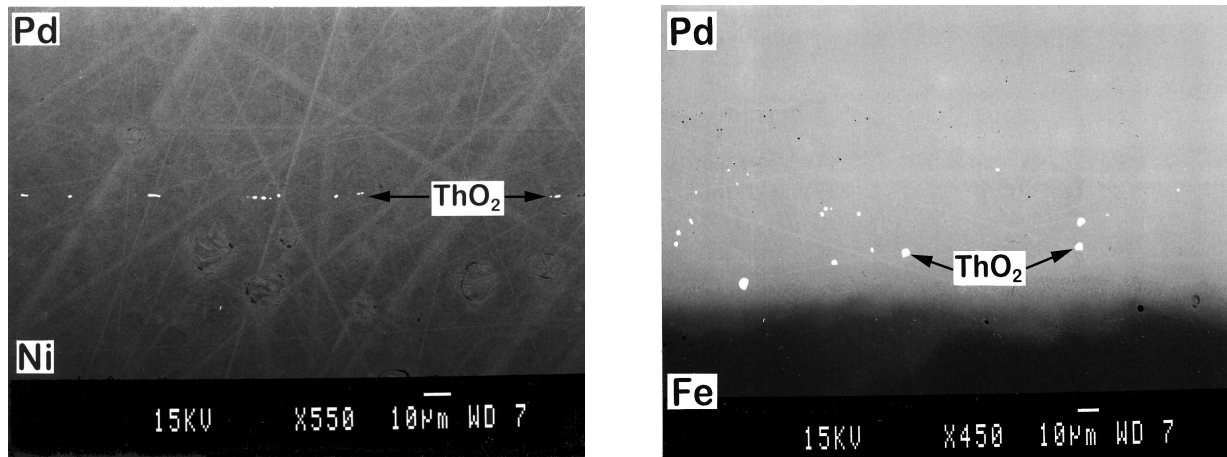
However, one should realise that only two of the three predicted “Kirkendall planes” can be found experimentally within the reaction zone. This can be appreciated by analysing the stability of the Kirkendall plane at the possible intersections. If markers, which ended up at the position  $K_1$  in Fig. 2, would (for whatever perturbation) be slightly ahead of this plane, they would slow down (lower velocity) and if these markers were behind this plane, they would move faster (higher velocity). In other words, the plane located at  $K_1$  tends to “attract” inert markers in its vicinity. Hence, a *stable* Kirkendall plane will emerge in the interdiffusion zone when the straight-line  $v = x/2t$  intersects the velocity curve at a position where the Kirkendall velocity has a *negative gradient*.

Following a similar line of argument, it can be concluded that an *unstable* Kirkendall plane will appear inside a diffusion zone when the gradient of the velocity is *positive* at the intersection point. Indeed, the markers which are slightly ahead of the plane situated at  $K_2$  in Fig. 2 will move faster, and markers slightly behind this plane will migrate slower. If such an unstable Kirkendall plane is situated between two stable ones (like in the example in Fig. 2), the stable planes will accumulate all markers during the initial stage of interdiffusion. Therefore, only two Kirkendall planes (at the positions  $K_1$  and  $K_3$ ) are expected to appear. The occurrence of two Kirkendall planes in the Au/AuZn<sub>2</sub> couple has been observed indeed (Fig. 1).

A particularly convincing example of the formation of stable and unstable Kirkendall planes is provided by the observations made in the study on the Kirkendall effect in Ni-Pd and Fe-Pd solid solution systems. Fig. 3 shows back-scattered electron images of a Ni/Pd and an Fe/Pd diffusion couple annealed at 1100°C.

One can see a remarkable difference in the appearance of the markers inside the interdiffusion zones. In the Ni-Pd system, the ThO<sub>2</sub> particles form a planar array of plate-like inclusions within the diffusion zone. In the Fe/Pd couple, on the other hand, a significant scattering of the particles occurred upon interaction.

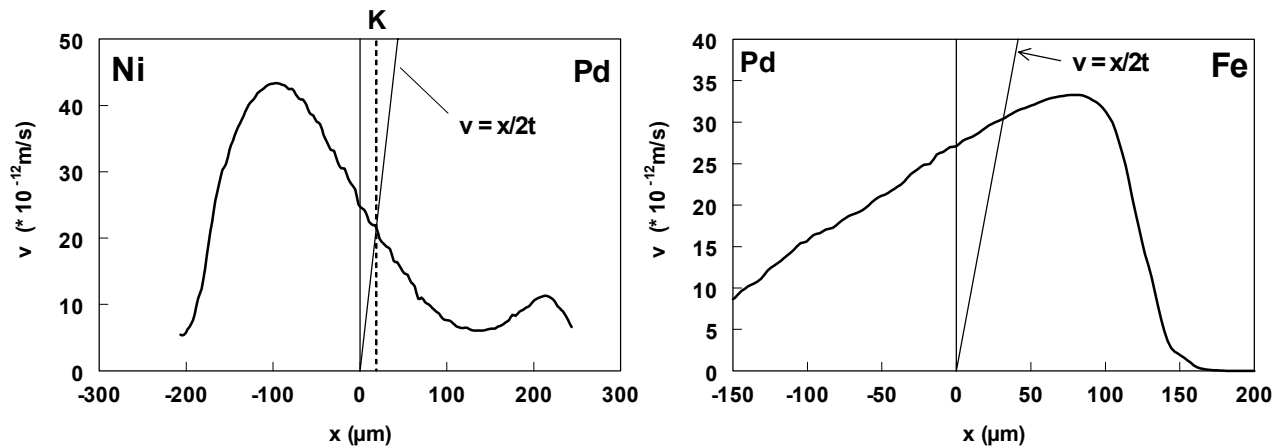
The Kirkendall velocity curves corresponding to the couples were constructed experimentally using the multi-foil diffusion couple technique [16] (Fig. 4).



a)

b)

Figure 3: BEI of (a) a Ni/Pd diffusion couple annealed at 1100 °C in vacuum for 196 h and (b) an Fe/Pd couple after interdiffusion at 1100 °C in vacuum for 144 h. The ThO<sub>2</sub> markers exhibit a white contrast.



a)

b)

Figure 4: Experimentally determined Kirkendall velocity curves of (a) a multi-foil Ni/Pd couple annealed at 1100 °C for 121 h and (b) a multi-foil Fe/Pd couple annealed at 1100 °C for 144 h.

In both cases, the line  $v = x/2t$  intersects the velocity curve once. In the Ni/Pd diffusion couple, the velocity curve at the intersection point has a negative slope, which results in the formation of a single, stable Kirkendall plane inside the interdiffusion zone (Fig. 4a). The appearance of the marker array as a straight row of plate-like ThO<sub>2</sub>-particles reflects the

tendency of a stable Kirkendall plane to accumulate the markers in its vicinity. By contrast, in the case of the Fe/Pd couple, the straight line intersects the velocity curve at a point where the Kirkendall velocity has a *positive* gradient, which will lead to an *unstable* Kirkendall plane (Fig. 4b). The initial planar array of the markers at the contact interface tends to transform into an array of ThO<sub>2</sub>-particles spatially distributed in the diffusion direction. One could say that no Kirkendall plane in the Fe/Pd diffusion couple exists at all. The latter result might have an important technological implication: diffusion bonds exhibiting a single unstable will probably exhibit better mechanical properties, since the “welding” plane (a notoriously weak spot from a mechanical point of view) “disappeared”.

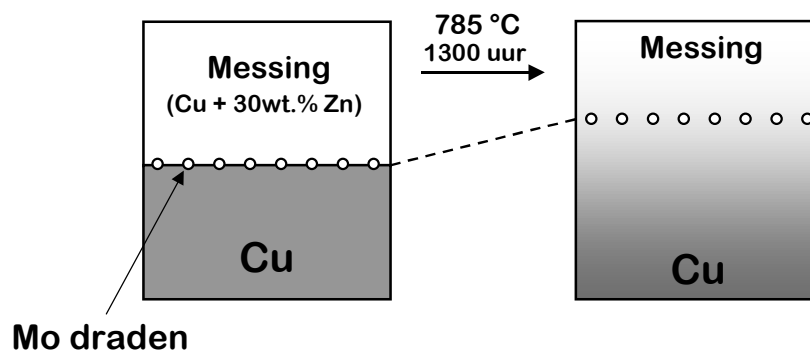
## References

1. A.D. Smigelskas and E.O. Kirkendall, *Trans. AIME* **171** (1947) 130.
2. L.S. Darken, *Trans. AIME* **175** (1948) 184.
3. M.J.H. van Dal, M.C.L.P. Pleumeekers, A.A. Kodentsov and F.J.J. van Loo, *Acta mater.* **48** (2000) 385.
4. M.J.H. van Dal, M.C.L.P. Pleumeekers, A.A. Kodentsov and F.J.J. van Loo, *J. Alloy Comp.* **309** (2000) 132.
5. M.J.H. van Dal, A.A. Kodentsov and F.J.J. van Loo, *Solid State Phenomena* **72** (2000) 111.
6. M.J.H. van Dal, A.M. Gusak, C. Cserháti, A.A. Kodentsov and F.J.J. van Loo, *Phys. Rev. Let.* **86** (2001) 3352.
7. M.J.H. van Dal, A.M. Gusak, C. Cserháti, A.A. Kodentsov and F.J.J. van Loo, *Defect and Diffusion Forum* **194-199** (2001) 195.
8. M.J.H. van Dal, D.G.M.M. Huibers, A.A. Kodentsov and F.J.J. van Loo, *Intermetallics* **9** (2001) 409.
9. M.J.H. van Dal, A.A. Kodentsov and F.J.J. van Loo, *Intermetallics* **9** (2001) 451.
10. M.J.H. van Dal, A.M. Gusak, C. Cserháti, A.A. Kodentsov and F.J.J. van Loo, accepted for publication in *Philosophical Magazine A*.
11. M.J.H. van Dal and A.M. Gusak, *Proceedings of Metal Physics and Advanced Technologies* **19** (2000) 5.
12. J.-F. Cornet and D. Calais, *J. Phys. Chem. Solids* **33** (1972) 1675.
13. F.J.J. van Loo, *Prog. Solid St. Chem.* **20** (1990) 47.
14. H. Okamoto and T.B. Massalski, Phase diagrams of binary gold alloys. Metals Park, Ohio, American Society for Metals (1988) p. 331.
15. D. Gupta and D.S. Lieberman, *Phys. Rev. B* **4** (1971) 1070 .
16. Th. Heumann, and G. Walther, *Z. Metallkde.* **48** (1957) 151.



## Samenvatting

In 1947 publiceerde Ernest Kirkendall de resultaten van zijn onderzoek naar diffusie van zink en koper in  $\alpha$ -messing [1]. In dit werk beschreef hij een experiment waarin een zgn. diffusiekoppel, dat bestond uit een messing staaf met een electrolytisch aangebrachte dikke laag zuiver koper, werd verhit op  $785^\circ\text{C}$ . Hij markeerde het oorspronkelijke grensvlak tussen het messing en koper met inerte molybdenen draden. Figuur 1 laat een gedeelte van de dwarsdoorsnee van het diffusiekoppel zien. Als gevolg van de verhitting gedurende enkele honderden uren diffundeerden de koper en zink atomen om het concentratieverschil op te heffen. Kirkendall ondervond dat tijdens de interactie de binnenste staaf kromp, m.a.w. de molybdenen draden bewogen naar de messing zijde van het diffusiekoppel (Fig. 1).



*Figuur 1: Schematische tekening van een gedeelte van de dwarsdoorsnede van het diffusiekoppel zoals geprepareerd door Kirkendall [1] voor en na de hittebehandeling. De Mo-draden bleken na de interactie te zijn verschoven in de richting van het messing eindstuk, dit als gevolg van de ongelijke diffusie van Cu en Zn atomen in de interactie zone.*

Op grond van volumeveranderingen kon dit niet verklaard worden. Hij concludeerde dat de verschuiving van de markeerdraden aantoonde dat de zink atomen veel sneller naar de ene kant van het diffusiekoppel (Cu-eindstuk) diffundeerden dan de koper atomen naar de andere kant. Dit experiment was het eerste directe bewijs van niet-gelijke diffusie van de elementen tijdens een interdiffusie proces in de vaste stof en de verplaatsing van inerte deeltjes dientengevolge staat sindsdien bekend als het **Kirkendall effect**. Het vlak waarin de markeerdraden liggen (ook wel lasnaad genoemd) wordt aangeduid met het **Kirkendall-vlak**.



Het was aan Darken in 1948 [2] om de theoretische grondslag achter het fenomeen te beschrijven. Hij gebruikte daarvoor de diffusietheorie zoals die beschreven is door Fick [3] (de eerste wet van Fick):

$$\tilde{J} = \tilde{D} \frac{\partial C}{\partial x}. \quad (1)$$

De term  $\tilde{J}$  staat voor de interdiffusie flux (mol/m<sup>2</sup>s),  $C$  voor de concentratie (mol/m<sup>3</sup>),  $x$  voor de diffusie parameter en  $\tilde{D}$  is de interdiffusiecoëfficiënt. Darken liet zien dat deze interdiffusiecoëfficiënt was opgedeeld in twee intrinsieke (onafhankelijke) diffusiecoëfficiënten:

$$\tilde{D} = V_A C_A D_B + V_B C_B D_A. \quad (2)$$

$D_i$ ,  $C_i$  en  $V_i$  representeren, respectievelijk, de intrinsieke diffusiecoëfficiënt (m<sup>2</sup>/s), de concentratie (mol/m<sup>3</sup>) en het partiële molaire volume (m<sup>3</sup>/mol) van component  $i$ .

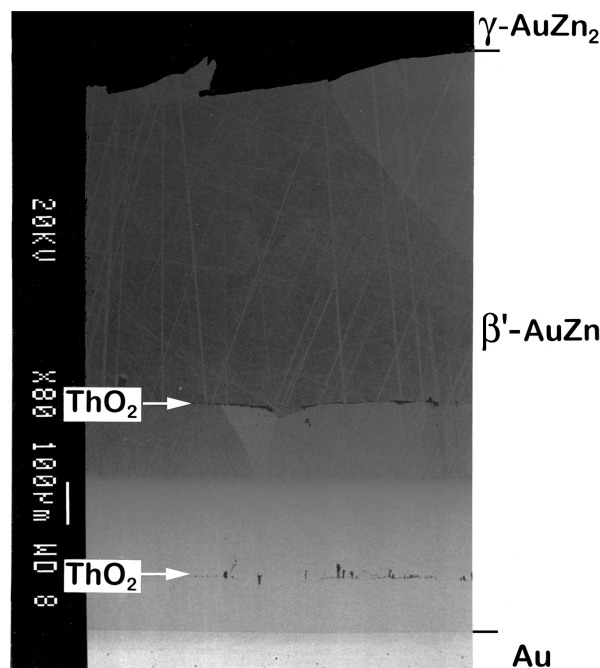
Heden ten dage staat het Kirkendall effect bekend als een fenomeen dat zich manifesteert in allerlei verschijnselen in een vast-vast interactie zoals de formatie van poriën, de ontwikkeling van spanning en zelfs deformatie van het materiaal. Dit soort processen zijn van betekenis in technologische vakgebieden waarbij verschillende materialen met elkaar worden verbonden: composiet materialen, coating technologie, dunne-film elektronische producten, las- en soldeertechnologie enzovoorts. Het is duidelijk dat een fundamenteel begrip van dit effect van groot belang is. Bijvoorbeeld, het Kirkendall-vlak is in deze constructies in het algemeen een mechanisch zwakke plek, waarover men zo veel mogelijk voorspelbare informatie wil bezitten.

Echter, ondanks het feit dat het Kirkendall effect sinds zijn ontdekking intensief is onderzocht, zijn er nog steeds enkele elementaire aspecten niet volledig duidelijk. Één daarvan is het volgende: is het oorspronkelijke contactvlak (Kirkendall-vlak), gemarkeerd door inerte deeltjes, uniek? Anders gezegd: kunnen de inerte deeltjes op het initiële contactvlak tijdens interactie verschillend migreren binnen de interdiffusie zone, zodat er

meer dan één Kirkendall-vlak ontstaan? In dit proefschrift is aangetoond dat het Kirkendall-vlak zowel enkelvoudig als meervoudig, stabiel of onstabiel kan zijn.

De vorming van meervoudige Kirkendall-vlakken werd gevonden toen we een goud-zink legering ( $\text{AuZn}_2$ ) en zuiver goud (Au) lieten reageren bij  $500^\circ\text{C}$ . Hierbij werd gebruik gemaakt van kleine homogeen verspreide  $\text{ThO}_2$ -deeltjes ( $0.5\text{-}5\ \mu\text{m}$ ) om het oorspronkelijke grensvlak tussen  $\text{AuZn}_2$  en Au te markeren [4]. Figuur 2 laat een dwarsdoorsnede van het diffusiekoppel zien. Zoals te zien, is er één verbinding gevormd:  $\beta'$ -AuZn.

De  $\text{ThO}_2$ -deeltjes zijn duidelijk waarneembaar vanwege het grijze contrast dat ze vertonen op de “back-scattered” elektronenmicroscopfoto. De deeltjes werden op twee gelokaliseerde posities binnen de AuZn-laag teruggevonden. Blijkbaar zijn er twee “Kirkendall-vlakken” gevormd uit één oorspronkelijk contactvlak!



*Figuur 2: Dwarsdoorsnede van een Au/ $\gamma$ -AuZn<sub>2</sub> diffusiekoppel gestookt bij  $500^\circ\text{C}$  gedurende 17.25 uur. Er ontstaat een intermetallische laag bestaande uit  $\beta'$ -AuZn. De  $\text{ThO}_2$ -deeltjes, gebruikt om het oorspronkelijke grensvlak te markeren, werden teruggevonden op twee gelokaliseerde posities.*

Om dit te kunnen verklaren zijn we in dit proefschrift dieper ingegaan op de theorie zoals die beschreven is door Darken [2]. Volgens Darken hebben we bij een binair A-B interdiffusie

proces te maken met twee onafhankelijke fluxen,  $J_A$  en  $J_B$ , die in een vast-vast interactie niet per definitie gelijk hoeven te zijn. Als gevolg van de ongelijkheid van deze fluxen ontstaat er een netto massaflux. Deze massaflux, die het interdiffusie proces vergezelt, kan worden gevisualiseerd door de migratie van inerte deeltjes aanwezig in de interactie zone. De snelheid van zulke deeltjes, de zgn. Kirkendall-snelheid  $v$ , is dus gelijk aan:

$$v = -(V_A J_A + V_B J_B), \quad (3)$$

en, gegeven dat de fluxen van A en B ( $J_A$  en  $J_B$ ) beschreven kunnen worden met Fick's eerste wet van diffusie met  $dC_B = (V_A / V_m^2) dN_B$ , wordt dit:

$$v = \frac{V_A V_B}{V_m^2} (D_B - D_A) \frac{\partial N_B}{\partial x}. \quad (4)$$

Hierin is  $V_m$  het molaire volume ( $\text{m}^3/\text{mol}$ ) en  $N_B$  de mol fractie van B.

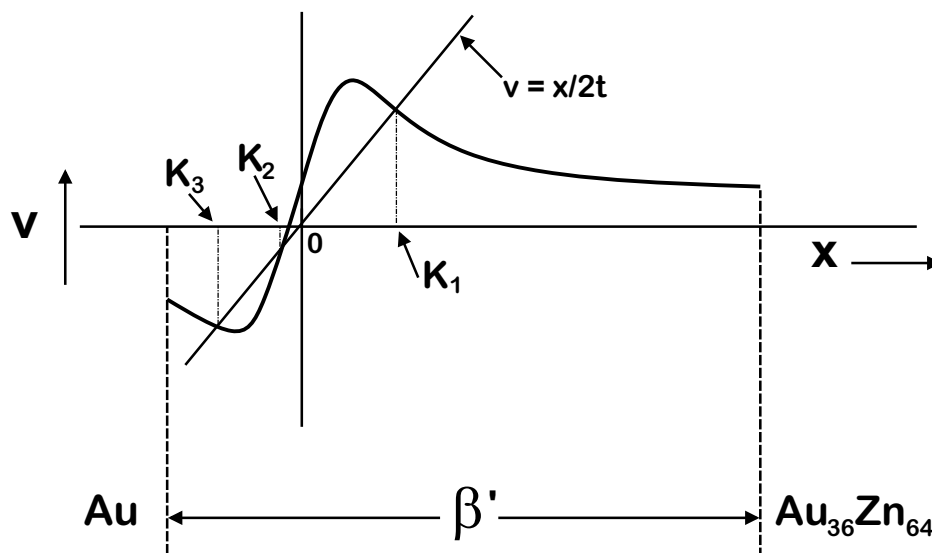
Nu is het zo dat de deeltjes, die op het oorspronkelijke grensvlak van het diffusiekoppel aanwezig zijn (de Kirkendall markeringen), de enige zijn die op tijd  $t = 0$  beginnen te bewegen. Omdat we hier alleen diffusie-gelimiteerde processen behandelen, bewegen deze deeltjes, en dus het Kirkendall-vlak, parabolisch met de tijd met een snelheid  $v = dx/dt = (x_K - x_0)/2t$ . De parameter  $x_K$  is de positie van de Kirkendall-deeltjes na stooktijd  $t$  en  $x_0$  is hun positie op  $t = 0$ ;  $x_K - x_0$  geeft dus de verplaatsing van de deeltjes weer.

Dit gegeven kan samen met vgl. (4) gebruikt worden om de positie van het Kirkendall-vlak in een willekeurig diffusiekoppel te bepalen als de intrinsieke diffusiecoëfficiënten van de diffunderende elementen bekend zijn over het relevante concentratiegebied. De locatie en snelheid van het Kirkendall-vlak kunnen dan immers grafisch gevonden worden via het snijpunt tussen de Kirkendall-snelheidscurve beschreven door vergelijking (4) en de rechte  $v = x/2t$ . Dit concept gaan we demonstreren aan de hand van het Au/AuZn<sub>2</sub> koppel van Fig. 2.

Hiervoor is het belangrijk te weten dat de  $\beta'$ -AuZn (B2; CsCl-structuur) bij hogere temperatuur (rond 500 °C) een breed oplosbaarheidsgebied heeft (van 38 – 57 at.% zink [5])

en dat aan de Zn-rijke zijde van deze fase Zn sneller diffundeert en aan de Au-rijke zijde Au de snelst diffunderende component is [6]. Dit betekent dat de Kirkendall-snelheidscurve (beschreven door vgl. (4)) voor het Au/AuZn<sub>2</sub> koppel waarin de  $\beta'$ -AuZn fase groeit een vorm heeft zoals die is weergegeven in Fig. 3.

Nu is het theoretisch voor te stellen dat de rechte  $v = x/2t$  de Kirkendall-snelheidscurve drie maal snijdt ( $K_1$ ,  $K_2$  en  $K_3$ ), waarbij gezegd moet worden dat  $x = 0$  overeen komt met de positie van het oorspronkelijke grensvlak. De inerte deeltjes aanwezig op het originele contactvlak tussen Au en AuZn<sub>2</sub> kunnen dus terechtkomen op deze drie posities wat, in principe, zou leiden tot drie “Kirkendall-vlakken”.



Figuur 3: Semi-kwantitatieve Kirkendall-snelheidscurve die overeenkomt met een Au/AuZn<sub>2</sub> diffusiekoppel gestookt bij 500 °C, waarin alleen de  $\beta'$ -AuZn fase groeit. In deze fase is het zo dat in het Au-rijke gedeelte Au sneller diffundeert en in de Zn-rijke gebied Zn de snelst diffunderende component is. De rechte  $v = x/2t$  snijdt de curve op drie plaatsen  $K_1$ ,  $K_2$  en  $K_3$  ( $x = 0$  is de positie van Kirkendall-markeringen op  $t = 0$ ).

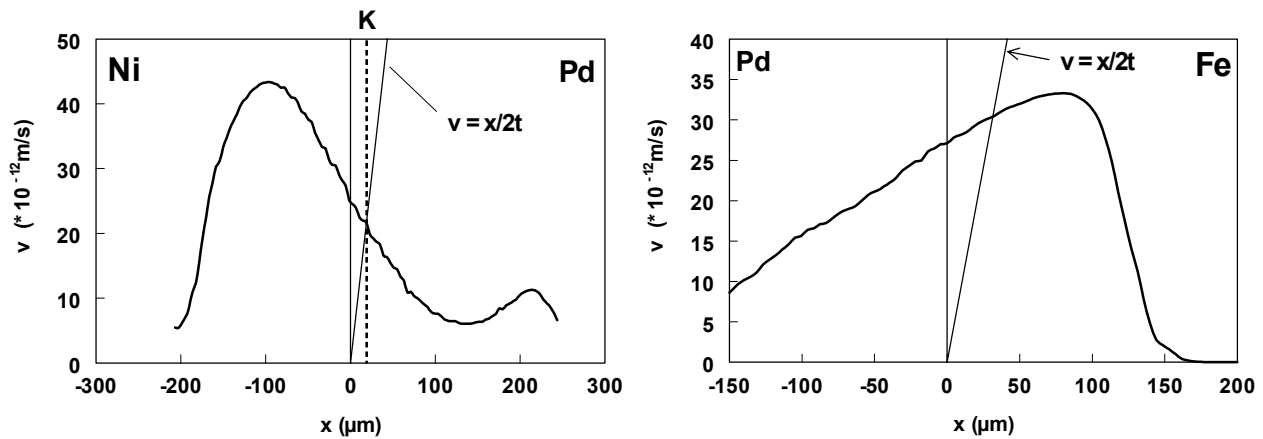
Het is echter zo dat alleen de Kirkendall-vlakken corresponderend met positie  $K_1$  en  $K_3$  zichtbaar zullen zijn omdat deze *stabiel* zijn. Om dit duidelijk te maken concentreren we ons even op het Kirkendall-vlak op positie  $K_1$ . Men kan zich voorstellen dat een inert deeltje, dat zich bevindt op deze positie, door een kleine verstoring iets vooruit is geraakt. Het heeft nu een lagere snelheid dan de deeltjes op het “echte” Kirkendall-vlak  $K_1$ . Als gevolg zal dit

deeltje worden ingehaald door dat Kirkendall-vlak. Zo kan men ook zeggen dat, als een deeltje een beetje achterop raakt, het een grotere snelheid zal hebben dan de deeltjes op Kirkendall-vlak  $K_1$ . Dit deeltje zal de Kirkendall-deeltjes weer inhalen. Concluderend kunnen we nu stellen dat het Kirkendall-vlak op positie  $K_1$  de neiging heeft de deeltjes in zijn omgeving naar zich toe te trekken, i.e. Kirkendall-vlak  $K_1$  is stabiel. Hetzelfde geldt voor Kirkendall-vlak  $K_3$ . Dus een stabiel Kirkendall-vlak komt overeen met een snijpunt tussen de rechte  $v = x/2t$  en de Kirkendall-snelheidscurve waar deze een *negatieve gradiënt* heeft.

Doorredenerend kunnen we nu ook stellen dat het Kirkendall-vlak op positie  $K_2$  *onstabiel* is. Inderdaad, als een deeltje iets voorop raakt, heeft het een grotere snelheid dan de deeltjes op positie  $K_2$  en zal niet terugkeren. Zo ook als een deeltje een beetje achter positie  $K_2$  terechtkomt heeft het een lagere snelheid en zal ook niet terugkeren. Dus een onstabiel Kirkendall-vlak kan beschreven worden als het snijpunt van lijn  $v = x/2t$  met de Kirkendall-snelheidscurve waar deze een *positieve gradiënt* heeft. Aangezien in de interdiffusiezone van Figuur 3 er twee stabiele Kirkendall-vlakken aanwezig zijn, zullen deze alle deeltjes in de beginfase van de interactie accumuleren en zal het onstabiele Kirkendall-vlak  $K_2$  niet zichtbaar zijn. Dit is de situatie zoals we die hebben gezien in het Au/AuZn<sub>2</sub> koppel.

Nu blijft de vraag: bestaan er systemen waarin alleen één *onstabiel* Kirkendall-vlak voorkomt, en hoe manifesteert dit zich? Dit gaan we demonstreren aan de hand van diffusiekoppel experimenten in de Ni-Pd en Fe-Pd systemen [9]. Figuur 4a en b tonen de experimenteel bepaalde Kirkendall-snelheidscurven voor, respectievelijk, een Ni/Pd diffusie koppel gestookt bij 1100°C gedurende 121 uur en een Fe/Pd diffusie koppel na een hittebehandeling bij 1100°C gedurende 144 uur. Deze curven zijn bepaald met behulp van de zgn. “multi-folie” diffusiekoppel techniek [7,8].

Zoals te zien is snijdt de rechte  $v = x/2t$  de snelheidscurven slechts eenmaal, dus in beide gevallen is er maar één Kirkendall-vlak te verwachten. Echter, in het geval van het Ni/Pd koppel heeft de snelheidscurve een negatieve gradiënt in het intersectiepunt en voor het Fe/Pd koppel een positieve gradiënt. Dit zou betekenen dat er in het Ni/Pd koppel een *stabiel* en het Fe/Pd geval een *onstabiel* Kirkendall-vlak ontstaat.

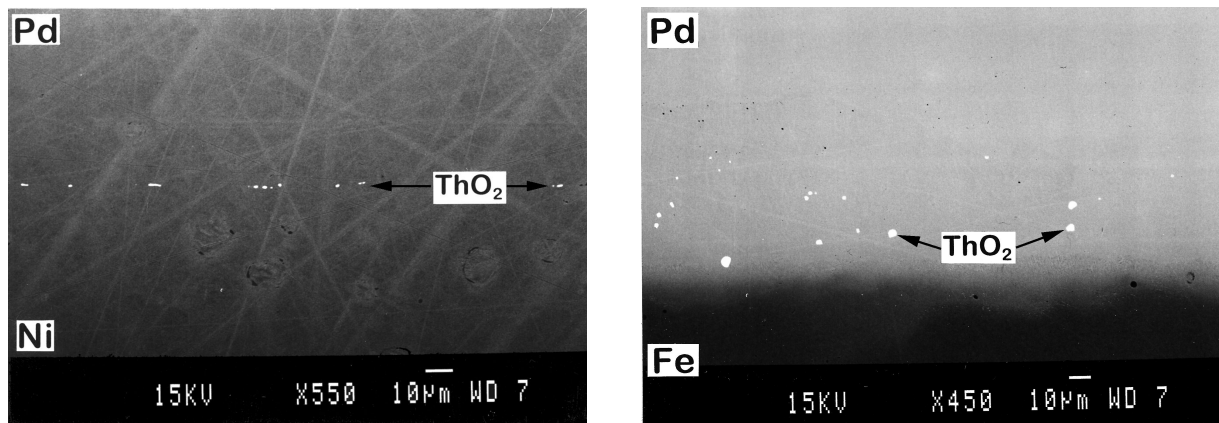


a)

b)

Figuur 4: Kirkendall-snelheidscurven corresponderend met a) een Ni/Pd diffusiekoppel (1100 °C; 121 uur) en b) een Fe/Pd diffusiekoppel (1100 °C; 144 uur).

De (on)stabiliteit van het Kirkendall-vlak in de interdiffusiezone openbaart zich door het gedrag van de inerte ThO<sub>2</sub>-deeltjes die aanwezig waren op het originele contact vlak van het diffusiekoppel. Figuur 5 a en b laten “back-scattered” elektronen microscoop foto’s zien van, respectievelijk, een Ni/Pd koppel (1100 °C; 196 uur) en een Fe/Pd koppel (1100 °C; 144 uur). In beide koppels vertonen de ThO<sub>2</sub> deeltjes een wit contrast.



a)

b)

Figuur 5: Dwarsdoorsneden van a) een Ni/Pd diffusiekoppel en b) een Fe/Pd diffusiekoppel die gestookt zijn bij 1100 °C gedurende, respectievelijk, 196 en 144 uur. De ThO<sub>2</sub>-deeltjes vertonen een wit contrast in de “back-scattered” elektronen-microscopfoto’s.

Als men kijkt naar het Ni/Pd koppel is te zien dat de agglomeraten van de ThO<sub>2</sub> deeltjes “netjes” in een rechte lijn gerangschikt zijn en hebben ze een “platte” vorm. Dit geeft aan dat het stabiele Kirkendall-vlak de neiging heeft de deeltjes aan te trekken.

Een ander beeld is te zien in het Fe/Pd koppel. De ThO<sub>2</sub> deeltjes zijn geheel verspreid over de diffusiezone. Omdat we hier te maken hebben met een enkel onstabiel Kirkendall-vlak en er dus geen stabiel Kirkendall-vlak is dat de deeltjes naar zich toe trekt, verspreiden de deeltjes zich en lijkt het wel of het systeem de “informatie” van het originele contact vlak verloren heeft. Dit laatste heeft een belangrijke technologische betekenis: een verbinding waarin alleen een onstabiel Kirkendall-vlak voorkomt zal andere (waarschijnlijk betere) mechanische eigenschappen vertonen dan een verbinding waarin allerlei mogelijke verontreinigingen zich kunnen ophopen in een enkel stabiel Kirkendall-vlak. Dat zal met name zo zijn in het vaak voorkomende geval waarbij dit stabiele Kirkendall-vlak gesitueerd is in een fasegrens waar de (mechanische) eigenschappen toch al sprongswijze veranderen.

**Referenties**

1. A.D. Smigelskas en E.O. Kirkendall, *Trans. AIME* **171** (1947) 130.
2. L.S. Darken, *Trans. AIME* **175** (1948) 184.
3. A. Fick, *Pogg. Ann.* **94** (1854) 59.
4. M.J.H. van Dal, A.M. Gusak, C. Cserhádi, A.A. Kodentsov en F.J.J. van Loo, geaccepteerd voor publicatie in *Phil. Mag. A*.
5. H. Okamoto en T.B. Massalski, Phase Diagrams of Binary Gold Alloys. Metals Park, Ohio, American Society for Metals, (1998) p. 331.
6. D. Gupta en D.S. Lieberman, *Phys. Rev. B* **4** (1971) 1070.
7. Th. Heumann en G. Walther, *Z. Metallkde.* **48** (1957) 151.
8. M.J.H. van Dal, M.C.L.P. Pleumeekers, A.A. Kodentsov en F.J.J. van Loo, *Acta mater.* **48** (2000) 385.





## Dankwoord

De afgelopen vier jaar, gedurende welke periode ik mijn promotieonderzoek bij de capaciteitsgroep Vaste Stof en Materialen Chemie heb volbracht, heb ik als enorm plezierig ervaren. Zowel op wetenschappelijk als menselijk vlak ben ik daarvoor een aantal mensen, zonder wie ik dit proefschrift nooit had kunnen schrijven, zeer dankbaar. Terugkijkend op deze periode besef ik pas hoeveel ze voor me hebben betekend.

Als eerste wil ik mijn eerste promotor Frans van Loo noemen. Tijdens de “diffusiegroep” bijeenkomsten en de individuele gesprekken heb ik enorm veel geleerd op het gebied van de diffusie en de thermodynamica. Zijn geduld, kennis en inzicht zijn bewonderingwaardig. Bij deze wil ik hem hartelijk bedanken.

Daarnaast wil ik Bert de With als tweede promotor bedanken mij de mogelijkheid en de vrijheid te geven om mijn onderzoek naar eigen inzicht uit te voeren.

Aan Sasja Kodentsov ben ik enorm veel dank verschuldigd. Hij heeft mij alle principes van de materiaalkunde geleerd en heeft zo de basis gelegd voor een erg vruchtbare (en soms vloeibare, met name alcoholische) samenwerking. Als Sasja aanwezig is, is er altijd leven in de brouwerij.

САША, СПАСИБО!

Csaba Cserhádi wil ik in het bijzonder bedanken. Hij heeft me tijdens zijn verblijf van twee jaren in de capaciteitgroep erg vaak geholpen vooral met elektronen microscopie. Csaba stond altijd voor me klaar.

Csaba, köszönöm szépen!

Prof. Andrei Gusak was very important for the development of the present work. He solved overnight the problem of the microstructural stability of the Kirkendall plane, which turned out to become a major topic of this thesis. It was an honour for me to co-operate with such a kind and bright man.

АНДРІЙ, ЩЕРО ДЯКУЮ!

I would also like to thank prof. Ülo Ugaste for the help during the initial stages of my promotion and for participating in the promotion committee.

Van de technische staf wil ik iedereen bedanken die me geassisteerd heeft. Daarvan wil ik er een paar speciaal vernoemen: Huub van der Palen, Han van Beek en Marco Hendrix. Huub heeft me met bijna alle diffusiekoppel experimenten geholpen en was (en is) onmisbaar voor het onderzoek. Ik zal de “multi-foil” experimenten die Huub voor me deed nooit vergeten! Han zal ik me altijd blijven herinneren door zijn onvermoeide werklust die hem zo lange tijd op de been hield. Han, het ga je goed! Naast de technische ondersteuning, heb ik met Marco met veel plezier menig kaartje gelegd en balletje getrapt.

Sergei Shulepov wil ik onder meer bedanken voor het schrijven van het computer programma (gegeven in Appendix 4.1) en het kampioen maken van ons voetbalteam *de ST-jers!* Ik zou ook graag Jos Jansen en Paul van de Varst willen noemen die mij met de wiskundige berekeningen (paragraaf 4.2) hebben geholpen.

Een belangrijk deel van het praktische werk is geleverd door de afstudeerders Matty Pleumeekers (hoofdstuk 3) en Dianne Huibers (hoofdstuk 5), die ik daarvoor ook zeer erkentelijk ben.

Mijn AiO-collega's wil ik allemaal bedanken voor de fijne sfeer binnen en buiten de vakgroep, met name Pascal en de Sevilla-gangers Emilio, Maru, Niels en Dennis. Al mijn kamergenoten wil ik ook bedanken voor de leuke gesprekken die verder gingen dan alleen over het werk: Gerben, Aggy, Prof. Andy Glaeser en Aloke Paul.

Ik wil ook graag de Wè-nun Henkers en mijn naaste vrienden (Joost, Hein, Wouter, Andor, Arno, de 10SC-mannen) bedanken voor de nodige afleiding tijdens deze vier jaar.

Lieve Katrien, zonder jou was het leven sowieso een stuk minder aangenaam.

Tenslotte wil ik mijn ouders, broers en de hele familie bedanken voor hun steun en vertrouwen.

## List of publications

### *The present work:*

1. M.J.H. van Dal, M.C.L.P. Pleumeekers, A.A. Kodentsov and F.J.J. van Loo, Intrinsic diffusion and Kirkendall effect in Ni-Pd and Fe-Pd solid solutions, *Acta mater.* **48** (2000) 385.
2. M.J.H. van Dal, M.C.L.P. Pleumeekers, A.A. Kodentsov and F.J.J. van Loo, Diffusion studies and re-examination of the Kirkendall effect in the Au-Ni system, *J. Alloys Comp.* **309** (2000) 132.
3. M.J.H. van Dal, A.A. Kodentsov and F.J.J. van Loo, The Kirkendall effect in multiphase systems, *Solid State Phenomena* **72** (2000) 111.
4. M.J.H. van Dal, A.M. Gusak, C. Cserháti, A.A. Kodentsov and F.J.J. van Loo, Microstructural stability of the Kirkendall plane in solid state diffusion, *Phys. Rev. Lett.* **86** (2001) 3352.
5. M.J.H. van Dal, A.M. Gusak, C. Cserháti, A.A. Kodentsov and F.J.J. van Loo, Instabilities of the Kirkendall plane, *Defect and Diffusion Forum* **194-199** (2001) 195.
6. M.J.H. van Dal, D.G.M.M. Huibers, A.A. Kodentsov and F.J.J. van Loo, Formation of Co-Si intermetallics in bulk diffusion couples: Part 1. Growth kinetics and mobilities of species in the silicide phases, *Intermetallics* **9** (2001) 409.
7. M.J.H. van Dal, A.A. Kodentsov and F.J.J. van Loo, Formation of Co-Si intermetallics in bulk diffusion couples: Part 2. Manifestations of the Kirkendall effect accompanying reactive diffusion, *Intermetallics* **9** (2001) 451.
8. M.J.H. van Dal, A.M. Gusak, C. Cserháti, A.A. Kodentsov and F.J.J. van Loo, Spatio-temporal instabilities of the Kirkendall-marker planes during interdiffusion in  $\beta'$ -AuZn, accepted for publication in *Philosophical Magazine A*.

9. M.J.H. van Dal and A.M. Gusak, Interdiffusive Big Bang – Bifurcations and instabilities of Kirkendall planes, *Proceedings of Metal Physics and Advanced Technologies* **19** (2000) 5.
10. M.J.H. van Dal, A.M. Gusak, C. Cserhádi, A.A. Kodentsov and F.J.J. van Loo, Reconsideration of the Kirkendall effect, submitted for publications to *Proceedings of DIFTRANS 2001*.
11. A.A. Kodentsov, M.J.H. van Dal, C. Cserhádi and F.J.J. van Loo, Reactive phase formation in binary and ternary silicide system, *Silicides: Fundamentals and Applications* L. Miglio and F. d'Heurle (eds.) (2001) 187.

*Others:*

12. A.A. Kodentsov, M.J.H. van Dal, C. Cserhádi, J.K. Kivilahti and F.J.J. van Loo, On Nitrogen Diffusion during the Internal Nitridation of N-Based Alloys, *Defect and Diffusion Forum* **143-147** (1997) 1619.
13. A.A. Kodentsov, M.J.H. van Dal, C. Cserhádi, L. Daróczi and F.J.J. van Loo, Permeation of nitrogen in solid nickel and deformation phenomena accompanying internal nitridation, *Acta mater.* **47** (1999) 3169.
14. A.A. Kodentsov, M.J.H. van Dal and F.J.J. van Loo, Thermodynamics and kinetics of phase formation in metal-ceramic joints, *9<sup>th</sup> Cimtec-World Ceramics Congress. Part C* (1999) 901.
15. S.L. Markovski, , M.J.H. van Dal, M.J.L. Verbeek, A.A. Kodentsov and F.J.J. van Loo, Microstructology of solid-state reactions, *J. Phase Equilibria* **20** (1999) 373.
16. A.A. Kodentsov, M.J.H. van Dal, and F.J.J. van Loo, Diffusion bonding of Si<sub>3</sub>N<sub>4</sub>-ceramic to transition metals: interfacial microchemistry, *Interfacial Science in Ceramic Joining*, A. Bellosi *et al.* (eds.) (1999) 15.

17. A.A. Kodentsov, M.J.H. van Dal, J.K. Kivilahti and F.J.J. van Loo, Thermodynamics and kinetics of internal reactions: nitridation of Ni-Cr alloys, *Ber. Bunsenges. Phys. Chem.* **102** (1998) 1326.
18. Yu. S. Nechaev, A.A. Kodentsov, M.J.H. van Dal and F.J.J. van Loo, The role of dislocations in the internal nitridation of Ni-Cr alloys, *Met. Phys. Adv. Tech.* **19** (2001) 107.
19. C. Cserhádi, Ü. Ugaste, M.J.H. van Dal, N.J.H.G.M. Lousberg, A.A. Kodentsov and F.J.J. van Loo, On the relation between interdiffusion and tracer diffusion coefficients in ternary solid solutions, *Defect and Diffusion Forum* **194-199** (2001) 189.
20. A.A. Kodentsov, M.J.H. van Dal, C. Cserhádi, A.M. Gusak and F.J.J. van Loo, Patterning in reactive diffusion, *Defect and Diffusion Forum* **194-199** (2001) 1491.
21. A.A. Kodentsov, M.J.H. van Dal, C. Cserhádi and F.J.J. van Loo, Deformation phenomena accompanying internal precipitation in solids, *High Temperature Materials Chemistry*, K. Hilpert, F.W. Froben and L. Singheiser (eds.) **Part II** (2000) 529.
22. A.A. Kodentsov, M.J.H. van Dal, C. Cserhádi and F.J.J. van Loo, Reactive phase formation in binary and ternary inorganic systems, *Nova Acta Leopoldina* **317** (2000) 205.

## Curriculum Vitae

Marcus Johannes Henricus van Dal werd geboren op 23 januari 1973, in Diessen, Noord Brabant, Nederland. Na het behalen van het atheneum eindexamen aan het Odulphus lyceum in Tilburg in 1991, begon hij de studie Scheikundige Technologie aan de Technische Universiteit Eindhoven.

In 1996 bracht hij 3 maanden door in Grenoble, Frankrijk op het ENSEEG-INP waar hij als stagiaire werkte aan het “Bevochtiginggedrag van Ni-Cr-Si legeringen op  $\text{Si}_3\text{N}_4$  substraten” onder de supervisie van prof. N. Eustatopoulos. In 1997, studeerde hij af aan de Technische Universiteit Eindhoven op het onderwerp “Nitridinggedrag van Ni-gebaseerde legeringen”.

In dat zelfde jaar begon hij als Assistent in Opleiding (AiO) bij het Laboratorium van Vaste Stof and Materialen Chemie onder de leiding van Prof. F.J.J. van Loo, wat resulteerde in dit proefschrift.

Marcus Johannes Henricus van Dal was born on the 23<sup>rd</sup> of January 1973, in Diessen, Noord Brabant, the Netherlands. After finishing Atheneum at the Odulphuslyceum in Tilburg in 1991, he decided to study Chemical Engineering at the Technical University of Eindhoven.

In 1996, he spent 3 months in Grenoble, France at the ENSEEG-INP where he worked on the “Wetting behaviour of Ni-Cr-Si alloys on  $\text{Si}_3\text{N}_4$  substrates” under the supervision of prof. N. Eustatopoulos. In 1997, he graduated at the Eindhoven University on the subject “Nitriding behaviour of Ni-based alloys”.

In the same year, he started his PhD project at the Laboratory of Solid State and Materials Chemistry under the guidance of Prof. F.J.J. van Loo, which resulted in the present thesis.